Helium and Tritium in Neutron-irradiated Beryllium

E. Rabaglino

Institut für Kern- und Energietechnik
Programm Kernfusion

Helium and tritium in neutron-irradiated beryllium

E. Rabaglino

Helium and tritium

in neutron-irradiated beryllium

Zur Erlangung des akademischen Grades eines

Doktors der Ingenieurwissenschaften

von der Fakultät für Maschinenbau der Universität Karlsruhe

genehmigte

Dissertation

von

Dott. Ing. Elisa Rabaglino

aus

Torino, Italien

Tag der mündlichen Prüfung: 20.07.2004

Hauptreferent: Prof. Dr.-Ing. Thomas Schulenberg (Universität Karlsruhe)

1. Korreferent: Prof. Dr. rer. nat. Dietrich Munz (Universität Karlsruhe)

2. Korreferent: Prof. Dott. Ing. Bruno Panella (Politecnico di Torino)

Helium and tritium in neutron-irradiated beryllium

Abstract

Beryllium is considered as a potential neutron multiplier in a Helium Cooled Pebble Bed tritium breeding blanket for future fusion power reactors. Under neutron irradiation, helium and tritium are produced in beryllium. The formation of helium bubbles induces swelling; tritium retention is a safety and waste handling issue. In-pile gas release should be sufficiently high to avoid the evacuation of the plant site in case of a serious accident leading to the abrupt release of all accumulated tritium. A reliable prediction of the behaviour of helium and tritium in beryllium, in-pile and during out-of-pile fast temperature transients, is necessary in order to prove the attractiveness of the blanket concept and to optimise design and materials. The lack of experimental data for beryllium pebbles, in the range of neutron fluence and temperature typical of the blanket module operation, imposes an extrapolation of models outside their validation range. A more sophisticated gas kinetics model and a more detailed validation of its single parts are necessary for beryllium in a fusion reactor blanket, than for uranium oxide in fission reactors. Since 1992 the code ANFIBE has been developed to predict the behaviour of helium and tritium in neutron-irradiated beryllium. The aim of the present work is to improve the code for both theoretical modelling and experimental validation, in order to increase confidence in its extrapolation to fusion reactor conditions. This requires to produce a more detailed, comprehensive and relevant experimental database than the one which was available during the early development phase of the code. The following milestones have been reached: (1) experimental characterisation of all helium and tritium diffusion and release stages in neutron-irradiated beryllium, also from a microscopic point of view; (2) assessment of helium and tritium thermal diffusion coefficients; (3) improvement of the model for gas precipitation into bubbles on the basis of the experimental study; (4) definition and application of an integrated validation procedure for the analytical model, based on the changes in the material microstructure related to different gas release stages. The final result of this study is a new version of the ANFIBE code, which can better describe gas atomic diffusion and precipitation into bubbles and the corresponding gas release. The code has then been applied to approximately assess tritium retention in beryllium at the End-Of-Life of a blanket module in a fusion reactor of 1.5 GW electric power. On the basis of such assessment, tritium retention in beryllium appears to be a much less critical issue than it was believed in the past.

Helium und Tritium in neutronenbestrahltem Beryllium

Zusammenfassung

Beryllium wird als Neutronenmultiplikator für einen heliumgekühlten Kugelschüttungs-Tritiumbrutmantel (das Helium-Cooled-Pebble-Bed-Blanket) für zukünftige Fusionskraftwerke betrachtet. Unter Neutronenbestrahlung werden Helium und Tritium im Beryllium produziert. Heliumblasenbildung verursacht Materialschwellung; Tritiumrückhaltung ist ein Sicherheits- und Abfallbehandlungsproblem. Um im Falle eines Störfalles, der das angesammelte Tritium freisetzten könnte, die Evakuierung der Umgebung zu vermeiden, muss die Tritiumfreisetzung während des Reaktor betriebs (in-pile) groß sein. Eine zuverlässige Vorhersage des Verhaltens von Helium und Tritium im Beryllium, in-pile und während schneller out-of-pile Aufheizung, ist notwendig, um die Attraktivität des Blanketkonzeptes zu prüfen und um Design und Materialien zu optimieren. Der Mangel an experimentellen Daten für Beryllium-Kugeln im Blanketbetrieb in Bezug auf Neutronenfluenzen und Temperaturen macht eine Extrapolation der Modelle außerhalb ihres Gültigkeitsbereiches notwendig. Verglichen mit Uranoxid in Spaltungsreaktoren, sind für Beryllium in einem Fusionsreaktorblanket eine Verfeinerung des Gaskinetikmodells und eine ausführliche Validierung der einzelnen Teile des Modells notwendig. Seit 1992 wurde der Code ANFIBE entwickelt, um das Verhalten von Helium und Tritium in neutronenbestrahltem Beryllium vorherzusagen. Das Ziel der hier vorliegenden Arbeit ist, den Code sowohl in Bezug auf die theoretischen Modelle, als auch auf die experimentelle Validierung zu verbessern, um damit das Vertrauen in die Vorhersagen für die Bedingungen eines Fusionsreaktors zu erhöhen. Im Vergleich zur ersten Version des Codes erfordert dies die Erstellung einer detaillierteren, umfassenderen und relevanteren experimentellen Datenbank. Die folgenden Meilensteine sind erreicht worden: (1) experimentelle Charakterisierung aller Helium- und Tritiumfreisetzungsstadien in neutronenbestrahltem Beryllium, im makro- als auch mikroskopischen Maßstab; (2) Abschätzung der Helium- und Tritiumdiffusionskonstanten; (3) Verbesserung des Modells für Gasausscheidung in Blasen auf der Grundlage der oben genannten experimentellen Studien; (4) Definition und Anwendung eines integrierten Validierungsverfahrens für das analytische Modell, basierend auf der Änderung der Mikrostruktur des Materials bei unterschiedlichen Gasfreisetzungsstadien. Das abschließende Ergebnis dieser Studie ist eine neue Version des ANFIBE Codes, die die Gasatomdiffusion und -ausscheidung in Blasen und die entsprechende Gasfreisetzung besser beschreibt. Der Code wurde dann angewandt, um die Tritiumrückhaltung in Beryllium am Ende der Lebensdauer eines Blanketmoduls in einem Fusionskraftwerk mit 1,5 GW elektrischer Leistung annähernd zu ermitteln. Auf der Basis dieser Abschätzung scheint die Tritiumrückhaltung in Beryllium ein viel geringeres Problem zu sein, als in der Vergangenheit angenommen wurde.

TABLE OF CONTENTS

1   Introduction

1.1   Neutron irradiation effects in beryllium

Beryllium is used as a neutron moderator in some research nuclear reactors and is a key material in the present design of future deuterium-tritium thermonuclear fusion reactors, where it is foreseen as a plasma facing material and as a neutron multiplier. Under neutron irradiation, as a consequence of the following reactions:

$$^{9}\text{Be} + n \rightarrow 2\ ^{4}\text{He} + 2\ n \qquad (E_n > 2.7\ \text{MeV}) \qquad\qquad\qquad (1\text{-}1)$$

$$^{9}\text{Be} + n \rightarrow\ ^{7}\text{Li} +\ ^{3}\text{H} \qquad (E_n > 10.5\ \text{MeV})$$
$$^{7}\text{Li} + n\ \ \rightarrow\ ^{4}\text{He} +\ ^{3}\text{H} + n \qquad\qquad\qquad\qquad (1\text{-}2)$$

$$^{9}\text{Be} + n \rightarrow\ ^{6}\text{He} +\ ^{3}\text{H} \qquad (E_n > 0.6\ \text{MeV})$$
$$^{6}\text{He} \rightarrow\ ^{6}\text{Li} + \beta^{-} + \nu \qquad\qquad\qquad\qquad (1\text{-}3)$$
$$^{6}\text{Li} + n \rightarrow\ ^{4}\text{He} +\ ^{3}\text{H}$$

helium and tritium are produced in beryllium. Gas production plays a much more important role than lattice damage in limiting the component lifetime. Gas atoms form bubbles and bubble growth and coalescence induce swelling. From this point of view, helium and tritium retention in beryllium under irradiation is an issue similar to gaseous fission product and helium accumulation in metallic uranium, uranium oxide or mixed uranium-plutonium oxide (MOX) nuclear fuels and in advanced Inert Matrix Fuels for the transmutation of actinides. Furthermore, tritium inventory is a safety and waste handling issue, in particular in fusion power plants, where the limits on accidental release of radioactivity are much lower than for fission reactors, the problem of handling, transport and storage of radioactive waste should be minimised and a recycling of the materials should be possible. The experimental characterisation and theoretical modelling of helium and tritium behaviour in beryllium are necessary in order to provide reliable predictions of swelling and tritium retention. It has to be proven that reactor components operate reliably until the End-Of-Life and that safety requirements are met in case of accident. On the basis of theoretical predictions, design parameters and material characteristics can be optimised in order to improve performance and safety.
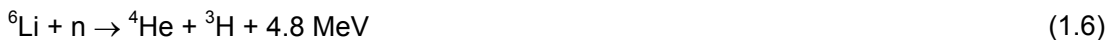
1.2   The tritium breeding blanket in a fusion power reactor

Nuclear fusion of hydrogen isotopes is an attractive option for electricity production starting from the second part of the 21$^{\text{st}}$ century. It is at present expected that a future fusion power reactor will be of a tokamak type (Fig. 1-1). A toroidal vacuum vessel contains a mixture of

hydrogen heavy isotopes (deuterium ^{2}H and tritium ^{3}H) at a very high temperature (of the order of 10^8 K). At such temperature hydrogen is in the state of plasma and the following fusion reaction occurs:

$$^2H + {}^3H \rightarrow {}^4He + n + 17.6 \text{ MeV} \tag{1.4}$$

Deuterium is a natural hydrogen isotope and can be extracted from water; tritium is a radio-active isotope and it has to be artificially produced by interaction of neutrons with lithium iso-topes, according to the reactions:

$$^7Li + n \ (E_n > 2.5 \text{ MeV}) \rightarrow {}^4He + {}^3H + n \tag{1.5}$$

$$^6Li + n \rightarrow {}^4He + {}^3H + 4.8 \text{ MeV} \tag{1.6}$$

The burning plasma is confined by a strong magnetic field, partially produced directly by su-perconducting coils located outside the vacuum vessel, partially by inducing a plasma current on the basis of the transformer principle. The energy from the fusion reactions is shared be-tween the reaction products: 1/5 goes to the alpha particles and, since they remain confined in the plasma, contributes to plasma heating; the remaining 4/5 are carried away by the neu-trons. The plasma chamber is surrounded by the tritium breeding blanket (Fig. 1-1), a series of modules where the neutrons coming from the plasma deposit their kinetic energy and in-teract with lithium atoms in order to breed tritium. Therefore the blanket has three main func-tions: to collect the heat deposited by the neutrons and to extract it by a cooling system; to
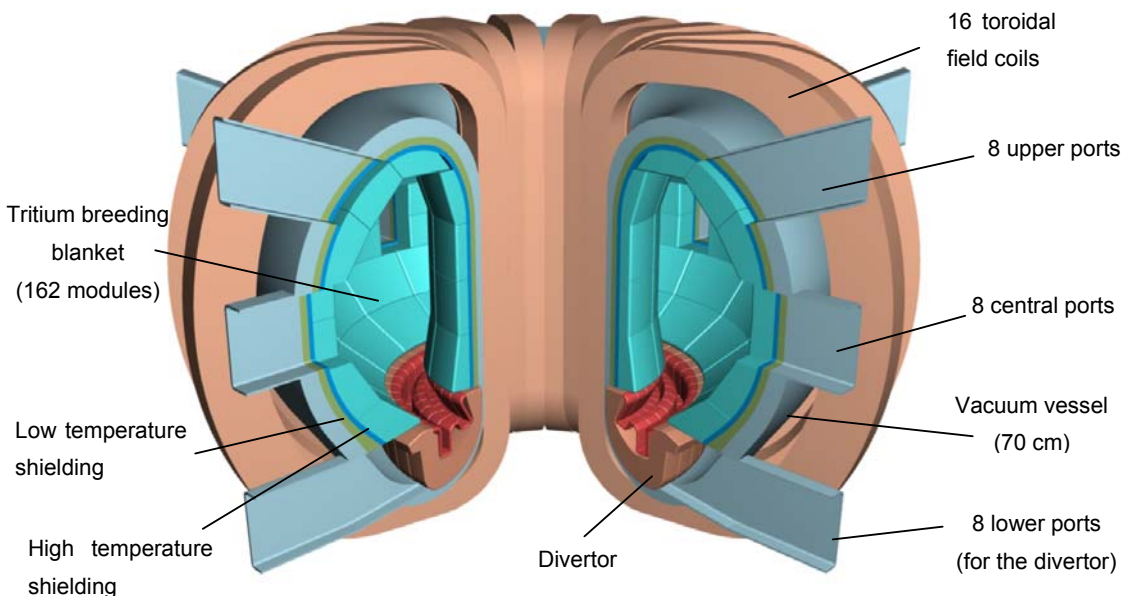
Fig. 1-1   View inside a future fusion power reactor.

breed tritium inside lithium based materials and to remove it by a purging system; finally, to act as a thermal and neutron shield for the superconducting coils located behind it.

1.3   Issues of beryllium in a solid tritium breeding blanket for fusion reactors

In the frame of the European fusion technology long term programme, a solid tritium breeding blanket is being developed as a possible solution for future fusion power reactors. Since the tritium breeder, i.e. lithium, is contained in a ceramic compound (orthosilicate Li_4SiO_4 or metatitanate Li_2TiO_3), beryllium is needed as a neutron multiplier to maintain a sufficiently high neutron flux for tritium breeding, in a ratio of at least 4 volume parts of neutron multiplier [Fis88] per ceramic breeder part. In the present reference concept, the Helium Cooled Pebble Bed (HCPB) blanket [Dal94] [Her99] [Her01], ceramic breeder and neutron multiplier are in the form of beds of small pebbles, separated by helium cooled steel plates (Fig. 1-2). The pebble beds are purged by an independent helium loop, in order to remove tritium. A recent assessment of operation conditions of the HCPB blanket in a fusion power plant [Che02] predicts a lifetime of the blanket module of 40000 hours. Beryllium pebble beds lay in a temperature range of 700 – 1050 K and neutron fluence reaches at End-Of-Life the peak value of $3 \cdot 10^{26}$ neutrons m^{-2} (E > 1 MeV), corresponding to a production of 25700 appm helium and 640 appm tritium, in conjunction with an integrated damage of 80 dpa. Swelling and tritium retention in beryllium are key issues of the concept [Mal99]. Swelling of beryllium pebbles leads to mechanical interaction of the bed with steel plates and bed deformation. The packing fraction of the beds and the contact area between pebbles are modified, with a consequent change in the macroscopic thermal conductivity and in the temperature profile [Sca95] [Sca97b]. Tritium accumulation is a concern in case of accidental temperature transients, where the whole inventory can be released in a short time, and in the transport, storage and recycling of spent blanket modules, since irradiated beryllium is considered to be a
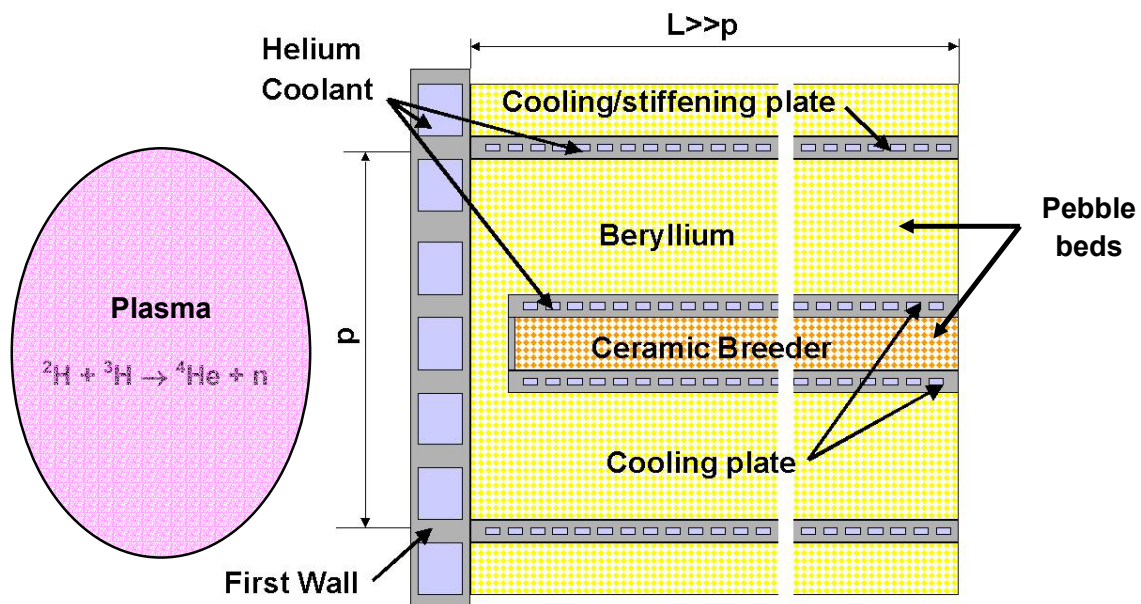
Fig. 1-2   Poloidal section of a module of the Helium Cooled Pebble Bed (HCPB) blanket.

special waste [Dru02], due to its toxicity and tritium content. In the 1.5 GW$_{el}$ fusion power plant presently considered as a reference in the European studies, tritium production in the neutron multiplier in the whole of the blanket has been assessed as about 24 kg in 390 tons of beryllium [Che02]. If a large fraction of such amount were retained in beryllium, it might be abruptly released during an off-normal temperature transient and the evacuation of the site of the fusion power plant would become necessary. Therefore the design requirement to keep a fusion power plant with a HCPB blanket attractive from the safety point of view is that most of tritium produced in beryllium should be continuously released in-pile and removed by the purging flow.

1.4 Characterisation and modelling of swelling and tritium retention in neutron-irradiated beryllium: the state of the art

1.4.1 The ANFIBE code

The code ANFIBE (Analysis of Fusion Irradiated BEryllium) was developed in the years 1992-1995 [Sca97a] [Sca98] to assess swelling and tritium retention in beryllium. ANFIBE is the result of an adaptation to beryllium of the code FUTURE [Ron88], previously developed for the description of gaseous fission product kinetics and swelling in uranium oxide.

The analytical model of helium kinetics, tritium kinetics and swelling in ANFIBE has been previously described [Sca97a] and it is presented in Annex A. It considers a set of average quantities which are representative of different states of gas atoms (helium or tritium) in the solid and of the related diffusion and release stages (Fig. 1-3). Under neutron irradiation, gas atoms are uniformly generated in the beryllium lattice. Their initial state is a non-equilibrium
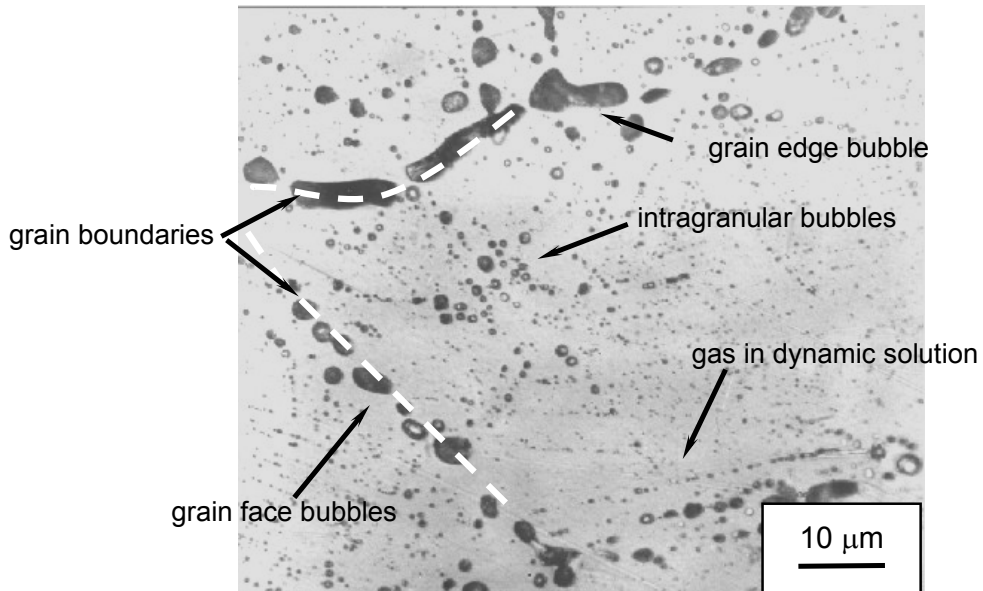
Fig. 1-3   Bubbles inside the grain and at grain boundaries in an irradiated beryllium pebble. Some of the average quantities described in the gas kinetics model of the ANFIBE code are shown.

4

solution (a *dynamic* solution). Therefore, if the temperature is sufficiently high to allow them to diffuse, they either precipitate into small bubbles inside the grain (*intra*granular bubbles) or migrate to grain boundaries, where they generate larger, elongated bubbles (*inter*granular bubbles, at grain surface or grain edge).

As time elapses and temperature or neutron fluence increase, bubbles diffuse, grow and coalesce until networks of interlinked porosities at grain boundaries are formed, which are connected to the free surface (*percolation paths*): these channels allow gas trapped into bubbles at grain boundaries being finally released. Gas percolation following pore interlinkage is the only release mechanism considered. The presence of free grain boundaries, which allow gas atoms reaching the grain boundary to be directly released, is neglected. Such assumption is correct for UO_2 pellets and also for standard beryllium blocks with fine grains which are used as a moderator in research reactors, since the external grain surface is practically negligible as compared to the total grain surface. Gas atoms which directly reach grain boundaries without being trapped by the population of intragranular bubbles are much faster released than those which precipitate inside the grain, since intragranular bubbles, in order to release their gas content, have to migrate to grain boundaries and their diffusion is much slower than the diffusion of single atoms. As a consequence, gas precipitation into intragranular bubbles is to be considered as a trapping phenomenon and the higher the precipitation rate is, the slower the release. In the analytical model of ANFIBE, the time evolution of gas balance terms (gas in dynamic solution, in intragranular bubbles, in intergranular bubbles per unit volume, fraction of gas released with respect to gas produced) and of bubble classes (intragranular, grain surface and grain edge bubbles per unit volume) is described as a competition of source and sink terms, which are functions of other gas balance terms, of bubble average features and of a number of key material properties (e.g. grain size, gas atomic diffusion coefficients and beryllium self-diffusion coefficient). As an example, the time derivative of the average concentration of helium or tritium in dynamic solution (Eq. A-1, Annex A) is given by the algebraic sum of four main terms:

1. the production rate of helium or tritium from nuclear reactions per unit volume (source term)

2. the gas precipitated into intragranular bubbles per unit time and volume (sink term, function of the atomic diffusion coefficient, of the intragranular bubble radius and concentration, of the gas-in-solid equilibrium solubility and of the concentration of gas in solution itself)

3. the gas migrated to grain boundaries per unit time and volume (sink term, function of the same quantities and in addition of the grain size)

4. the gas re-dissolved from intragranular bubbles (source term, function of the concentration of gas in intragranular bubbles and of the helium generation rate) per unit time and volume

One set of reaction-rate equations describes helium kinetics; a second one tritium kinetics, with similar equations; a third set describes bubble kinetics (nucleation, diffusion, growth, coalescence). On the basis of bubble population parameters (average radius and concentration, pressure) calculated by the bubble kinetics model, swelling is described as the result of the creep of the solid matrix under the influence of pressurized bubbles. It is considered as a non-equilibrium phenomenon and it mainly depends on the governing creep law.

1.4.2 Issues of ANFIBE

The main issues of the 1995 version of ANFIBE (from now on referred to as ANFIBE 0) are related to the scantiness of relevant experimental information at that time, as far as material properties and opportunity of detailed model validation are concerned. Swelling predictions were validated on the basis of macroscopic density measurements at End-Of-Irradiation. Helium release predictions could not be validated due to the absence of data both in-pile and out-of-pile. Tritium release predictions were validated on the basis of a set of out-of-pile measurements during temperature transients, due to the absence of in-pile data [Sca95]. In general:

1. materials were of a much lower quality and remarkably different from the one that is presently considered as a reference for the HCPB blanket in some key characteristics, i.e. shape, grain size and impurity content, especially oxygen

2. irradiation conditions (temperature and neutron fluence) were far from the expected operation range of beryllium pebble beds in the HCPB blanket (Fig.1-6)

3. no data on the material microstructure were available to validate models of bubble nucleation and kinetics from a microscopic point of view

4. some key material properties, which have a strong influence on the prediction of gas diffusion and release and swelling, were not available and were assessed on the basis of available literature

1.4.2.1 Issues related to material type

In the HCPB blanket, beryllium is in the form of pebble beds, in order to prevent material break-up, to reduce interaction with walls under irradiation, to avoid hot spots at the wall and to facilitate gas purge. Pebble beds have an actual packing factor of about 0.62-0.64 [Rei02]. Beryllium pebbles have been developed explicitly for the blanket since the beginning of the '90s, in collaboration with different companies (BrushWellmann, USA; NGK, Japan). At present, the reference pebble size is 1 mm (Fig. 1-4). Pebbles from 0.1 to 5 mm diameter have also been considered. Pebbles from 1 to 5 mm diameter are produced by Rotating Electrode Process (REP): a high purity beryllium electrode melts in an arc ejecting spherical drops which solidify during their flight in helium. Such process gives a perfect spherical shape, but a hole in the centre of the pebble may appear as a result of the solidification process. Very
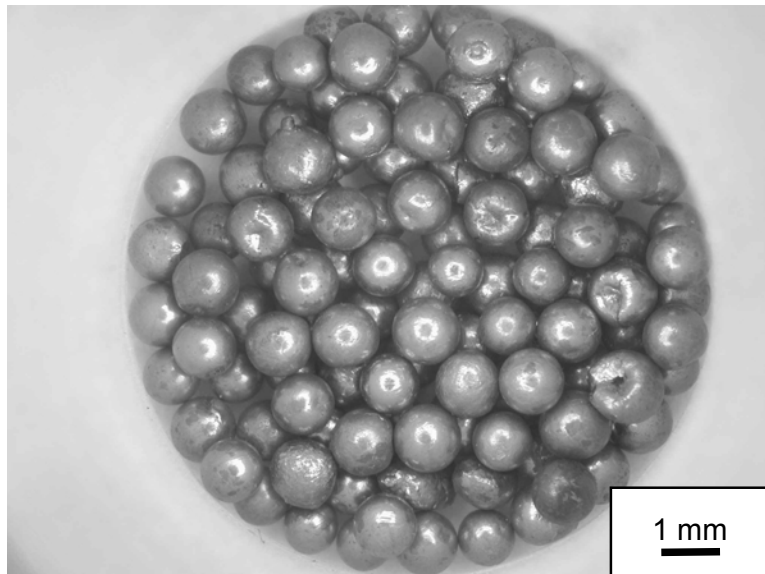
Fig. 1-4   The present reference material as a neutron multiplier for the HCPB blanket, 1-mm beryllium pebbles produced by NGK by REP [Pia02][Kle01].
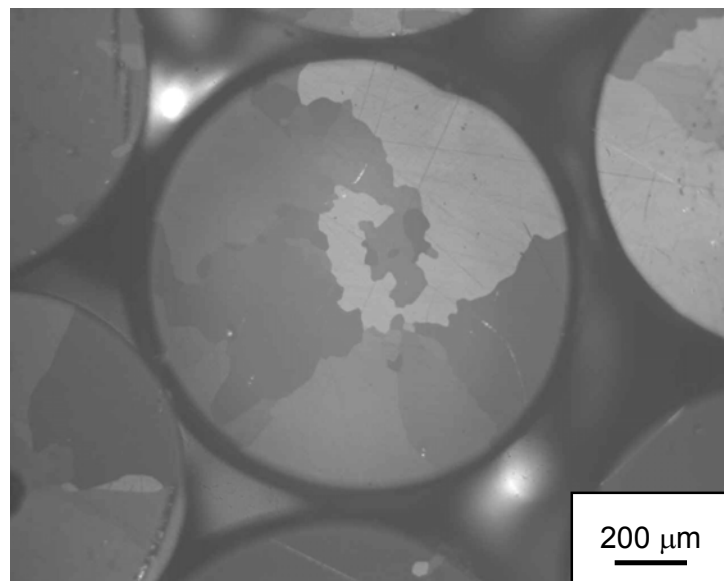

Fig. 1-5   Microstructure of the reference beryllium pebbles for the HCPB blanket in Fig. 1-4. Coarse columnar grains are visible.

small pebbles (0.1-0.2 mm) are produced by spraying molten beryllium in an inert atmosphere (Inert Gas Atomisation process, IGA). In a previous development stage, 2 mm pebbles were a by-product of beryllium fluoride reduction with magnesium (Fluoride Reduction Process, FRP). Pebbles have always a coarse grain microstructure (Fig. 1-5), with much larger grains than beryllium bricks or tiles produced by Hot Isostatic Pressing for nuclear reactors or plasma facing components (40 to 200 μm grain size, as compared to about 10 μm). Inside the grains the dislocation density is very low. When studying the behaviour of pebbles under irradiation, the following main peculiarities have to be considered: the controlled impurity content [Pia02], the unusually large grain size and the large free surface per unit mass (17 m^2 kg^{-1} for 1 mm diameter pebbles [Iwa99]), related to a large ratio of free surface to grain boundary surface. This implies different characteristics in terms of mechanical properties (e.g. creep rate, which is fundamental to predict swelling) and gas release properties. Such characteristics make the material absolutely peculiar. A model developed on the basis of experimental results obtained with standard beryllium bricks cannot be easily extrapolated to pebbles. Likewise, the analytical description of relevant gas release mechanisms, in particular the formation of open porosity networks, cannot be simply borrowed from sintered ceramics (e.g. UO_2 pellets) and needs ad-hoc experimental data and model developments.

1.4.2.2 Issues related to irradiation conditions

As far as the present irradiation possibilities in fission research reactors are concerned, it has been shown [Fis04] that conditions similar to a fusion reactor, as far as the ratio of tritium to helium production and of dpa to helium production are concerned, can be very well simulated in the High Flux Reactor (HFR) located in Petten (the Netherlands), with a suitable design of the irradiation experiment. Nevertheless, a very long time is needed to reach the End-of-Life (EOL) conditions of beryllium in a fusion power reactor (> 20000 appm helium production), with prohibitive costs. The irradiation programme HIDOBE (HIgh DOse BEryllium) [Heg04] will be started in late 2004 in the HFR with the aim of reaching 3000 appm helium production in 2 years and 6000 in 4 years, in two separate irradiation rigs, in a range of 400 to 800 °C. In HIDOBE the reference beryllium pebbles will be irradiated for the first time at blanket relevant temperatures. The Post Irradiation Examinations (PIE) are foreseen starting from 2007.

In the long term, the possibility to irradiate beryllium under conditions typical of a fusion reactor, reaching the EOL fluence in the same time (40000 hours, 4.5 years), will be provided by the International Fusion Material Irradiation Facility (IFMIF) [Fis04]. In the international programme for the development of nuclear fusion energy, the construction and operation of a neutron source, dedicated to testing the behaviour of materials (in particular structural materials) under reactor relevant irradiation conditions, is foreseen as a necessary complementary step to the International Thermonuclear Experimental Reactor (ITER), in order to prepare for the construction of a demonstration fusion power reactor around 2035 (the DEMO reactor). In IFMIF neutrons with the same spectrum as in a fusion reactor will be generated by the impact of accelerated deuterons onto a liquid lithium target [Moe02].

Fig. 1-6 sums up the irradiation conditions of beryllium samples available for model development and validation before 1995, today and in the next years. In the next future, before an

irradiation in IFMIF can be carried out, the maximum dose of available beryllium pebbles will not exceed 6000 appm, only about ¼ of the EOL fluence at the typical operation temperatures of the blanket in a fusion reactor (700-1050 K).

1.4.2.3 Issues related to model extrapolation

Due to the absence of data in a fusion reactor relevant range of irradiation conditions and for a representative material, the extrapolation of models outside their validation range is needed in order to assess End-Of-Life conditions of beryllium in the blanket. The need for extrapolation imposes a much more careful and detailed validation procedure for ANFIBE than for presently available codes which calculate gas kinetics in nuclear fuels, i.e. the CO-PERNIC code developed by Framatome ANP [Ber02] [Las00]. A validation based on integral quantities as macroscopic swelling and gas release alone is not sufficient, because these are cumulative effects resulting from complex diffusion phenomena occurring in the solid. It is necessary to check if the prediction of macroscopic quantities complies with the description of microscopic gas diffusion. Single gas kinetics stages, i.e. atomic diffusion, precipitation into intragranular bubbles or migration to grain boundaries, bubble migration, growth and coalescence, formation of percolation paths at grain boundaries, should be correctly described. Gas release stages should be put in connection to microstructure evolution, in order
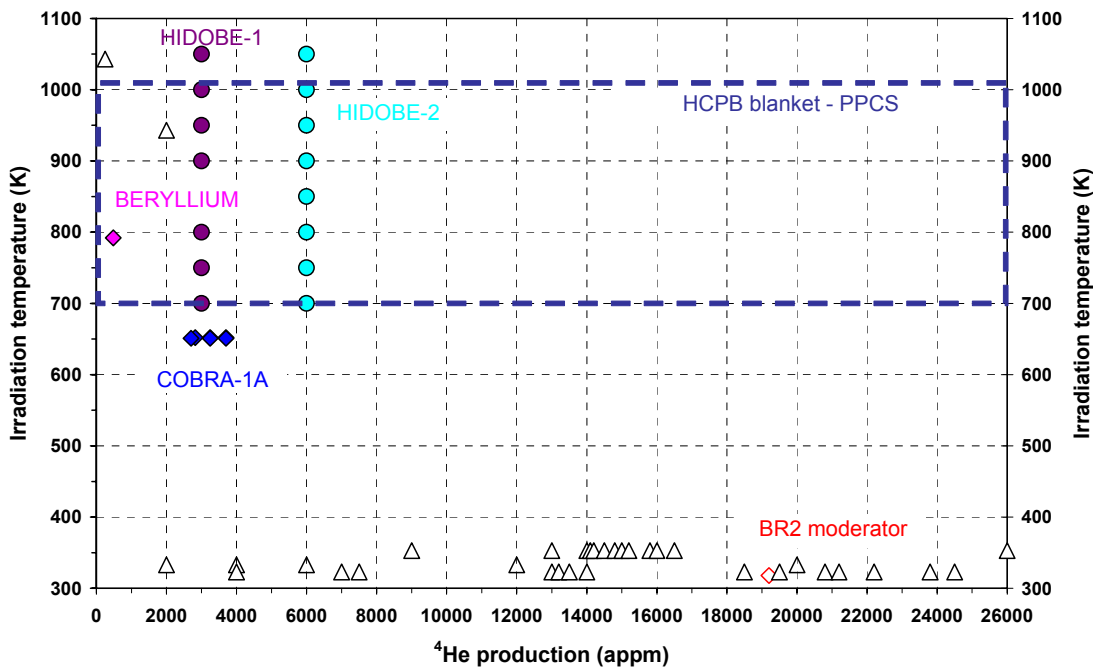

Fig. 1-6   Irradiation conditions of beryllium specimens available for the validation of models: before 1995 (triangles, validation of ANFIBE 0), from 1995 to nowadays (squares, validation of ANFIBE 1) and expected in the next future (circles). Material type: pebbles (full symbols), other (empty symbols).

to understand to which particular diffusion phenomenon they are related. In order to validate each part of the model from the microscopic point of view, an exhaustive characterisation of microstructure and of its evolution corresponding to different gas release stages has to be performed. Furthermore, the experimental tests should make it possible to check and validate single parts of the model, which describe different diffusion stages, separately and independently of others.

1.5 Recent progress in the experimental characterisation of neutron-irradiated beryllium

The main issue of the validation of ANFIBE in 1995 was the absence of a complete characterisation in-pile and out-of-pile of a relevant material, irradiated under representative conditions. In particular the relationship between macroscopic gas release and microscopic diffusion phenomena had to be understood and quantitatively characterised in terms of key atomic-scale quantities in the model.

After 1995, relevant progress in the experimental characterisation has been made, in conjunction to material development. Beryllium pebbles, similar to the present reference material although in an earlier development stage, have been irradiated in two experiments:

1. The BERYLLIUM irradiation in the High Flux Reactor in Petten, the Netherlands [Con96]: pebbles fabricated by BrushWellmann (0.1 and 2 mm diameter) were irradiated at about 790 K to a fast neutron fluence of 1.0 - 1.24 $\cdot 10^{25}$ neutrons m^{-2} (480 appm ^{4}He, 12 appm ^{3}H) from 21st April to August 8th, 1994;

2. The COBRA-1A irradiation in the Experimental Breeder Reactor II in Idaho Falls, USA [Gel97]: pebbles fabricated by BrushWellmann (1, 3, 5 mm diameter) and by NGK (1 mm) were irradiated at about 653 K to a fluence of 3.62 - 4.88 $\cdot 10^{26}$ neutrons m^{-2} (2700-3700 appm ^{4}He) from November 26th, 1992 to September 26th, 1994.

Both irradiations are well documented. The complete Post Irradiation Examinations (PIE) of pebbles from the COBRA-1A irradiation was performed in 1997 [Gel97]. A detailed PIE and out-of-pile study of pebbles from the BERYLLIUM irradiation is presented in Chapter 2 of this study. At the same time, a number of out-of-pile helium and tritium release measurements during temperature transients with different irradiated beryllium samples were performed [Sca97c].

The recent progress in the experimental characterisation of irradiated beryllium samples, in particular the availability of a first database for beryllium pebbles, enables a revision of the ANFIBE code.

1.6   Aim and milestones of the present study

The general aim of this study is to improve and better validate gas kinetics models in the ANFIBE code, in order to enable a reliable extrapolation to the EOL conditions of beryllium pebbles in a fusion power reactor. The strategy to approach this goal consists of the following main steps:

1. study of out-of-pile helium and tritium release from weakly irradiated pebbles, during out-of-pile thermal ramp annealing to the melting point. During this kind of temperature transients, it is possible to reproduce in a short time the evolution of gas diffusion phenomena which occur in pile as the dose increases, from atomic diffusion to gas release through open porosity networks

2. study of microstructure evolution during the temperature transient, corresponding to different gas release stages. This study makes it possible to relate macroscopic gas release to microscopic diffusion phenomena occurring inside the grains and at grain boundaries

3. inverse analysis of experimental gas release curves, by an analytical model that takes into account gas atomic diffusion and precipitation into intragranular bubbles or migration to grain boundaries. The study enables to provide elementary material properties for a part of the general gas kinetics model in ANFIBE and to improve, calibrate and validate it independently from other parts

4. on the basis of the inverse analysis, assessment of helium and tritium thermal diffusion coefficients, of a characteristic distance for the migration of gas atoms to grain boundaries and of the probability that gas atoms are trapped in bubbles instead of reaching the grain boundaries

5. improvement of the model for gas precipitation and migration to grain boundaries in ANFIBE, in order to match the experimental results

6. integrated validation of the improved version of ANFIBE on the basis of microscopic data on the microstructure and macroscopic data on gas release

The first four milestones are described in Chapter 2. Chapter 3 presents the improvements of the gas kinetics model which, on the basis of the experimental study and of other data in the available literature, have been implemented in a new version of ANFIBE, called ANFIBE 1. An integrated macroscopic/microscopic validation procedure of the gas kinetics model (milestones 5 and 6) is also defined and applied. In Chapter 4, finally, the improved version of the code is applied to assess tritium retention in the reference beryllium pebbles at End-Of-Life of a HCPB blanket module in a fusion reactor of 1.5 GW electric power.

ANFIBE shall be further improved in the next years as soon as the same methodology developed and applied in this study will be extended to characterise other irradiated beryllium

samples. The confirmation of the ANFIBE code up to 3000 and to 6000 appm ^{4}He production will be possible as soon as the Post Irradiation Examinations of the HIDOBE irradiation will be completed around 2010. It is expected that the confirmation at these two fluences will enable, by linear extrapolation, also a fully reliable prediction at fusion reactor End-Of-Life conditions. Nevertheless, the final confirmation up to 26000 appm will be possible only in the long-term (10-15 years from now), after irradiation of beryllium pebbles in the International Fusion Material Irradiation Facility.

2 Experimental study - Characterisation of gas diffusion and release in irradiated beryllium

2.1 Introduction

An experimental study of the kinetics of helium and tritium in irradiated beryllium has been performed, in order to improve the understanding of gas diffusion phenomena, to provide key material properties for the models and relevant experimental information to validate and improve them also from the microscopic point of view. The main part of the study concerns weakly irradiated pebbles from the BERYLLIUM experiment: for this material a study of the out-of-pile gas release during fast thermal ramp annealing to the melting point has been performed. As a second step, the different gas release stages which appear during such temperature transient have been correlated to microstructure evolution. As a third step, an inverse analysis of gas release, coupled to a quantitative analysis of bubble population characteristics, has made it possible to assess the atomic thermal diffusion coefficients of helium and tritium and to validate and improve the model of gas precipitation into intragranular bubbles and consequently of gas release. In order to investigate gas kinetics at different irradiation conditions and with different microstructure, other two types of irradiated beryllium have been examined: weakly irradiated pebbles from the EXOTIC 8 irradiation and highly irradiated fragments from the disposed moderator of Belgian Reactor 2 (BR2).

2.2 The samples

Three types of irradiated beryllium have been investigated:

1. weakly irradiated pebbles from the BERYLLIUM irradiation

2. weakly irradiated pebbles from the EXOTIC 8 irradiation

3. highly irradiated fragments from the disposed moderator of BR2

Table 2-1 summarizes their relevant characteristics and compares them to the reference pebbles for the Helium Cooled Pebble Bed (HCPB) blanket.

The pebbles from the BERYLLIUM irradiation, though of low quality and with higher impurity content, have similar shape and microstructure (coarse grains, 40-200 μm) to the reference material. Their irradiation history is very well documented [Con96]. Due to their relatively high irradiation temperature and low fluence, they are suitable to investigate early gas diffusion stages, i.e. atomic diffusion and precipitation into intragranular bubbles, as well as the effect of radiation damage on them. By out-of-pile heating to high temperatures, it is possible to partially reproduce in these pebbles diffusion stages which would occur under irradiation at higher fluences, i.e. bubble growth and formation of interlinked porosities. The pebbles from the EXOTIC 8 irradiation have similar grain size, but much smaller diameter, therefore they

Irradiation conditions	BERYLLIUM irradiation	EXOTIC 8-3/13 irradiation	BR2 moderator 2nd matrix channel B120	*HCPB blanket*
Material type	BrushWellmann FRP pebbles, 2 mm diameter	BrushWellmann IGA pebbles, 0.1 to 0.2 mm diameter	Fragments from VHP bricks	*NGK REP pebbles, 1 mm diameter*
Grain size	40 to 200 µm	40 to 200 µm	20 µm	*40 to 200 µm*
Main impurities	3125 ppm BeO, 1200 ppm Mg	3400 ppm Be0, 100 ppm Mg	19500 ppm BeO, 28 ppm Mg	*2300 ppm BeO, 300 ppm Mg, controlled ratios between impurities*
Irradiation time	97.4 days	449.8 days	15 years	*40000 hours (≈ 4.5 years)*
Neutron spectrum	Fast fission	Fast fission	Fast fission	*fusion*
Irradiation fluence	$1.24 \cdot 10^{25}$ m^{-2} (E > 0.1 MeV)	$2.70 \cdot 10^{25}$ m^{-2} (E > 0.1 MeV)	$9.90 \cdot 10^{26}$ m^{-2} (E > 0.1 MeV)	*Up to $3 \cdot 10^{26}$ m^{-2} (E > 1 MeV)*
Irradiation temperature	780 K	800 - 900 K	420 K	*770 – 1030 K*
^{4}He content	480 appm (*)	285 appm (*)	19200 appm (*)	*Up to 25700 appm at EOI*
^{3}H content	12 appm (*) at EOI (1994) 8 appm in 2001 (**)	1.16 appm (*) at EOI (2000)	2256 appm (*) at EOI (1995) 1522 appm in 2002 (**)	*Up to 640 appm at EOI*

(*) calculated on the basis of the irradiation history; (**) at the time of the characterisation

Tab. 2-1   Main material and irradiation characteristics of irradiated beryllium samples investigated in this study [Con96] [Van02] [Sca01] [Aal02], compared to the reference material for the solid blanket [Pia02] [Che02].

are useful to investigate the effect of a larger ratio of free surface to grain boundary surface on gas release.

Fragments from BR2 disposed moderator bricks are a material very different from the reference pebbles: they have fine grains and a much higher content of oxygen [Van02]. Beryllium oxide affects tritium diffusion at low temperatures (< 600 K), since it traps tritium as beryllium hydroxide. Furthermore, the irradiation conditions (temperature and neutron spectrum) are far from the expected operation conditions of the blanket. Nevertheless, all available materials with a ^{4}He content representative of blanket End-Of-Life (EOL) conditions exhibit the same issue: no pebbles are available to study gas kinetics at high dose (Fig. 1-6, Chapter 1). The results of the characterisation of highly irradiated beryllium from BR2 are useful to understand qualitatively gas diffusion and release phenomena at high dose and with much smaller grains, but in the extrapolation of the results to pebbles the different microstructure and irradiation conditions have to be taken into account.

2.3   Study of out-of-pile gas release

2.3.1   The Knudsen cell technique

The effusion of helium and tritium from irradiated beryllium samples was measured by a technique based on the principle of the Knudsen cell, coupled to a mass spectrometer [Hie00] [Gag92]. The facility was originally developed to study vapour effusion and fission gas release from irradiated nuclear fuel up to high temperatures. The main peculiarities of this technique if applied to irradiated beryllium, as compared to similar studies in the literature [Sca01a] are the following: (1) the melting point of beryllium (T_m = 1556 K [Kle01]) can be exceeded and this makes it possible to follow release stages until complete exhaustion of the gas inventory; (2) gas release is measured in a vacuum and not with a purge flow; (3) tritium is measured, like helium, by the mass spectrometer located in the vicinity of the source and not by an ionisation chamber or a proportional counter.

The scheme of the set-up is shown in Fig. 2-1. The furnace can reach temperatures up to 2500 K and is mounted in a lead-shielded glove-box. The Knudsen cell, a tungsten cell of 12 mm outer diameter containing the sample (Fig. 2-2), is lifted up into a thermally shielded tungsten heating coil and an ultra-high vacuum of 10^{-6} Pa is created. Gaseous products effuse out through a hole in the top of the cell and a small fraction of the particle beam goes through the ionisation chamber of a quadrupole mass spectrometer located directly above the oven. A liquid-nitrogen loop around the ion source acts as a cold trap for condensable hydrocarbons and rest vapours, so that background noise in the mass spectrometer signal can be significantly reduced. Irradiated beryllium is heated above the melting point with temperature ramps of about 10 or 30 K/min, which are obtained by automatic control of the heating resistor voltage. The temperature is measured by a thermocouple inserted in the base of the sample holder. To account for the difference between the temperature measured by the thermocouple and the real temperature of the sample inside the cell, the following calibration procedure is applied: standard samples of silver, zinc, platinum and beryllium are melted and cooled-down; at the freezing point of the sample a thermal arrest occurs at which both temperature and vaporisation rate remain constant for a sufficiently long time, providing fixed points to correct the thermocouple temperature on the basis of the actual melting temperature. After this correction the residual temperature error is less than 5 K.
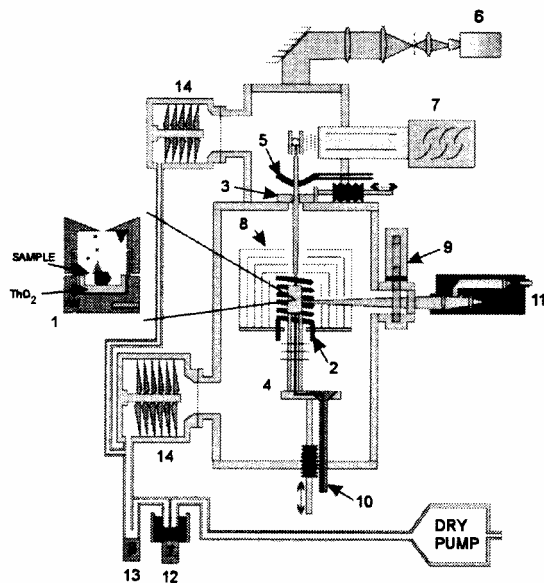
Fig. 2-1   The Knudsen-cell facility [Ron99]. (1) Knudsen-cell with black-body hole and ThO$_2$ coating inside; (2) tungsten heating coil; (3) chopper; (4) facilities to move the cell up and down; (5) liquid nitrogen cold trap to reduce background noise; (6) CCD camera to align the cell and the chopper holes; (7) quadrupole mass spectrometer; (8) thermal shields (tungsten/tantalum); (9) pyrometer windows revolver; (10) inlet gas capillary (to introduce purge gases into the cell); (11) linear pyrometer; (12) γ counter with cold trap; (13) β counter; (14) turbo-molecular pumps. The whole facility is inside a lead shielded glovebox.

Fig. 2-2   Some tungsten Knudsen cells, fabricated by PLANSEE (Reutter, Austria).

The mass spectrometric detection of $^9Be(g)$ and ^4He in the vapour effusing from the irradiated beryllium samples is straightforward, since no noise related to the presence of isobaric nuclides affects their measurement. For ^4He though, a small contribution of $^1H^3H$ to mass 4 signal was detected, the ratio $^3H/^4He$ in the samples being approximately 1.7%. On the other hand, particular care had to be taken in detecting ^3H and ^3He. Normal mass spectrometers are unable to resolve the small difference between their atomic weight (3.016049 uma ^3H, 3.016029 ^3He) in order to detect them separately. Furthermore, during blank tests, a non-negligible background noise in mass-3 channel was observed, increasing with temperature. This is caused by the presence of hydrogen formed from thermal or electron-induced decomposition of residual hydrocarbons, which in the ion source undergoes the reaction: H_2^+ + $H_2 \rightarrow H_3^+$ + H [Ses01]. Furthermore, on the basis of the natural abundance of deuterium in hydrogen (0.015%), 0.03% of hydrogen molecules consists of $^1H^2H$. A number of blank tests have been performed in order to study the background noise in mass-3 channel: with the cold trap on, a constant ratio of mass-3 to mass-1 signals is observed (of the order of 0.015). During tests with irradiated beryllium, the background noise in mass-3 channel can be calculated from the mass-1 signal and then subtracted.

Further issues in the measurement of tritium arise from its possible appearance in different forms: monatomic ^3H, di-tritium gas $^3H_2$ or protium[1]-tritium $^1H^3H$. Since the mean free path of atoms in ultra-high vacuum is much longer than the distance between the sample and the mass spectrometer, if tritium leaves the beryllium surface as a single atom, it is very likely detected as such (mass 3). Blank tests revealed that no background noise affected mass 6; for ionisation potentials above 30 eV the possible contribution of $^1H^3H$ to the mass-4 signal was considered to be negligible with respect to the much larger ^4He inventory in the samples.

In order to verify the appearance of molecular tritium at the beryllium surface and to measure it separately from ^3He, the difference in their first ionisation energy (13.6 eV for hydrogen and 24.6 eV for helium) was considered. Blank tests with increasing energy of the ionising electrons in the presence of a helium-hydrogen flow showed that the helium signal clearly appeared above 30 eV, whereas only hydrogen was visible at 25 eV. By comparing the gas release curves from irradiated beryllium at 25 and 30 eV ionising electron energy, it is possible to isolate the contribution of tritium and to understand in which form it is released. The method allows performing precise and reproducible measurements of tritium release even from weakly irradiated pebbles, which have a very small tritium inventory (some appm).

2.3.2 Pebbles from the BERYLLIUM irradiation

Fig. 2-3 shows a plot of helium and tritium release rates from weakly irradiated pebbles from the BERYLLIUM experiment, with a heating rate of about 10 K/min and ionising electron energy of 70 eV, in a logarithmic scale and in terms of the ion current of the mass spectrometer. The release rate is proportional to the product of the mass spectrometer current times

---

[1] Protium (^1H) is the most abundant isotope of hydrogen (99.985 % of natural hydrogen)
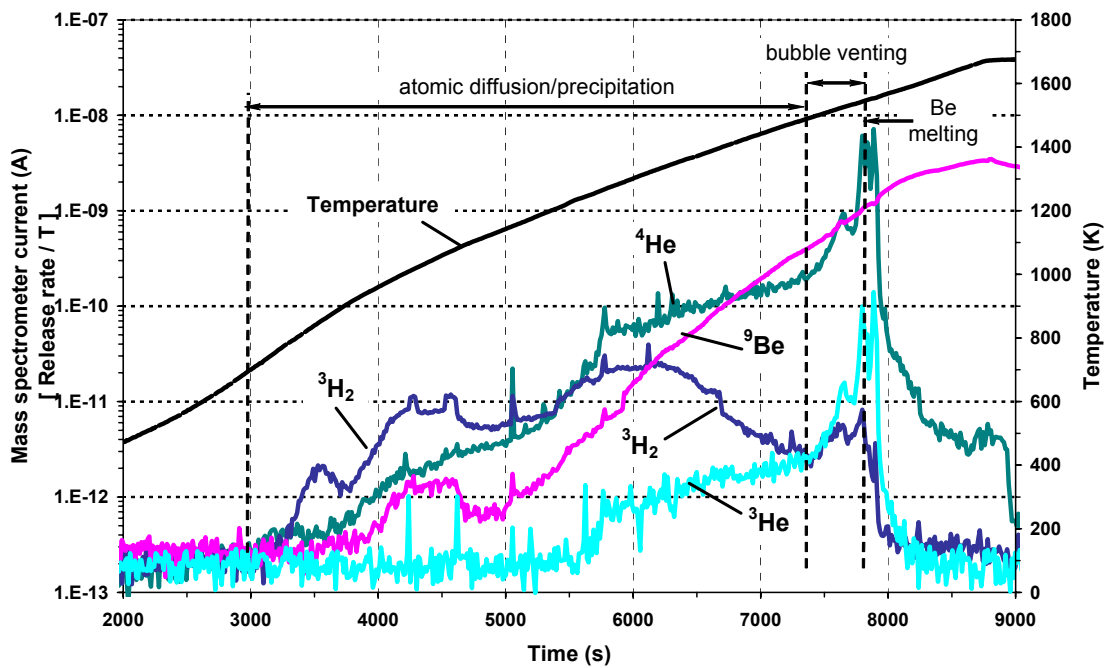
Fig. 2-3   Gas release in a vacuum from weakly irradiated pebbles from the BERYLLIUM experiment (2 mm diameter, 40-200 micron grains, 780 K irradiation temperature, 480 appm ^{4}He, 8 appm ^{3}H, 4 appm ^{3}He). Temperature ramp: about 10 K/min. Ionising electron energy: 70 eV. (Experiment 114bei) [Rab02a]
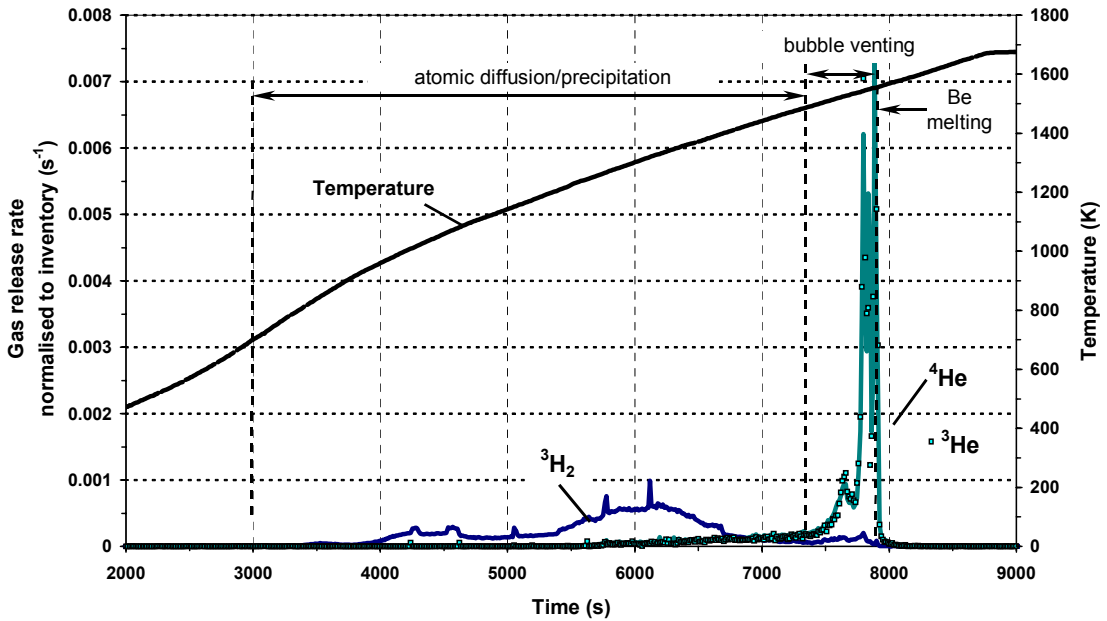
Fig. 2-4   The same experiment as in Fig. 2-3, but here gas release rate normalized to total gas inventory is shown, in a linear scale. The curves of ^{4}He and ^{3}He overlap.
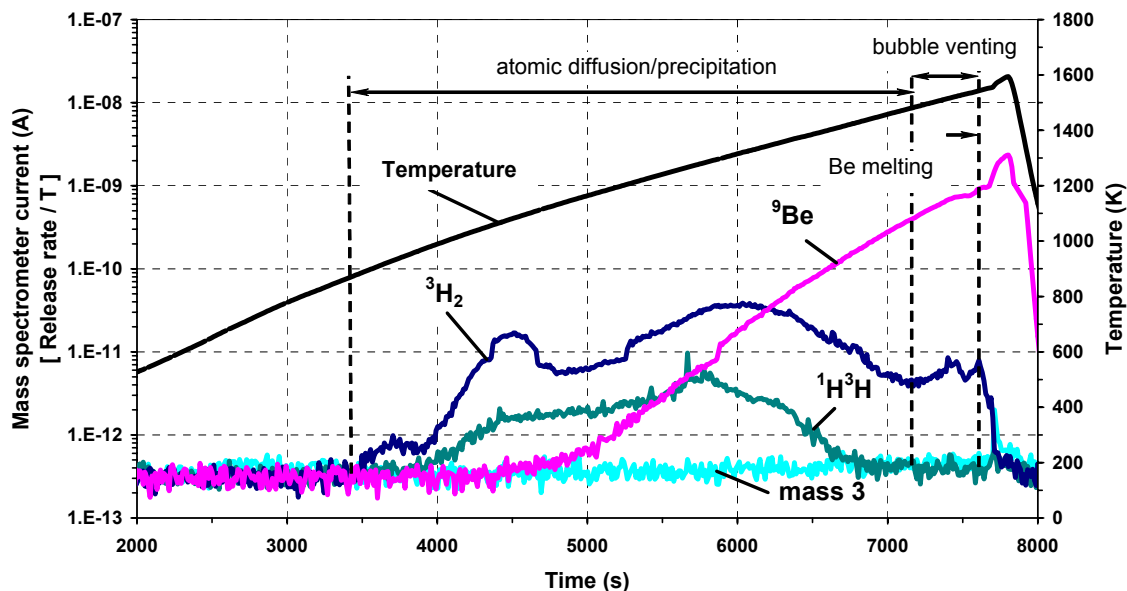
Fig. 2-5   Gas release in a vacuum from weakly irradiated pebbles from the BERYLLIUM experiment (2 mm diameter, 40-200 micron grains, 780 K irradiation temperature, 480 appm ^{4}He, 8 appm ^{3}H, 4 appm ^{3}He). Temperature ramp: about 10 K/min. Ionising electron energy: 25 eV. At 25 eV, helium is not detected.(Experiment 255bei) [Rab02a]
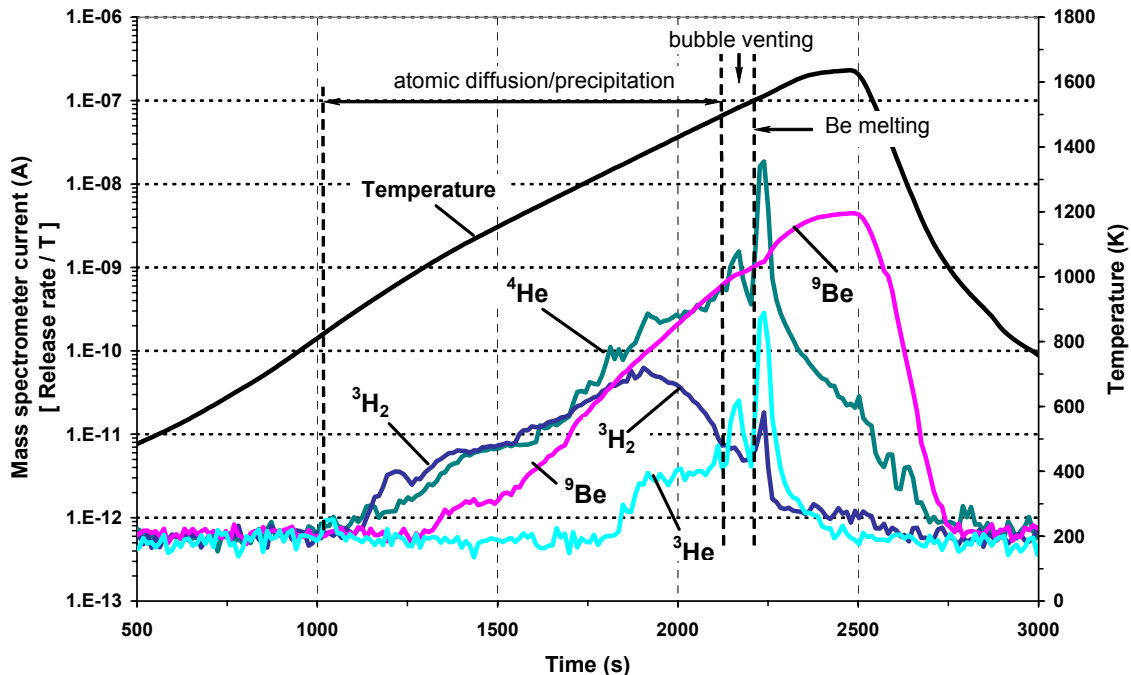

Fig. 2-6   Gas release in a vacuum from weakly irradiated pebbles from the BERYLLIUM experiment (2 mm diameter, 40-200 micron grains, 780 K irradiation temperature, 480 appm ^{4}He, 8 appm ^{3}H, 4 appm ^{3}He). Temperature ramp: about 30 K/min. Ionising electron energy: 70 eV. (Experiment 160bei) [Rab02a]

the temperature, therefore the ion current describes gas release rate unless a linear correction. The same experiment, in a linear scale, is shown in Fig. 2-4: here the release rate is normalised, for ^{4}He, ^{3}He and ^{3}H, to the respective inventory, i.e. to the integral of the curves in Fig. 2-3. A similar experiment, with ionising electron energy of 25 eV, is shown in Fig. 2-5: here hydrogen is detected (^{3}H$_2$ and ^{1}H^{3}H) but not helium. Fig. 2-6 shows the effect of a faster heating (about 30 K/min). Fig. 2-7 shows the integral release rate for ^{4}He and ^{3}H, normalised to the total inventory, as a function of temperature. The relationship between release stages and microscopic diffusion phenomena described in the following paragraphs has been deduced from the analysis of microstructure evolution of the samples during a 10 K/min heating transient, presented in paragraph 2.4.

2.3.2.1 Helium kinetics

With a temperature ramp of 10 K/min, ^{4}He release starts above 700 K. As temperature increases, three stages of ^{4}He release can be identified (Fig. 2-3): (1) atomic diffusion, in the range 700-1300 K; (2) precipitation into bubbles, in the range 1300-1500 K; (3) bubble venting, from 1500 K to the melting point $T_m = 1556$ K.

The release of helium in the range 800 - 1500 K is due to the diffusion of helium atoms, initially frozen in the lattice in a dynamic solution, to free grain boundaries. At the same time, a consistent part of the gas precipitates into bubbles: the helium trapped in bubbles cannot be released because the time constant for bubble migration to open surfaces is much larger than the duration of the experiment. In the first stage, up to 1300 K, precipitation is in progress but diffusion to free surfaces is dominant. Starting from 1300 K, most of the helium inventory, which was not released, has already precipitated and the helium in solution is practically exhausted: as a consequence, the release rate curve increases at a lower rate.

Above 1500 K a sharp release peak starts (Fig. 2-3, Fig. 2-4): in this third stage, approximately 75% of the total initial ^{4}He inventory is released via extensive bubble coalescence and venting, i.e. by a percolation phenomenon. Above $\approx$ 1100 K beryllium becomes brittle, so that pressurised pores can easily produce microcracks (above 1100 K the ultimate tensile strength is < 40 MPa [Pok96]). This release stage crosses first the phase transition of beryllium (1542 K [Kle01]) from the hexagonal closed packed (α phase) to the body centred cubic structure (β phase) and then the melting point (1556 K [Kle01]): during the first phase transition, which involves a large transformation enthalpy (6100 J mol^{-1}, compared to 7200 J mol^{-1} for melting), there is a full restructuring of the metallographic structure and this leads to a partial closure of the percolation channels and, consequently, to a temporary arrest of the gas release peak (Fig. 2-3, Fig. 2-4). A small part of the helium inventory is finally released during melting. Though in these experiments, due to the constant temperature increase, the gas release peak crosses a first order phase transition, it starts at lower temperatures (1500 K): therefore percolation occurs independently from phase transition. This conclusion is confirmed by the fact that a sharp helium release peak has been observed also by other authors after longer annealing times at constant temperature (1300 K [Sca01a], 1120 K [Sca95b]) well below the phase transitions.

As far as ^{3}He (from ^{3}H decay) is concerned, the comparison of the mass-3 release rate at ionising electron energy of 70 eV (Fig. 2-3) and 25 eV (Fig. 2-5) proves that mass-3 signal consists essentially of ^{3}He, which is present in a ratio of about 0.8 % of ^{4}He. This is confirmed by the fact that the curves of mass 3 and ^{4}He have a very similar shape and, if the release rate curve normalised to the total inventory are considered, the two curves overlap (Fig. 2-4). In particular, the similar precipitation and venting stages suggest that ^{4}He and ^{3}He were initially in the same state and that they behave exactly in the same way during the temperature transient.

2.3.2.2 Tritium kinetics

Comparison of the release rate of masses 3, 4 and 6 at 70 eV (Fig. 2-3) and at 25 eV (Fig. 2-5) proves that tritium is essentially released as di-tritium gas (^{3}H$_2$, mass 6). A small fraction of tritium combines with protium, giving a negligible contribution to mass 4. No atomic tritium has been detected. Since single tritium atoms are unlikely to combine after leaving the beryllium surface, it can be concluded that most of tritium is released already in a molecular form. As tritium is generated and diffuses in solid beryllium as a single atom, a recombination at the beryllium surface probably occurs. Effusion of tritium is also influenced by the presence of a thin oxide surface layer and of intragranular precipitates of BeO. At low temperature, tritium can be trapped as Be(OH)$_2$, a compound which decomposes above 600 K. This makes tritium release modes at low temperature somewhat different from those of helium, but, due to the very low tritium inventory in the samples, this range could not be examined in this study due to the detection limit. Starting from 800 K up to 1500 K, tritium release appears
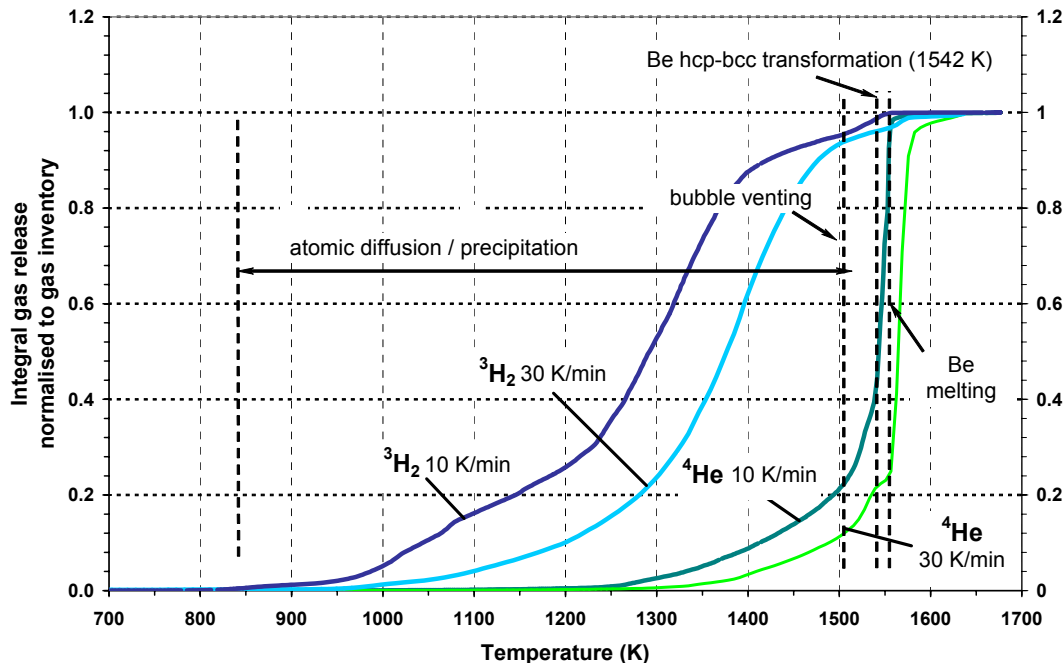

Fig. 2-7   Helium and tritium integral release, normalised to inventory, as a function of temperature, in the experiments in Fig. 2-3 and Fig. 2-6. [Rab02a]

to be essentially driven by atomic diffusion, with a decrease of the release rate starting from 1300 K due to progressive exhaustion (Fig. 2-3). During this phase, helium bubbles capture a small fraction ($\approx$ 6%) of tritium, which is finally released together with helium, as extensive bubble venting takes place at higher temperatures (such fraction can be assessed as the integral of the tritium release curve above 1500 K, Fig. 2-7). It can be concluded from these experiments that, if tritium is not trapped in helium bubbles before the beginning of the heating transient, it diffuses out much faster than helium.

2.3.2.3 Effect of a faster heating

With a faster heating (30 K/min, Fig. 2-6) the same release stages as at 10 K/min are observed, both for helium and for tritium, but the first diffusion stage starts at higher temperatures (850 K). This is because the same temperature is reached in a shorter time and the time constants for diffusion are the same. In this case (Fig. 2-6), though the percolation phase starts at the same temperature than with 10 K/min (1500 K), most of helium (78%, Fig. 2-7) is released during melting.

2.3.3 Pebbles from the EXOTIC 8 irradiation

In order to study the influence of material type on the gas release stages and to increase confidence in the extrapolation of the conclusions to the reference material for the HCPB blanket, the study of gas release from pebbles from the BERYLLIUM irradiation was repeated with pebbles from the EXOTIC 8 experiment. Though size and production method are very different (Tab. 2-1), both types of pebbles have coarse grains and low irradiation fluence in a similar temperature range.

Beryllium pebbles were irradiated in EXOTIC 8 together with lithium orthosilicate pebbles, enriched in ^{6}Li at 50%. Due to a ^{6}Li contamination, which probably occurred during the manipulation or storage of the samples, it was not possible to measure tritium release in this study, because the very small amount of tritium in the pebbles is released as di-tritium gas (mass 6) and measured by the mass spectrometer together with ^{6}Li.

By comparing Fig. 2-8, Fig. 2-9 and Fig. 2-10 to, respectively, Fig. 2-3, Fig. 2-6 and Fig. 2-7 it can be concluded that pebbles from the BERYLLIUM and from the EXOTIC 8 irradiations have a very similar behaviour in terms of helium diffusion and release kinetics. The same release stages appear in similar temperature ranges above 700 K. The very small helium peaks below 700 K in Fig. 2-8 are probably due to noise related to the furnace degassing which often occurs at such temperatures. Helium release starts at about 700 K with a temperature ramp of 10 K/min and only at 1000 K with 30 K /min. The burst release stage starts from about the same temperature (1510 K), independently from the heating rate and consists of two separate peaks, suggesting that the same restructuring of the material as in the pebbles from the BERYLLIUM irradiation occurs across the phase transition of beryllium. The fraction of helium inventory released in the various stages is also approximately the same (Fig. 2-10): only a small amount is released by migration of gas atoms to grain boundaries, most of helium precipitates and is released by bubble venting or after melting.
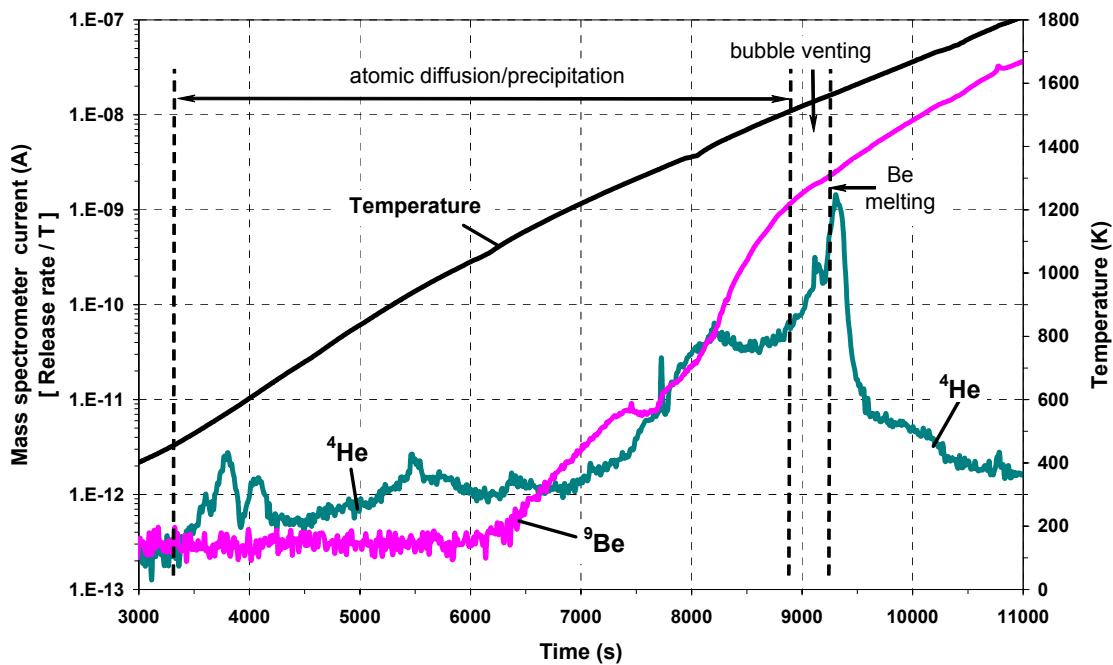
Fig. 2-8   Helium release in a vacuum from weakly irradiated pebbles from the EXOTIC 8 experiment (0.1 mm diameter, 40-200 micron grains, about 285 appm ^{4}He). Temperature ramp: about 10 K/min. (Experiment 235bei)
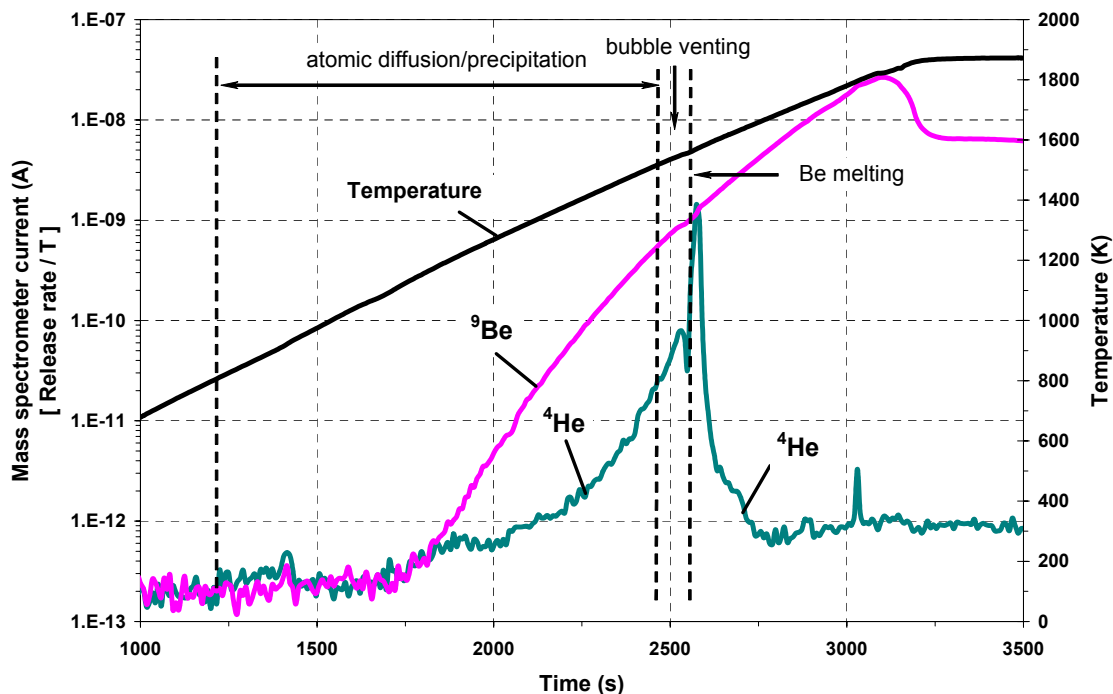

Fig. 2-9   Helium release in a vacuum from weakly irradiated pebbles from the EXOTIC 8 experiment (0.1 mm diameter, 40-200 micron grains, about 285 appm ^{4}He). Temperature ramp: about 30 K/min. (Experiment 237bei)
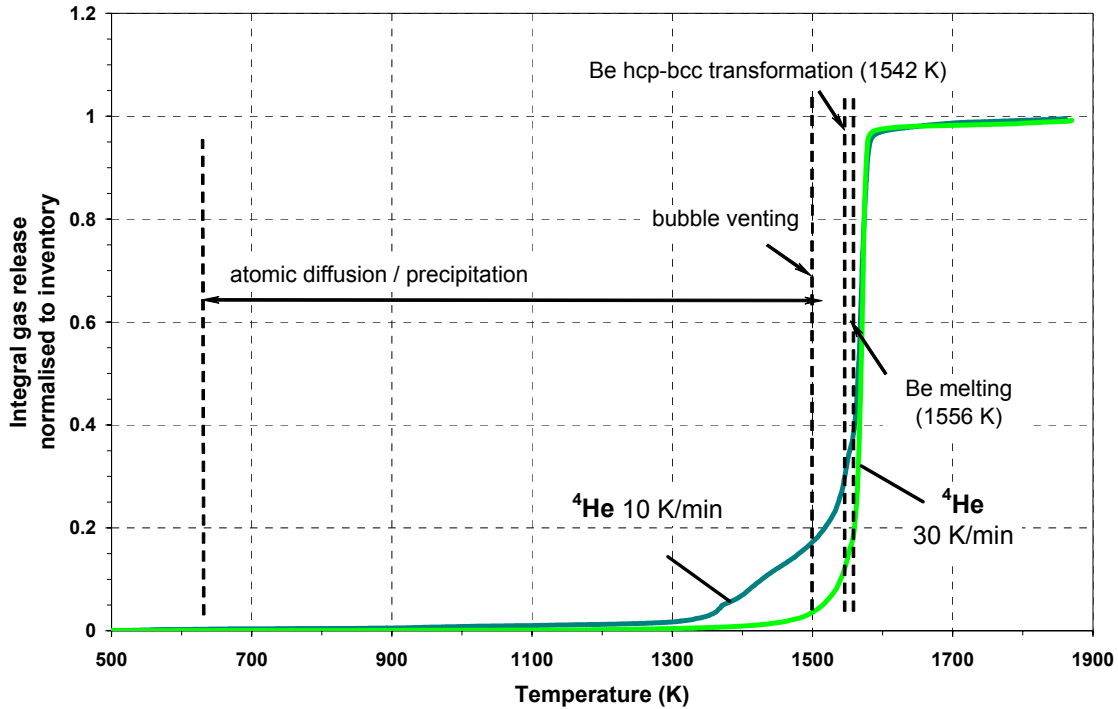
Fig. 2-10   Helium integral release, normalised to inventory, as a function of temperature, in the experiments in Fig. 2-8 and Fig. 2-9.

Apart from the different irradiation dose, the pebbles from EXOTIC 8 differ substantially from the ones from BERYLLIUM both in the production method and in the size (Inert Gas Atomisation (IGA) instead of Fluoride Reduction Process (FRP), 0.1 mm diameter instead of 2, Tab. 2-1). The only common feature of these two materials is the grain size, since also IGA pebbles, being a melting product, have coarse grains. The similar gas release kinetics suggests that *grain size is the material property which has the largest influence on gas diffusion, precipitation into intragranular bubbles, migration to grain boundaries and release.* As a consequence, it is reasonable to expect that also the reference pebbles, having a similar microstructure, will have a similar behaviour and that, in the absence of irradiated reference pebbles, a study of gas diffusion and precipitation performed on a different material is also representative, provided that the material are pebbles with coarse grains.
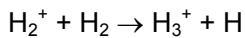
Nevertheless, an effect of pebble size is expected (Chapter 3, paragraph 3.8). Smaller pebbles have a larger fraction of grain surface which is directly exposed to the outside; as a consequence a larger fraction of gas atoms reaching grain boundaries can immediately be released before interlinked porosities are formed. As a consequence, with the same average grain size, smaller pebbles should release gases better than larger ones. Though experimental evidence of this phenomenon has been provided [Sca97c], no influence of pebble size was detected in this study (Fig. 2-7, Fig. 2-10). This is attributable to differences in the irradiation dose, in the average grain size and in the quantities examined of the two kinds of

pebbles, as well as to the very low gas inventories measured, which limit the possibility to make quantitative comparisons of gas release.
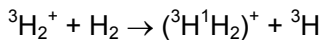
2.3.4 Fragments from BR2 moderator

In order to investigate gas release mechanisms at very high dose and gas content, representative of the HCPB blanket module End-Of-Life (EOL) conditions, fragments from the disposed moderator of BR2 were examined (Tab. 2-1), under the same conditions as for weakly irradiated pebbles. This material has a ^{4}He content of the order of the production at EOL in the blanket, but the ^{4}He inventory has been generated during a much longer irradiation time and at much lower temperature, as well as with a different neutron spectrum. A consequence of the soft neutron spectrum and the long irradiation time is a much higher ^{3}H production and much more radiation damage than it would have occurred in a fusion reactor for the same ^{4}He generation. During the long out-of-pile storage between the End-Of-Irradiation (EOI) and this study (7 years), a consistent fraction of ^{3}H inventory (33 %) decayed into ^{3}He.

Similarly to pebbles, in fragments from BR2 moderator tritium is released during the thermal ramp as molecular di-tritium gas. Nevertheless, the signal of mass 5 of the mass spectrometer, which is in the experiments with weakly irradiated pebbles at the level of the background noise, becomes important and assumes the same shape as the signal of mass 6. This has been explained as a consequence of the same reaction responsible for the noise in mass-3 signal mentioned in paragraph 2.3.1, which occurs in the ion source of the mass spectrometer [Ses01]:

$$H_2^+ + H_2 \rightarrow H_3^+ + H$$

This reaction can involve a molecule of di-tritium gas and produce an ion of mass 5:

$$^3H_2^+ + H_2 \rightarrow (^3H^1H_2)^+ + ^3H$$

Probably this phenomenon occurs also in the experiments with weakly irradiated pebbles, but no ion $(^3H^1H_2)^+$ is detected due to the very low amount of tritium in the samples.

Fig. 2-11 shows, in a logarithmic scale, helium and tritium release rates with a heating rate of 10 K/min and an ionising electron energy of 40 eV. The same experiment, in a linear scale, is shown in Fig. 2-12. Fig. 2-13 shows the signals of mass 1, 5 and 6 during the same experiment, corresponding to ^1H, $(^3H^1H_2)^+$ and $^3H_2$. Fig. 2-14 shows the effect of a faster heating (30 K/min). Fig. 2-15 shows the integral release rate for ^{4}He and ^{3}H, normalised to the total inventory, as a function of temperature.

2.3.4.1 Helium kinetics

Helium release kinetics in fragments from BR2 moderator (Fig. 2-11, Fig. 2-12) appears to be substantially different from weakly irradiated pebbles (Fig. 2-3, Fig. 2-4). With a heating
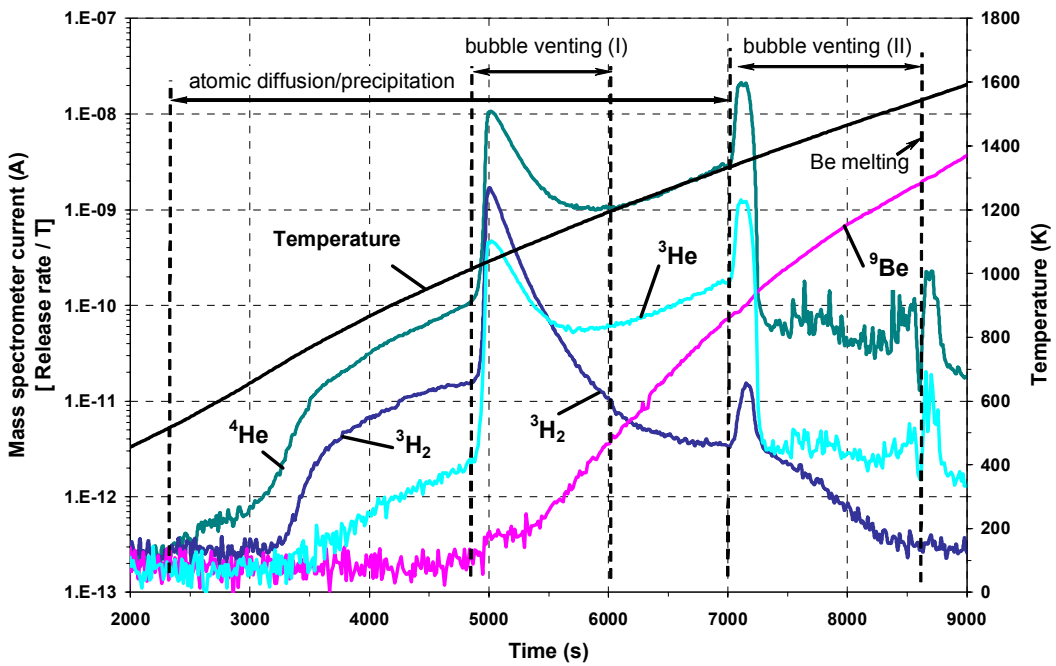
Fig. 2-11   Gas release in a vacuum from highly irradiated fragments from BR2 moderator (20 micron grains, 420 K irradiation temperature, 19200 appm ^{4}He, 1522 appm ^{3}H, 731 appm ^{3}He). Temperature ramp: about 10 K/min. Ionising electron energy: 40 eV. (Experiment 232bei)
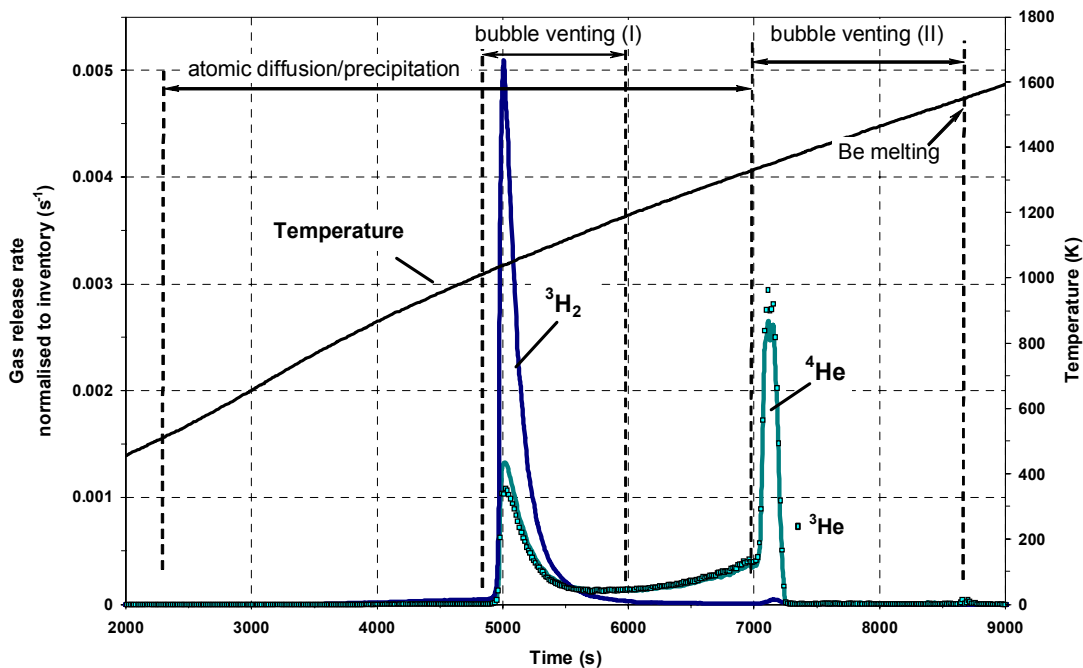
Fig. 2-12   The same experiment as in Fig. 2-11, but here gas release rate is normalized to total gas inventory and represented in a linear scale. The curves of ^{4}He and ^{3}He overlap almost completely.
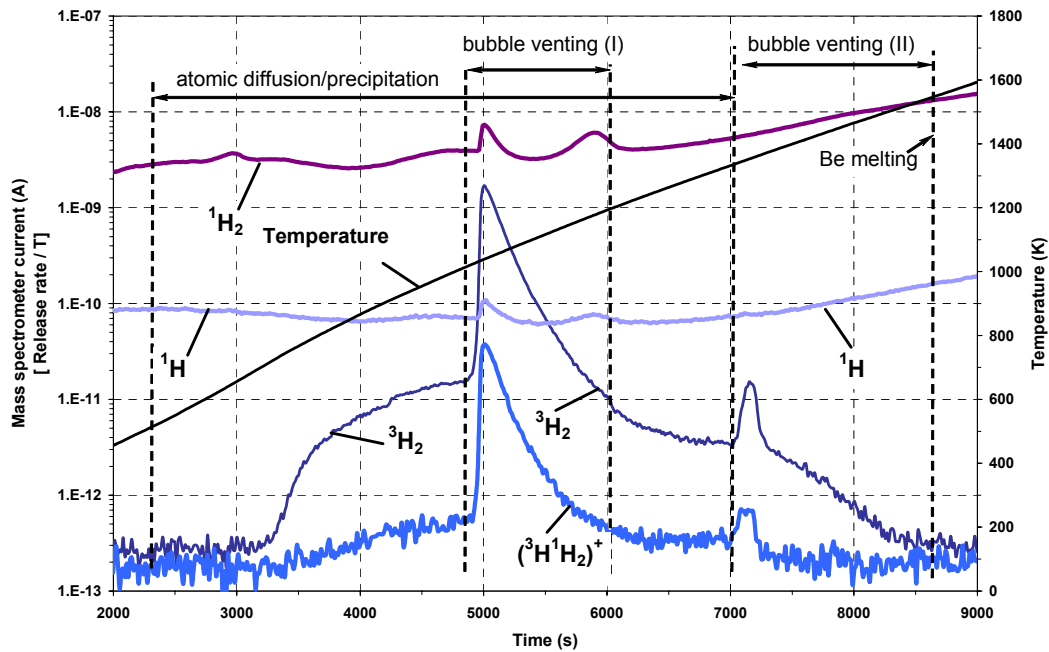
Fig. 2-14   Hydrogen release rate in the same experiment as in Fig. 2-11. Masses 1 and 2 are related to the presence of hydrocarbons, masses 5 and 6 to tritium contained in the irradiated beryllium sample.
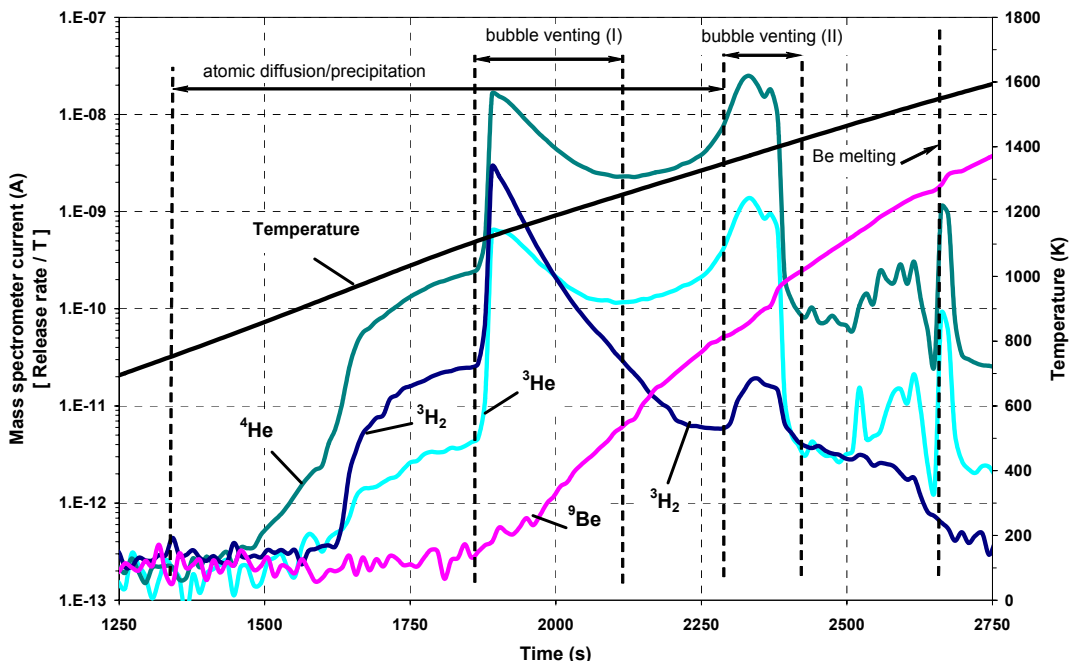

Fig. 2-13   Gas release in a vacuum from highly irradiated fragments from BR2 moderator (20 micron grains, 420 K irradiation temperature, 19200 appm ^{4}He, 1522 appm ^{3}H, 731 appm ^{3}He). Temperature ramp: about 30 K/min. Ionising electron energy 40 eV. (Experiment 234bei)
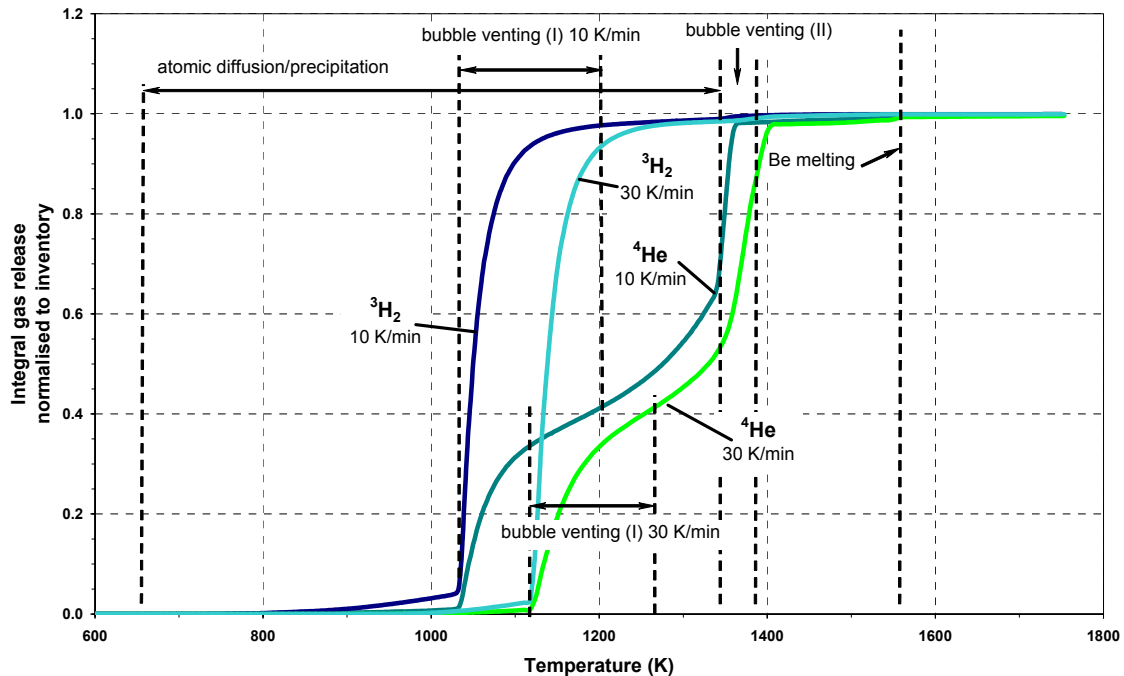
Fig. 2-15   Helium and tritium integral gas release, normalised to inventory, as a function of temperature, in the experiments in Fig. 2-4 and Fig. 2-6.

rate of 10 K/min, ^{4}He release starts already at 500 K and goes through 4 stages: (1) atomic diffusion, in the range 500-1000 K; (2) bubble venting, in the range 1000-1200 K; (3) a second diffusion stage, in the range 1200-1330 K; (4) a second bubble venting stage from 1330 to 1400 K, in which practically the whole residual inventory is released, well below the melting point T_m = 1556 K. Nevertheless, the apparently different release modes in respect of the weakly irradiated beryllium pebbles can be explained as the result only of a different combination of the same microscopic phenomena in different temperature ranges.

A preliminary Scanning Electron Microscopy (SEM) examination of the surface of the fragments [Rab03b] shows that, in spite of the very high gas content in the material, no bubbles in the range of microns are present at grain boundaries. On the basis of Transmission Electron Microscopy (TEM) studies of similar materials in the literature, where at End-Of-Irradiation no bubbles were observed [Cha02], and considering the very low irradiation temperature which prevents gas atoms from diffusing, it is expected that a large fraction of gas inventory is still frozen in a dynamic solution in the lattice or trapped in the vicinity of dislocations. As temperature increases, gas atoms migrate to grain boundaries or precipitate into intragranular bubbles. The ^{4}He release measured starting from 500 K is related to gas atom migration to external grain surfaces: this is a similar diffusion stage as observed in the weakly irradiated pebbles, but it starts earlier, due to the much smaller grain size, which implies a higher probability that gas atoms reach grain boundaries instead of precipitating inside the grain. Above 1010 K, a burst release is observed, which slowly exhausts at 1200 K: this phenomenon is probably due to the sudden formation of interlinked porosities at grain boundaries. It is reasonable to assume that, even though no large bubbles were present at

28

the beginning of the transient, a big amount of gas had in any case already collected at grain boundaries, in a supersaturated solution or trapped by dislocations, giving rise to a sudden formation of grain boundary bubbles during the first phase of the transient. After the end of the first gas release peak, the diffusion stage continues as an ideal follow-up of the curve in the range 500 K-1000 K. Finally, at 1330 K, a second peak appears, much less intense than the first one: during this phase, practically all the remaining ^{4}He inventory is released. The high temperature peak is due to the venting of intragranular bubbles which have formed and grown inside the grains during the temperature transient, therefore it is in some extent similar to the peak ending the gas diffusion phase in weakly irradiated pebbles (Fig. 2-3, Fig. 2-8). Nevertheless, it occurs at much lower temperature probably because of the smaller grain size, which makes intragranular cracking easier. An important conclusion of the study of highly irradiated beryllium is that a high dose, as expected, is beneficial for gas release, since, e.g. at 1200 K already 90% of ^{3}H has been released (Fig. 2-15), as compared to only 10-30% in weakly irradiated pebbles (Fig. 2-7). In order to extrapolate this conclusion to pebbles, it has to be considered that they have much larger grains, therefore the fraction of gas atoms which reach grain boundaries during irradiation will be smaller, as a consequence a consistent release fraction will be shifted from the peak at low temperature to the one at high temperature, making the release curve for highly irradiated pebbles more similar to the one in Fig. 2-3. But pebbles will be irradiated in the blanket at much higher temperature, which enhances grain boundary bubble formation even at lower dose.

As far as ^{3}He from ^{3}H decay is concerned, it has exactly the same release kinetics as ^{4}He (the normalised release rate curves overlap almost completely in Fig. 2-12), like in weakly irradiated pebbles (Fig- 2-4). This confirms that all ^{3}He microscopic diffusion stages (atomic diffusion, precipitation into intragranular bubbles or migration to grain boundaries) are the same as for ^{4}He and that the spatial distribution of the 2 isotopes during the transient remains the same, independently of the global amount present, of the irradiation dose, of the decay time and of the material type.

2.3.4.2 Tritium kinetics

The stages of tritium release are the same as for helium (Fig. 2-11, Fig. 2-13): two peaks, which correspond to bubble venting, add themselves to a regular curve which represents migration of atoms to external grain surfaces. This confirms that also at high dose and helium content, tritium and helium diffuse and precipitate together. The first burst release stage is attributable to tritium already at grain boundaries at EOI, which suddenly form intergranular bubbles and interlinked porosities, together with helium, as soon as the temperature increases. The second peak is related to the venting of intragranular bubbles formed during the temperature transient and corresponds to the only tritium peak of weakly irradiated pebbles, due probably to the same phenomenon.

Nevertheless, there are some important differences which can be attributed, like in the weakly irradiated pebbles, to a faster atomic diffusion of tritium to grain boundaries. Fig. 2-12 shows that most of tritium inventory is released during the first peak at low temperature, whilst the second peak gives only a negligible contribution, comparable to the contribution of

the only tritium release peak in weakly irradiated pebbles (Fig. 2-4): as a matter of fact, after the end of the first peak, the curve of diffusional release of tritium decreases instead of increasing like the curve of helium, showing that the amount of tritium remaining in a dynamic solution in the lattice is exhausted. This means that during the early phase of the temperature transient, a much larger fraction of tritium migrates to grain boundaries with respect to helium.

The same phenomenon is responsible for a different weight of the burst release stage in the two kinds of materials for tritium. In both weakly irradiated pebbles and highly irradiated fragments, the percentage of helium inventory released via bubble venting is by far dominating. But, as far as tritium is concerned, diffusion is dominating for the weakly irradiated pebbles, because at the beginning of the transient no helium bubbles are present and tritium, if it is not trapped, migrates to grain boundaries much faster than helium. If bubbles are already present, or a large amount of gas has already collected at grain boundaries without forming bubbles, then tritium is released only when helium bubbles are vented and the fraction of tritium released by percolation is also dominating, like in the highly irradiated fragments.

A fundamental conclusion can be drawn: even though helium and tritium precipitate together in bubbles inside the grain and at grain boundaries, tritium reaches grain boundaries more easily than helium; therefore the fraction of tritium to helium trapped in intragranular bubbles is smaller than in grain boundary bubbles. Intragranular bubble are poorer in tritium than grain boundary ones. The trapping mechanism of precipitation into bubbles is the same for the two gases, but in respect of release it acts more favourably for tritium because bubbles at grain boundaries are more easily vented than intragranular ones. This implies finally that, as interlinked porosities are formed at grain boundaries, a larger fraction of tritium inventory than of helium inventory will be released. This conclusion is general, because the same effect has been observed in this study in two different materials at very different irradiation conditions and microstructure and it can be extended to pebbles in the blanket; furthermore, it is confirmed by the theory of tritium precipitation on the basis of an inverse analysis of tritium release curves presented in paragraph 2.5 (paragraph 2.5.4 in particular).

2.3.4.3 Effect of a faster heating

If the heating rate is faster (30 K/min, Fig. 2-14 and Fig. 2-15) the same release stages as at 10 K/min are observed, both for helium and for tritium, but the first diffusion stage starts at much higher temperatures (830 K). This is because the same temperature is reached in a shorter time and the time constants for diffusion are the same, like in the weakly irradiated pebbles. Also the first gas release peak is shifted to higher temperatures (1100 K instead of 1020 K), whilst the second one seems to be practically unaffected (1350 K instead of 1340 K): this happens also in the weakly irradiated pebbles and is a confirmation of the fact that the second peak in the highly irradiated material and the only peak in weakly irradiated pebbles are due to the same phenomena.

2.4 Characterisation of the microstructure of weakly irradiated pebbles from the BERYLLIUM irradiation

2.4.1 The microscopy techniques

A detailed characterisation of the evolution of the microstructure of pebbles from the BERYL-LIUM irradiation during a Knudsen cell experiment at 10 K/min heating rate (like the one in Fig. 2-3) has been performed, in order to relate gas release to microscopic diffusion phenomena and to confirm the explanations of different gas release stages in paragraph 2.3.2. Different microscopy techniques have been applied, depending on the size and type of features which had to be studied.

Optical microscopy is suitable to investigate bubbles in the range of some microns, which are present inside the grain and at grain boundaries at the end of the precipitation stage, when a growth and coalescence process is already in an advanced stage. Optical metallography is based on the use of visible light and requires the preparation of a polished surface. It is a destructive analysis and enables the examination of one random cross section of the sample, therefore it is typically two-dimensional. In analysing bubble parameters (size and concentration), it has to be taken into account that an optical microscopy micrograph shows a cut of 3D bubble population along a surface [Luc84], which is fully representative of the actual 3D population only for a homogeneous and isotropic distribution of bubbles and pores.

In order to investigate irradiation damage and the very early stage of gas precipitation, when bubbles have a diameter of the order of some nanometres, a Transmission Electron Microscopy (TEM) examination is necessary [Hir65] [Wil96]. An extremely thin film has to be prepared starting from the original sample, where areas of a thickness of the order of some hundred nm, transparent to electrons, should be present. A preparation method has been developed for obtaining a TEM film starting from pebbles. As a first stage, the pebble is reduced to a disk with perfectly parallel surfaces and about 0.1 mm thickness (Fig. 2-16a). As a second step, the centre of the disk is electrolitically thinned until it reaches the desired thickness. A TEM examination is also destructive, but instead of a cross section a TEM micrograph is a projection of a 3D volume where, typically, bubbles at different depths are seen in transparency as if they overlapped (Fig. 2-21, Fig. 2-23b).

Scanning Transmission Microscopy (SEM) is suitable for surface examinations. It has been used in order to investigate modifications of the surface of the pebbles during the temperature transient.

Interlinked porosities resulting from the growth and coalescence of lenticular grain boundary bubbles have typically a complex 3D structure and are S-shaped, therefore from a 2D cross section obtained by optical microscopy it is impossible to identify the morphology and topology of such features across the pebble. An X-ray absorption computer aided microtomography (CMT) has been therefore performed. Since beryllium is generally transparent to X-rays, except in a very narrow energy band, a monochromatic and at the same time very intense and parallel X-ray beam is necessary. This requirement is fulfilled only by a synchrotron light

source. The experimental technique for the CMT of weakly irradiated beryllium pebbles has been developed at the European Synchrotron Radiation Facility in Grenoble [Rab03], on the basis of previous studies of non irradiated pebble beds [Sca01b].

Fig. 2-16b shows the experimental setting for a CMT scan: the sample, an irradiated pebble embedded in Plexiglas inside a Plexiglas cylinder, is mounted on a rotating/translating positioning support between the X-ray source and the optics. The 2D detector system consists of magnifying lenses and a CCD camera with a 2048 x 2048 pixel chip. The magnification can be changed to adapt the spatial resolution and the field of view of the detector to the sample under investigation. The vertical rotation axis of the sample is aligned with the central axis of the detector with a precision between 0.1 and 0.5 pixels. The X-ray scan of the sample consists in the acquisition of 900 2D images by the CCD camera, along a global rotation angle of 180°. The energy of the monochromatic beam has been set in the range 7 – 11 keV. By changing optics and binning, the resolution can be varied in the range 0.35 to 4.9 microns, depending on the size and the extension of the features which have to be identified in the sample. In order to make a 3D reconstruction and rendering of the pebble volume and of the features inside, a phase segmentation on the basis of grey tones in the 2D cross sections has to be performed, i.e. the different phases (beryllium matrix, Plexiglas, pores and impurity phases in beryllium) have to be univocally identified on the basis of grey tones in the 2D cross sections, in order to be able to visualize them separately. Grey tone contrast can be negatively affected by the appearance of bias effects due the experimental


2 mm	20 mm
(a)	(b)
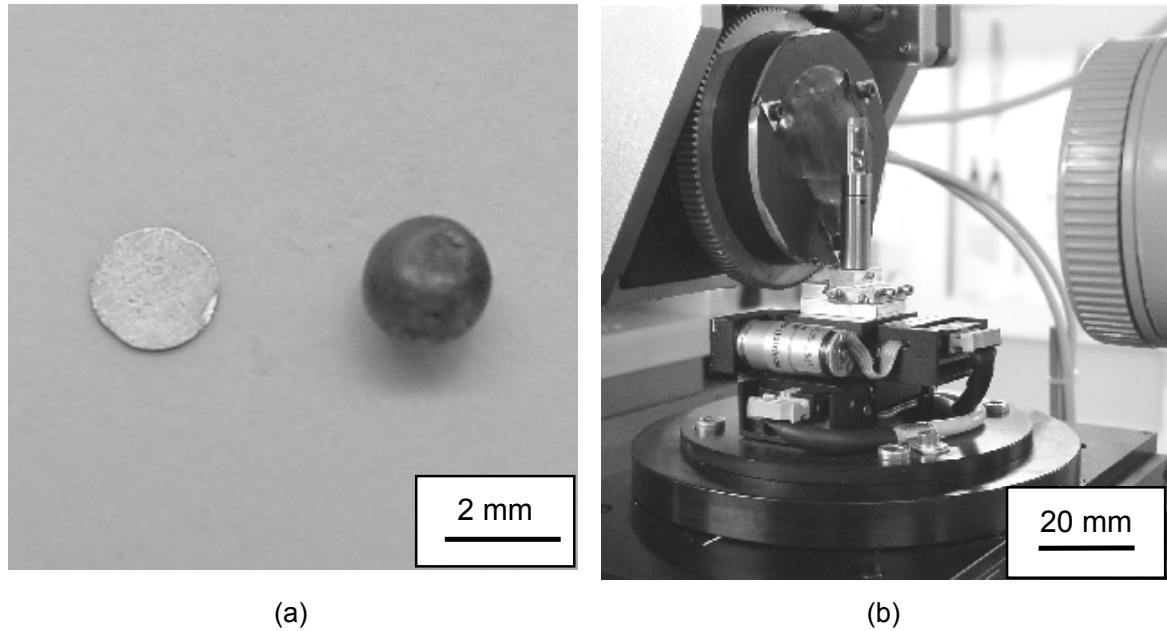
Fig. 2-16   Techniques for the characterisation of the microstructure of beryllium pebbles. (a) As a first stage of the TEM preparation technique, pebbles are reduced to a thin disk. (b) The microtomography technique. A pebble from the BERYLLIUM irradiation, inside a sample holder, is positioned on a rotating-translating support between the synchrotron light source (right) and the optics of the CCD camera (left). [Rab03]

negatively affected by the appearance of bias effects due the experimental settings (Plexiglas embedding of the sample, resolution, field of view, position of the sample with respect to the X-ray source), which, as a consequence, have to be carefully optimised.

2.4.2 Before irradiation

The pebbles irradiated in the BERYLLIUM experiment were produced by BrushWellmann as an intermediate stage in the fabrication of beryllium by Fluoride Reduction Process (FRP). The pebbles collect on the bottom of a bath where beryllium fluoride is reduced by magnesium fluoride. As compared to the reference material, they have much lower quality, but some important similarities in the microstructure. Fig. 2-17 shows the surface and a cut of these pebbles, before irradiation. The shape is spherical but more irregular and the surface rougher than in the reference pebbles produced by Rotating Electrode Process (Fig. 1-4, Fig. 1-5), which are a melting product. Sometimes, large internal porosities appear, both open and closed (Fig. 2-17b, Fig. 2-18a): these are a residue of the fabrication process. Grains are very large and columnar, with an impurity phase segregated at grain boundaries (Fig. 2-18a). Inside the grains no dislocations are present (Fig. 2-18b), as it has to be expected in the reference pebbles for the Helium Cooled Pebble Bed blanket (Fig. 1-5). A very fine dispersion of incoherent impurities appear (about 10^{20} m^{-3}), probably magnesium precipitates.

2.4.3 End of irradiation

At End-Of-Irradiation (EOI), in spite of a relatively high in-pile temperature and a low dose (Tab. 2-1), a very high density of dislocation loops appear inside the grains, about $3 \cdot 10^{20}$ m^{-3} (compare Fig. 2.18b with Fig. 2.19a). No gas bubbles have been observed, therefore gas atoms are still in a non-equilibrium solution in the lattice or they are trapped at sites with minimized electron density in the vicinity of dislocations and incoherent impurities. The presence of gas atoms nearby dislocations explains why dislocation healing is hindered: dislocations are "pinned" by gas atoms and their movement and annihilation is prevented.

2.4.4 The gas precipitation stage

As temperature increases, gas atoms are free to diffuse and precipitate. At 1000 K the early precipitation stage is detected: a population of very small bubbles (from 1 to 12 nm size) appear inside the grains. Intragranular bubbles nucleate on dislocations [Tur71] (Fig. 2-20), which is a further confirmation of the assumption that at EOI gas atoms were trapped nearby dislocations. A strong interaction between radiation damage and intragranular gas kinetics has to be assumed. Intragranular bubbles are ellipsoids with 2 equal semi axes end the same direction of elongation: this is probably related to the fact that beryllium has a hexagonal cell; therefore in one direction lattice resistance to deformation is lower. Similar intragranular bubbles have been previously observed at EOI in the pebbles irradiated in the CO-BRA-1A experiment [Gel97]. Larger bubbles at grain boundaries are also observed (Fig. 2-21b).

No modifications on the surface with respect to the non-irradiated state are detected.

(a)

(b)
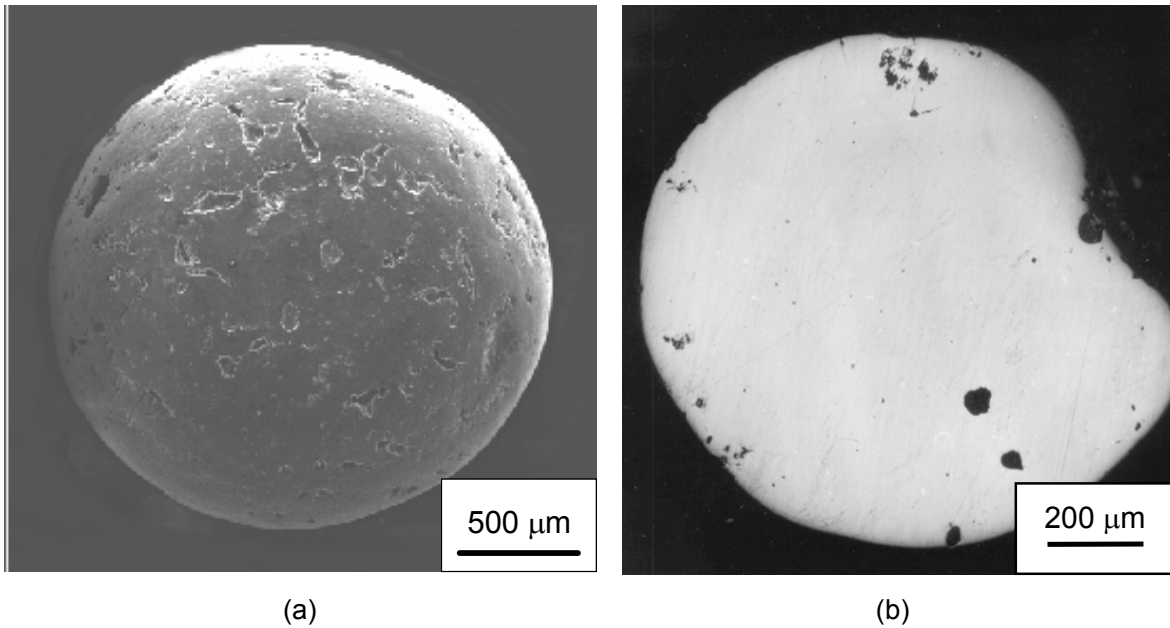
Fig. 2-17   *BERYLLIUM experiment, before irradiation*. Pebble microstructure. (a) Surface (SEM) (b) Cross section (OM).
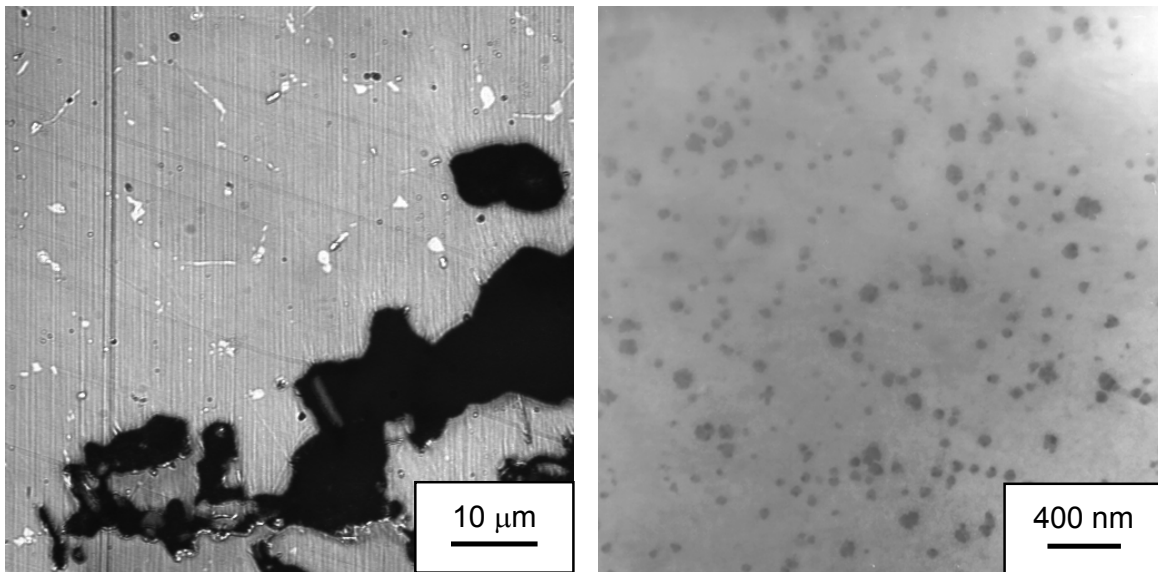

Fig. 2-18   *BERYLLIUM experiment, before irradiation*. (a) Mg impurities segregated at grain boundaries (white) and large porosities (black). (b) Intragranular microstructure (TEM). No dislocations, but a very fine dispersion of incoherent impurities (black dots) are visible.

(a)   (b)
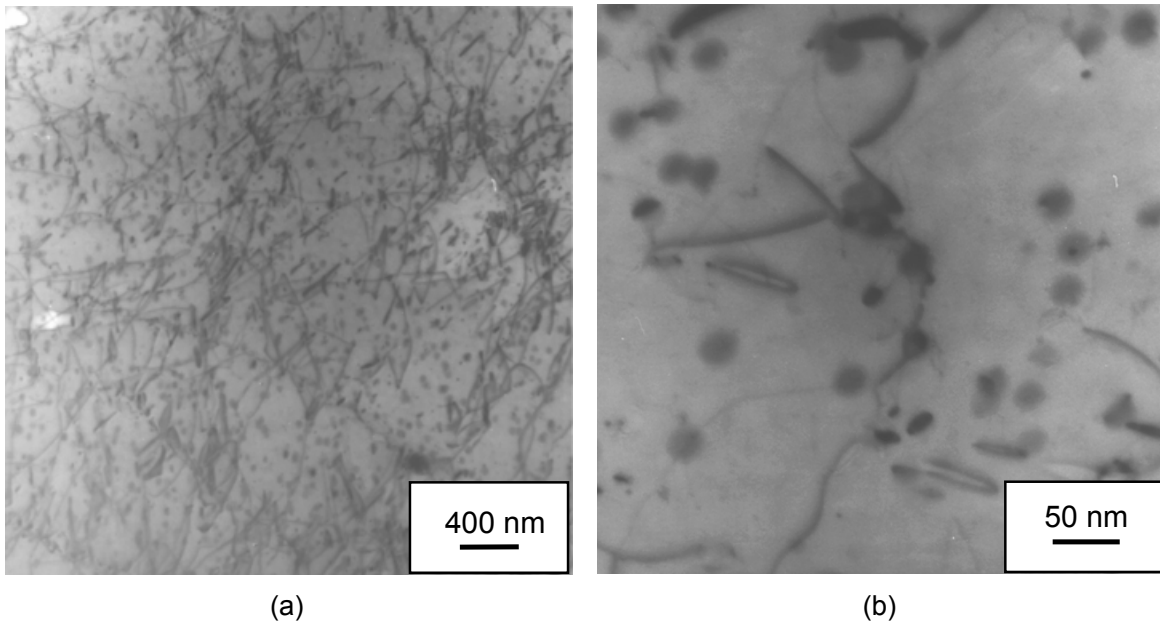
Fig. 2-19   *BERYLLIUM experiment, end of irradiation*. Irradiation-induced dislocations inside the grains (TEM). No gas bubbles are present. Gas atoms are still dissolved in the lattice or trapped in the vicinity of dislocations and incoherent impurities.


(a)   (b)
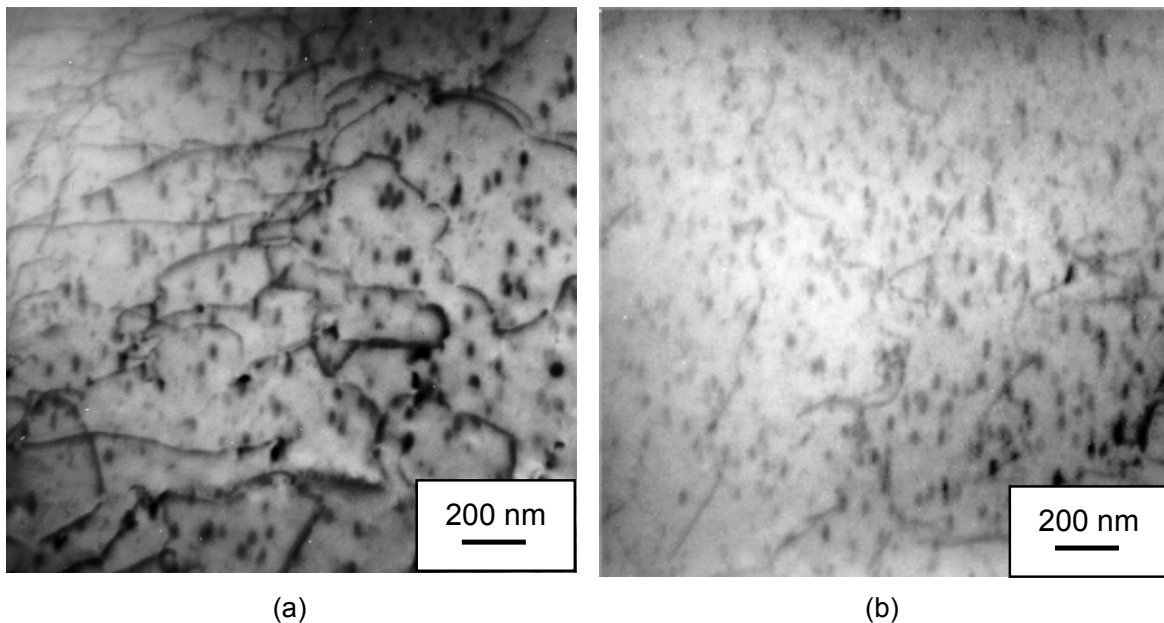
Fig. 2-20   *BERYLLIUM irradiation, the gas precipitation stage*. After irradiation and out-of-pile heating at 10 K/min to 1000 K (TEM). Gas atoms precipitate into small intra-granular bubbles.

(a)   (b)
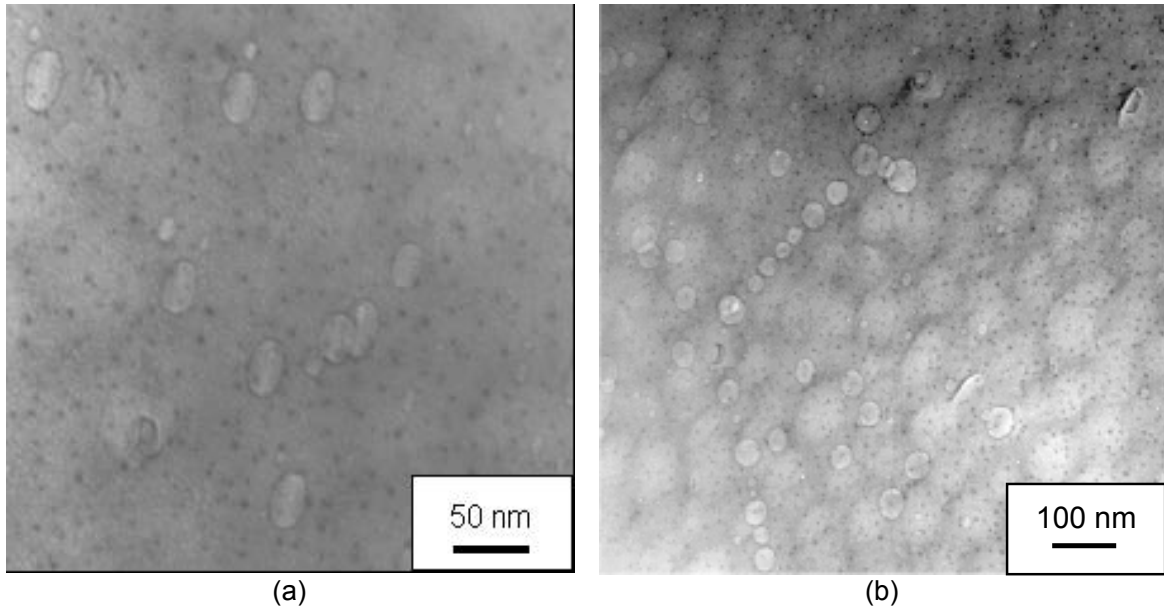
Fig. 2-21   *BERYLLIUM irradiation, the gas precipitation stage*. After irradiation and out-of-
pile heating to 1000 K (TEM). (a) Small elliptic intragranular bubbles (statistical
analysis of bubble radii in Fig. 2-30) [Rab03c]. (b) 3D projection of a grain bound-
ary bubble chain.

2.4.5 Bubble growth and coalescence

At 1340 K a large fraction of the gas inventory has precipitated. In spite of the low gas con-
tent (about 480 appm ^{4}He), very large bubbles are visible (Fig. 2-23): a dramatic process of
bubble growth has occurred, due to the deterioration of the mechanical properties of beryl-
lium at this temperature [Pok96]. Intragranular bubbles have become spherical and their size
lies in the range of some microns. They are aligned along straight lines, which gives confir-
mation to the assumption that they have nucleated on dislocations and that dislocations af-
fect also bubble kinetics. A process of formation of sub-grains is in progress. At grain
boundaries bubbles are much larger and lenticular: the formation of S-shaped interlinked
porosity, similar to those observed in UO_2 [Fis02], is in progress.

A SEM examination of the surface (Fig. 2.22a) shows the appearance of cracks along pref-
erential directions, corresponding to bundles of grains.

2.4.6 The gas percolation stage

At 1500 K bubble venting begins. The appearance of a gas release peak suggests that inter-
linked porosities at grain boundaries are reaching at this temperature the outer surface of the
pebble. The 3D development of percolation paths in pebbles from the BERYLLIUM irradia-
tion, after out-of-pile heating to 1500 K, has been examined by microtomography [Rab03].
Figure 2-24 shows two sections of the same pebble, perpendicular to one another and to two

(a) (b)
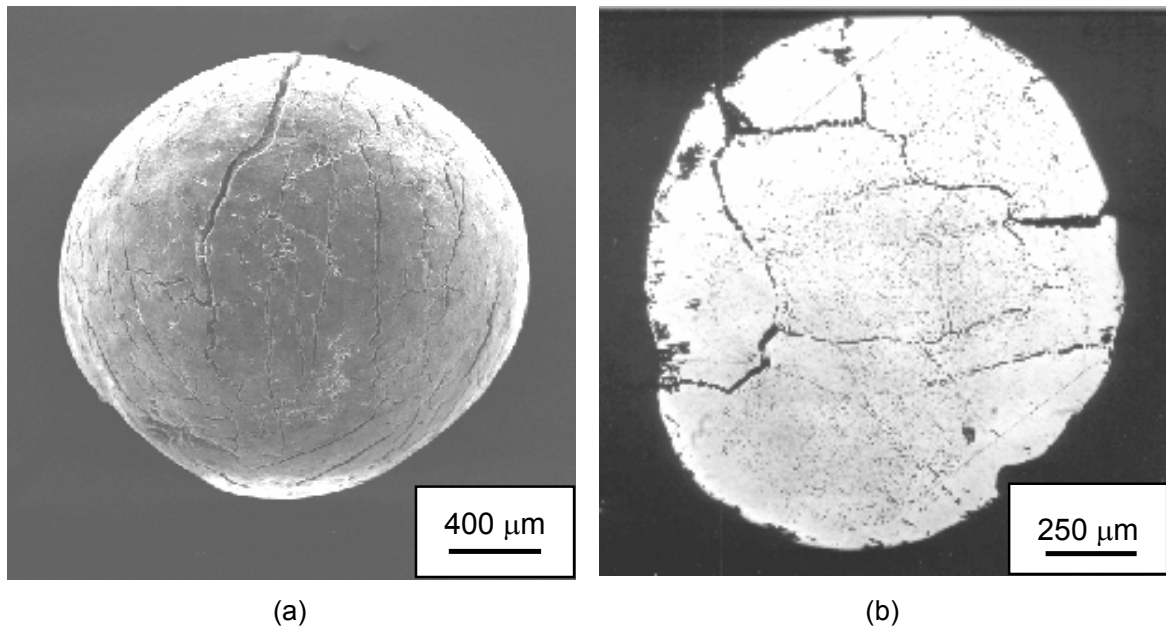
Fig. 2-22 *BERYLLIUM irradiation, bubble growth and coalescence*. After out-of-pile heating at 10 K/min to 1340 K. (a) Microcracks appear on the surface (SEM) (b) Cross section (OM).


(a) (b)
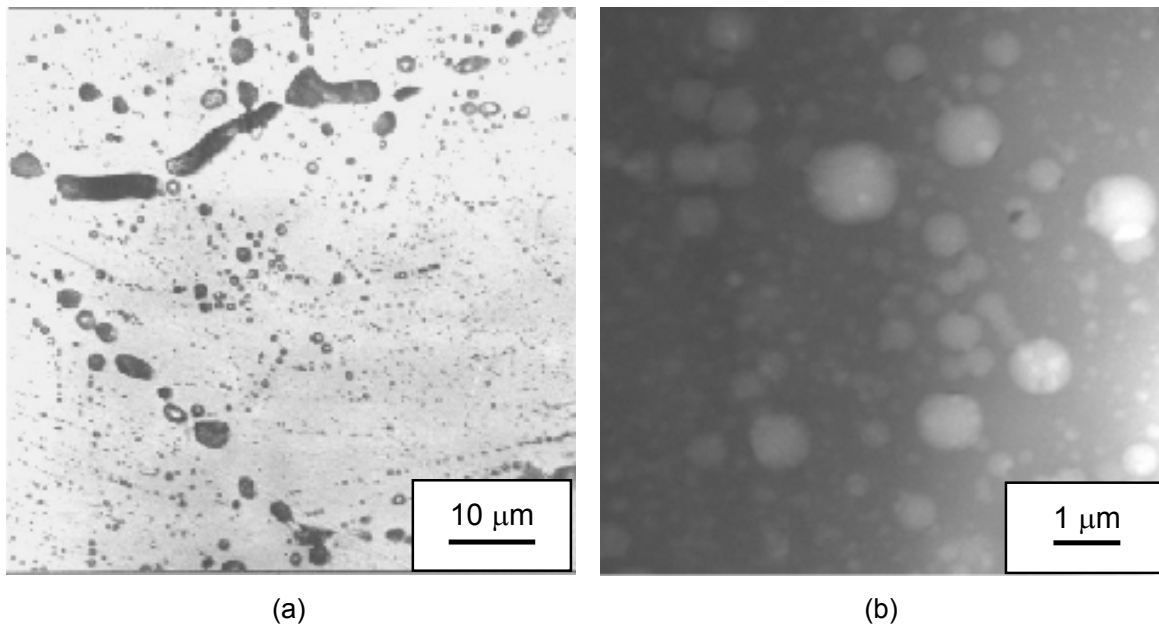
Fig. 2-23 *BERYLLIUM irradiation, bubble growth and coalescence*. Intragranular and grain boundary bubbles. (a) Lenticular bubbles at grain boundaries and large intragranular bubbles (detail of Fig. 2-22a) (b) Smaller intragranular bubbles (STEM, statistical analysis of bubble radii in Fig. 2-31) [Rab03c].

(a) (b)
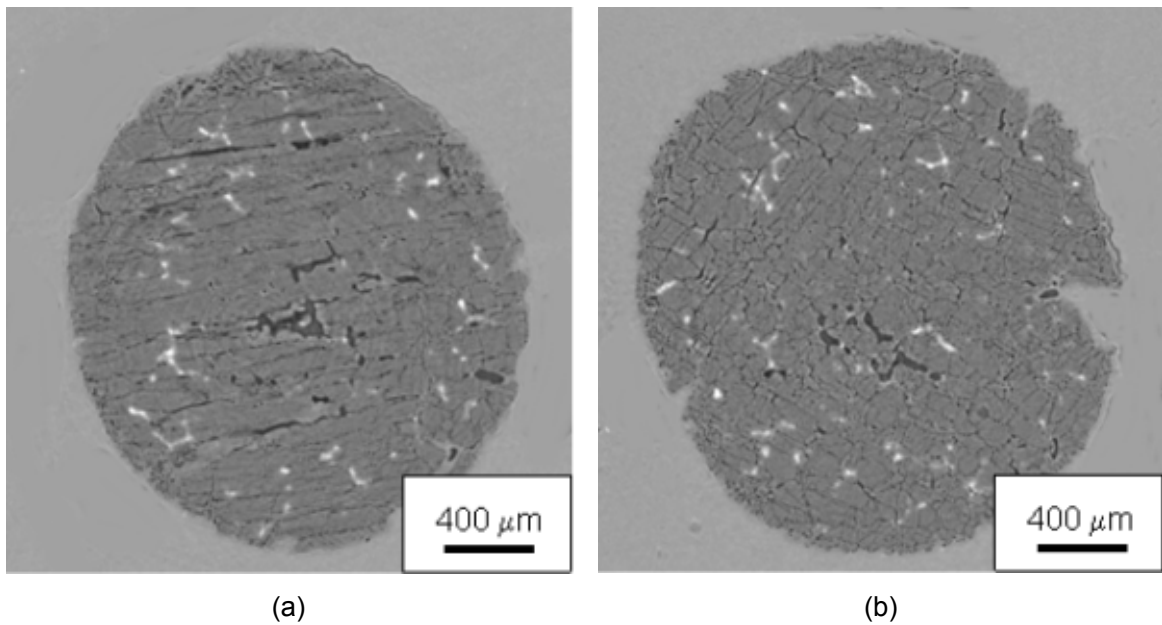
Fig. 2-24   *BERYLLIUM irradiation, the gas percolation stage*. Perpendicular cross sections of a pebble, after irradiation and out-of-pile heating to 1500 K (microtomography) [Rab03]. Gas percolation paths at grain boundaries have formed. They are related to the beginning of a burst release.


(a) (b)
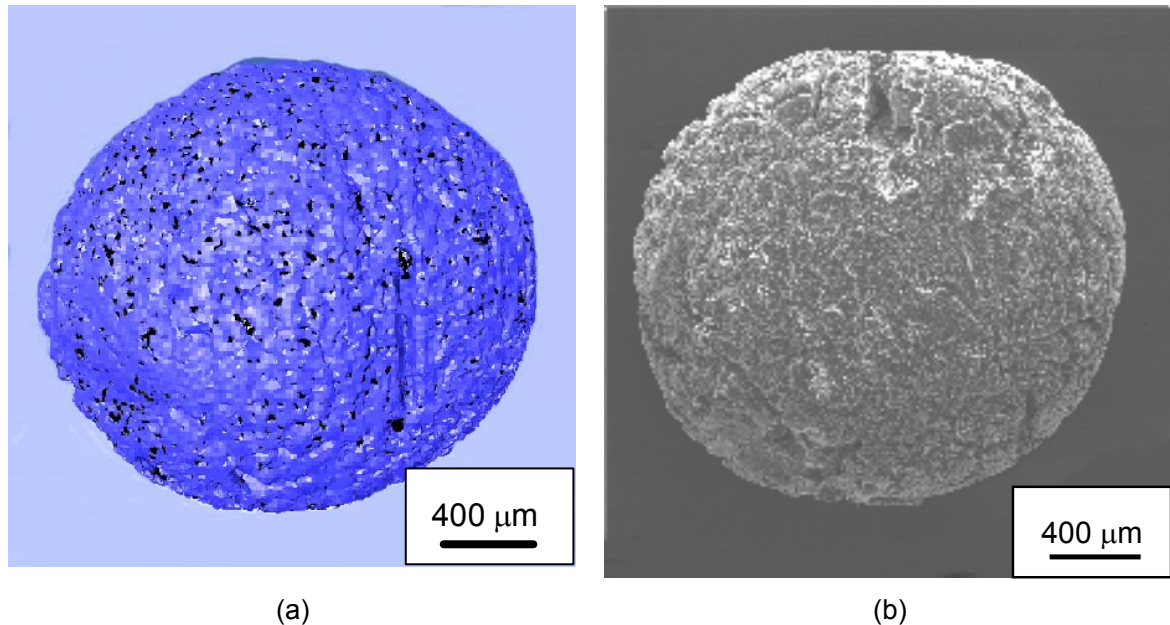
Fig. 2-25   *BERYLLIUM irradiation, the gas percolation stage*. Pebble surface after out-of-pile heating to 1500 K (two different samples). (a) Microtomography with phase segmentation. On the beryllium surface (blue) the emerging open porosities are shown (black) [Rab03]. (b) SEM examination

different axes (z and x), in a position corresponding to the maximum diameter of the sample, with a resolution of 4.9 microns. The features below 4.9 microns are here not visible.

In Fig.2-24a extended parallel percolation paths running across the whole pebble are observed. They are in part the result of a grain separation induced by crack propagation in the presence of chains of pressurised bubbles at grain boundaries.

In Fig. 2-24b the parallel paths are not visible any more and a cell structure is observed. By comparing the two perpendicular cross sections, it can be concluded that the percolation paths are not isotropic and have a columnar structure along a few preferential directions. These correspond to bundles of basaltic grains which grew during the fabrication process. Coarser porosities with a different shape are also visible: these are no irradiation effect but a residue of the fabrication process. White impurity phases (essentially Mg) are segregated at grain boundaries.

Figures 2-25a shows a 3D view of the reconstructed surface of the same pebble as in Fig. 2-24, after the phase segmentation process. The black phase represents the emerging porosity channels. As expected from the porosity texture in the 2D cross sections, their distribution at the surface is not isotropic: their surface concentration substantially increases around the axes of the columnar grain bundles shown in Fig. 2-24. It can be therefore concluded that gas release was much more intense in these zones than in the equiaxed grain regions.

The SEM examination of a similar sample in the same conditions (Fig. 2-25b) shows that, in agreement with the results of the microtomography after phase segmentation, at the beginning of the bubble venting the surface of the pebble is completely restructured. A cell structure is present also on the surface, which is completely different from the smooth surface, with some cracks, which was observed at 1340 K (Fig. 2-22a).

2.5 Inverse analysis of out-of-pile gas release from pebbles from the BERYLLIUM irradiation

2.5.1 Theory and methodology

For the pebbles from the BERYLLIUM irradiation, out-of-pile gas release during the Knudsen-cell experiments described in paragraph 2.4 is, up to approximately 1500 K, the result of gas migration to grain boundaries, in the presence of a precipitation phenomenon into intragranular bubbles. Starting from 1500 K, the gas inventory trapped in bubbles is abruptly released. For both helium and tritium, gas release below 1500 K can be described by a simple model taking into account simultaneous atomic diffusion, precipitation into intragranular bubbles and migration to grain boundaries only. Bubble migration and coalescence phenomena and, in general, all gas diffusion phenomena, which have a large time constant and are relevant during long-term irradiation, can be neglected during this short experiment. Irradiation-related phenomena, e.g. gas generation and bubble re-solution due to interaction with neutrons are also absent in an out-of-pile transient. Consequently, the gas kinetics model in the

ANFIBE code (Eq. A-1, A-2, A-3, A-4, Annex A) can be reduced to the following set of reaction-rate equations [Ron99] [Ron87b]:

$$\frac{dc}{dt} = -Kc - Hc \tag{2.1}$$

$$\frac{db}{dt} = Kc - Ub \tag{2.2}$$

$$\frac{dg}{dt} = Hc + Ub \tag{2.3}$$

c is the average concentration of gas atoms (helium or tritium) in dynamic solution in the lattice (number of atoms per unit volume of beryllium), b of gas in intragranular bubbles, g of gas migrated to grain boundaries: these quantities describe the average gas balance. Since in pebbles with coarse grains a large fraction of the grain surface is external, g represents, to a good approximation, the quantity of gas released. The larger the grains and the smaller the pebble, the closer the approximation to reality (see paragraph 3.8): the model would be exact if the pebble consisted in one grain only or in the case of very fast gas diffusion along grain boundaries.

All concentrations are normalised to the total gas inventory at the beginning of the out-of-pile transient I, as a consequence:

$$c + b + g = 1 \tag{2.4}$$

Eq. 2.1 describes the out-of-pile kinetics of gas atoms in a dynamic solution. The concentration c of gas in solution decreases if gas atoms, as they diffuse in the lattice, precipitate into intragranular bubbles (precipitation term Kc) or if they reach grain boundaries (grain boundary loss term Hc). The precipitation term gives a positive contribution to the increase of gas concentration in bubbles b (Eq. 2-2), whilst the grain boundary loss term increases the quantity of gas at grain boundary and, consequently, released g (Eq. 2-3). In the absence of relevant bubble migration to grain boundaries, the only mechanisms which allows gas trapped in bubbles to be released is bubble venting (bubble venting term Ub).

2.5.1.1 Diffusion, precipitation and migration to grain boundaries

The inverse of the time constant for precipitation K is related to the probability that gas atoms are captured in a given time by a population of intragranular bubbles (containing both helium and tritium):

$$Kc = \chi \; k_{sc}^2 Dc = \chi \; 4\pi \; r_i N_i Dc \tag{2.5}$$

According to the classical random capture theory [Boo57], this probability depends on the gas atomic diffusion coefficient D and on the average size r_i and concentration N_i of bubbles, which are contained in the *intragranular sink strength* k_{sc}. The diffusivity describes gas atom mobility; bubble size and concentration determine the total capture cross section of bubbles. Nevertheless, studies of gas release from a variety of irradiated materials have shown that the pure random capture theory gives in most cases an incorrect description of gas precipitation [Ron87]. In particular, gas precipitation is overestimated and correspondingly, gas migration to grain boundaries is underestimated. The observed reduction of the intragranular sink strength with respect to the random capture theory is due to the fact that, at the beginning of the precipitation stage, bubbles have the dimension of some nanometres (Fig 2-21a) and the gas pressure inside can reach 1 GPa (paragraph 3.5). Elastic equilibrium around the bubble is established by the balance between capillarity forces and gas bubble pressure. Any addition of gas atoms to a bubble through precipitation creates large stresses, unless a proportionate number of vacancies are simultaneously captured by the bubble. If this cannot occur, the stress field surrounding the bubble creates an additional free energy barrier which makes more difficult the jump of gas atoms into the bubble. The decreased effectiveness of bubbles as gas precipitation sinks is described by introducing a *precipitation hindering factor* χ [Ron87a] smaller than 1. The product $\sqrt{\chi}k_{sc}$ we define as the *hindered intragranular sink strength.*

A second reason for the precipitation delay is the possible finite solubility of gas atoms in the lattice. In fact, the precipitation rate is proportional to the gas-in-solid concentration only in the case where its solubility is negligible. Otherwise, the precipitation rate is proportional to the supersaturated fraction of gas in dynamic solution. In this case (for example for tritium, paragraph 3.4), if c_S is the equilibrium solubility, the precipitation term in Eq. 2-5 has to be modified into $K(c-c_S)$. Since c_S can be independently established, the same analytical description as in Eq. 2-5 can be maintained, the effect of solubility being included into the precipitation hindering factor:

$$K(c-c_S)=\left(1-\frac{c_S}{c}\right)Kc = \chi\ k_{sc}^2 Dc = \chi\ 4\pi\ r_i N_i Dc = \left(1-\frac{c_S}{c}\right)\chi^{'}\ 4\pi\ r_i N_i Dc \tag{2.5a}$$

whereby Eq. 2-5a is valid only for $c \geq c_S$. In such case the precipitation hindering factor χ is the product of a factor χ', which takes into account the stress field around the bubbles, and of the factor $0 \leq (1-c_S/c) \leq 1$, which represents the effect of the solubility.

The inverse of the time constant for migration to grain boundaries H is related to the probability that gas atoms, escaping to capture by intragranular bubbles, reach grain boundaries:

$$Hc = k_{sg}^2 D = 3\frac{\sqrt{\chi}k_{sc}}{\alpha}Dc \tag{2.6}$$

The *grain boundary sink strength* k_{sg} depends on the hindered intragranular sink strength k_{sc} and on a characteristic length of migration to grain boundaries α , which is a material property and can be expected to roughly correspond to the average grain size. The ratio of the precipitation and boundary loss time constants is [Ron99]:

$$\frac{H}{K} = \frac{3}{\alpha\sqrt{\chi k_{sc}}}$$

(2.7)

It is a function of the grain size, of the precipitation hindering factor and of bubble population parameters, but *it does not depend on the gas diffusion coefficient*.

Atomic diffusion, in the absence of irradiation enhancement, is single-energy thermally activated:

$$D = D_0 \ \exp\left(-\frac{Q_D}{kT}\right)$$

(2.8)

D_0 is the entropic factor (or diffusion constant) and Q_D the activation energy of the thermal diffusion coefficient; T is the temperature, k the Boltzmann's constant.

In conclusion, long-range gas diffusion and precipitation processes are controlled by two fundamental material properties, diffusion coefficient and migration length, as well as by the characteristics of intragranular bubble population contained in the intragranular sink strength, with a bias represented by the precipitation hindering factor. The assessment of these quantities, for the material considered, is essential in order to be able to describe gas migration phenomena and, consequently, release.

2.5.1.2 Bubble venting

Gas precipitated into bubbles cannot be released via bubble diffusion to grain surfaces, because the time constant of bubble motion is much larger than the duration of the transient. In fact, only starting from 1500 K up to the melting point of beryllium (1556 K [Kle01]) gas trapped in intragranular bubbles is rapidly released, via bubble coalescence and venting. In order to describe gas release in this range, a sink term for the inventory of gas in bubbles has been introduced in Eq. 2-2. The bubble venting stage has been modelled as a thermally activated phenomenon related to material creep under the influence of bubble pressure. Therefore, in order to be able to complete the analytical description of helium and tritium release above 1500 K, the inverse of the time constant for bubble venting has been described as:

$$U = TU_0 \exp\left(-\frac{Q'}{kT}\right)$$

(2.9)

Q' is an activation energy related to thermal creep, U_0 a pre-exponential factor.

A high temperature release of gas trapped in bubbles occurs also in Knudsen-cell experiments with irradiated UO_2, but it is due to a completely different mechanism as in beryllium pebbles. In UO_2 at high temperatures evaporation becomes relevant and bubbles are vented due to the evaporation of the surrounding matrix. This phenomenon can be described by a similar term as in beryllium, but with U proportional to $1/\sqrt{T}$ instead of T [Ron96]. It has been proven in this study that, due to the lower equilibrium vapour pressure of beryllium at the explored temperatures, a matrix evaporation model does *not* describe correctly high temperature ^{4}He release from beryllium pebbles and, consequently, such phenomenon does not play any relevant role.

2.5.1.3 Methodology of the inverse analysis

The model in Eq. 2-1, 2-2 and 2-3 is parametrically dependent on thermal diffusivity (activation energy Q_D and effective entropic factor D_0), migration length to grain boundaries α and hindered intragranular sink strength $\sqrt{\chi}k_{sc}$, as well as activation energy Q' and entropic factor U_0 of the bubble venting stage (Eq. 2-9). The set of equations can be analytically solved in order to express gas release as a function of time during the Knudsen-cell experiment. The solution has been used to fit the experimental curves of the fractional integral release of ^{4}He and ^{3}H by a least square method, implemented in the EFFUSX code [Ron02], in order to assess the values of the above-mentioned parameters.

Since the analytical model of gas diffusion and precipitation, except for radiation-resolution effects, which are absent in out-of-pile experiments, is the same as in the ANFIBE code (Eq. A-1, Eq. A-2, Eq. A-3 and Eq. A-4, Annex A), the results of the inverse analysis are of fundamental importance to calibrate and check the gas diffusion and precipitation model in ANFIBE, for irradiated beryllium pebbles.

2.5.2 Fitting of gas release curves

Fig 2-26 shows the fitting of an experimental curve of ^{4}He release from pebbles from the BERYLLIUM irradiation during out-of pile heating at about 10 K/min to the melting point, as a function of temperature. The experimental curve is the time integral of a ^{4}He release rate curve similar to the one in Fig 2-3. The inverse analysis is performed by means of the EFFUSX code in the temperature range 300 – 1556 K (melting point), on the basis of the diffusion/precipitation/bubble venting model described in paragraph 2.5.1: a solution of the set of equations 2-2, 2-3 and 2-4 for the concentration of helium at grain boundaries/released g is fitted to the experimental curve. The prediction of the fraction of gas inventory precipitated into bubbles b, corresponding to the theoretical gas release curve obtained by the fitting, is also plotted.

A set of 14 experiments were examined (4 at 10 K/min, 3 at 30 K/min for ^{4}He, 3 at 10 K/min, 4 at 30 K/min for ^{3}H). Fig. 2-27 shows a typical fitting of a ^{4}He curve at 30 K/min, Fig. 2-28 and Fig. 2-29 similar fittings at 10 and 30 K/min, but for ^{3}H.
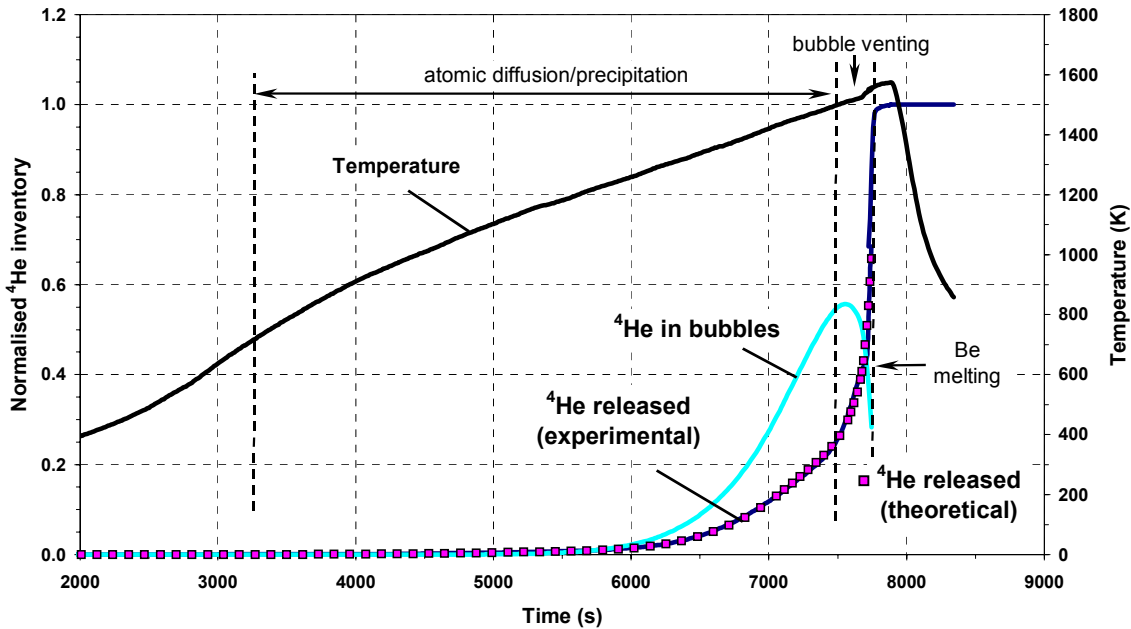
Fig. 2-26   Fitting, by the EFFUSX code, of an experimental ^{4}He release curve from pebbles from the BERYLLIUM irradiation, during out-of-pile heating at 10 K/min, in the range 300 K – 1556 K (beryllium melting point) [Rab03c]. The prediction of ^{4}He inventory in intragranular bubbles corresponding to the theoretical prediction of ^{4}He release is also shown. (Experiment 159bei, Tab. 2-2).
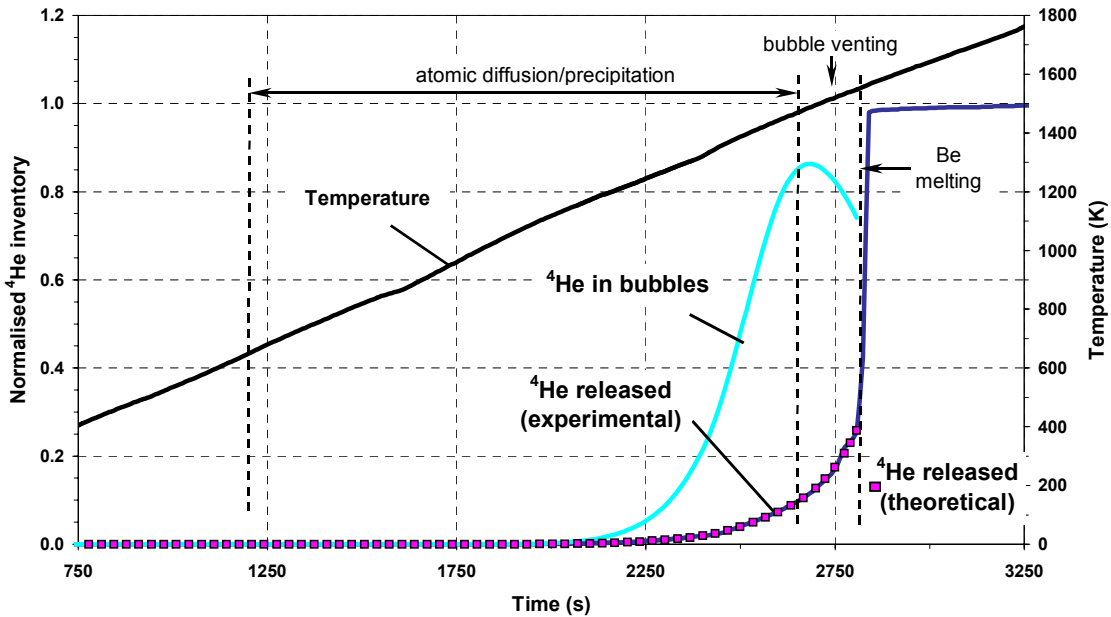

Fig. 2-27   A similar fitting as in Fig. 2-26, but of ^{4}He release during out-of-pile heating at 30 K/min. (Experiment 233bei, Tab. 2-2).
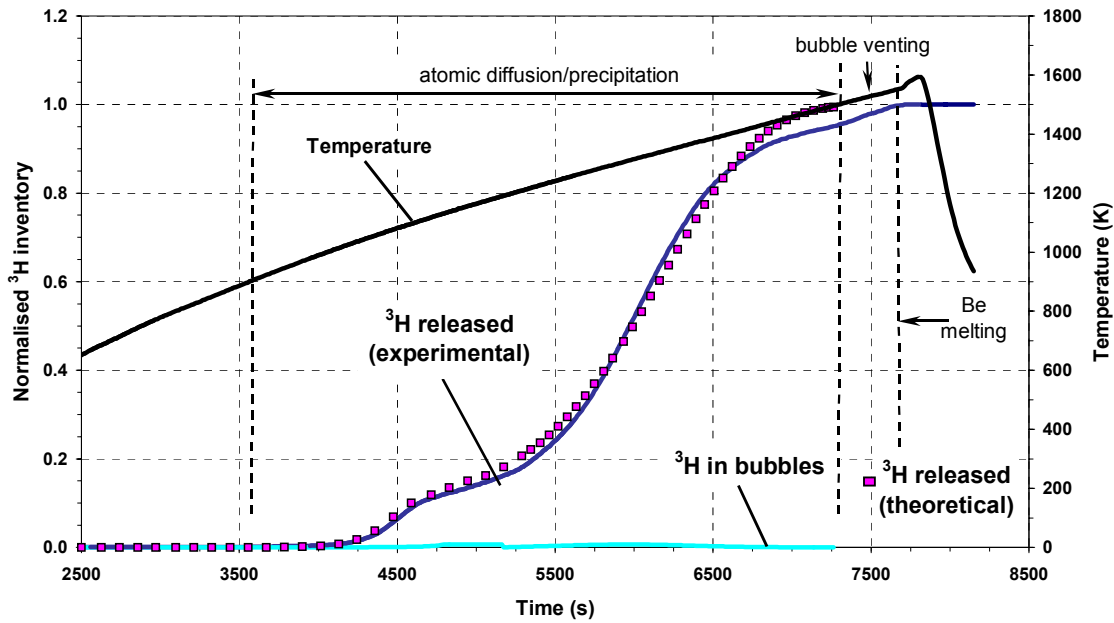
Fig. 2-28   A similar fitting as in Fig. 2-26, but of ^{3}H release during out-of-pile heating at 10 K/min. (Experiment 155bei, Tab. 2-3).
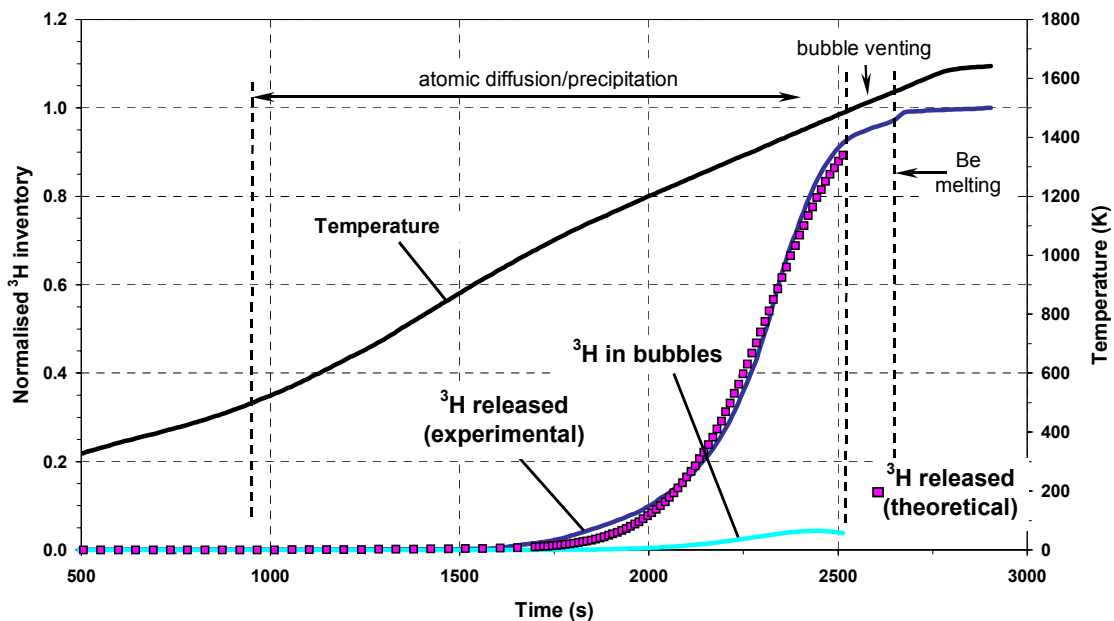
Fig. 2-29   A similar fitting as in Fig. 2-26, but of ^{3}H release during out-of-pile heating at 30 K/min, in the range 300 K – 1500 K. (Experiment 160bei, Tab. 2-3).

For ^{4}He, in the whole set of experiments examined, the theoretical prediction which results from the inverse analysis is generally in excellent agreement with the measured gas release in the full range of temperatures considered. Up to 1500 K gas release is due to the migration to grain boundaries of a limited fraction of gas atoms, whilst most of them precipitate, therefore the inventory of gas trapped in bubbles increases. For ^{4}He, precipitation in the range 300 K –1500 K is much more intense than migration to grain boundaries: in the whole set of experimental curves of ^{4}He release fitted, the peak value of the gas in bubbles at the end of the precipitation stage is in the range of 55 to 75%, which corresponds to the fraction of gas released above 1500 K (Fig. 2-7). Therefore the theoretical prediction, fitted on the experimental curve, reproduces correctly the fact that all gas accumulated in bubbles during the precipitation stage must be released during bubble venting and melting. Precipitation is more intense if the heating is faster (compare Fig. 2-26 to Fig. 2-27): this is a possible explanation of the delay in release observed at 30 K/min. For tritium, the fitting of the release curve with the model including the bubble venting stage used for ^{4}He, though numerically stable, gives an unsatisfactory prediction of gas inventory in bubbles: in particular, the appearance of the bubble venting stage is largely anticipated with respect to reality. This is due to the fact that, for tritium, the bubble venting stage has in the least square fitting process a very low weight as compared to the diffusion stage: the limited number of experimental points available in this range does not allow fitting the experimental curve, without negatively affecting the description of the rest of the transient. Therefore, for tritium the model was limited to diffusion and precipitation, with a fictitious evaporation stage similar to the one occurring in UO_2 (paragraph 2.5.1.2). The fitting range was therefore limited to the end of the diffusion stage (1500 K).

Also for tritium the inverse analysis confirms the conclusions of the study of the release rate curves (Fig. 2-3): practically the total inventory is released by diffusion, with a very small fraction precipitating into bubbles, much smaller than for ^{4}He (in the range of 0 to 10%). In the whole set of Knudsen cell experiments performed, the quality of the fitting for ^{3}H is somewhat lower than for ^{4}He, though very satisfactory taking into account the extremely small amount of tritium in the samples. In particular the fitting is less precise in the first part of the release curve: this can be attributed to the irregularities observed in the ^{3}H release rate curve, related to the presence of other phenomena than diffusion. The prediction of the maximum amount of tritium precipitated is also reasonable, though the maximum amount of tritium precipitated varies in the range of 0 to 10%. The slight decrease of gas inventory in bubbles at high temperature is an effect of the fictitious evaporation stage assumed.

The main input quantities to the EFFUSX code for the fitting of a gas release curve are the gas migration characteristic length of the material α and the value of the entropic factor of the thermal diffusivity D_0; the main output quantities are the activation energy of the thermal diffusivity Q_D and the hindered intragranular sink strength $\sqrt{\chi}k_{sc}$. The last quantity is actually dependent on temperature, but since in the model it is considered to be constant, the fitting provides an average value during the transient. The values of the input quantities are determined by trial and error, on the basis of the quality of the resulting fitting. It has been observed that the fitting is, numerically, completely unsuccessful if input parameters far from the right values, due to the extreme sensibility of the inverse analysis.
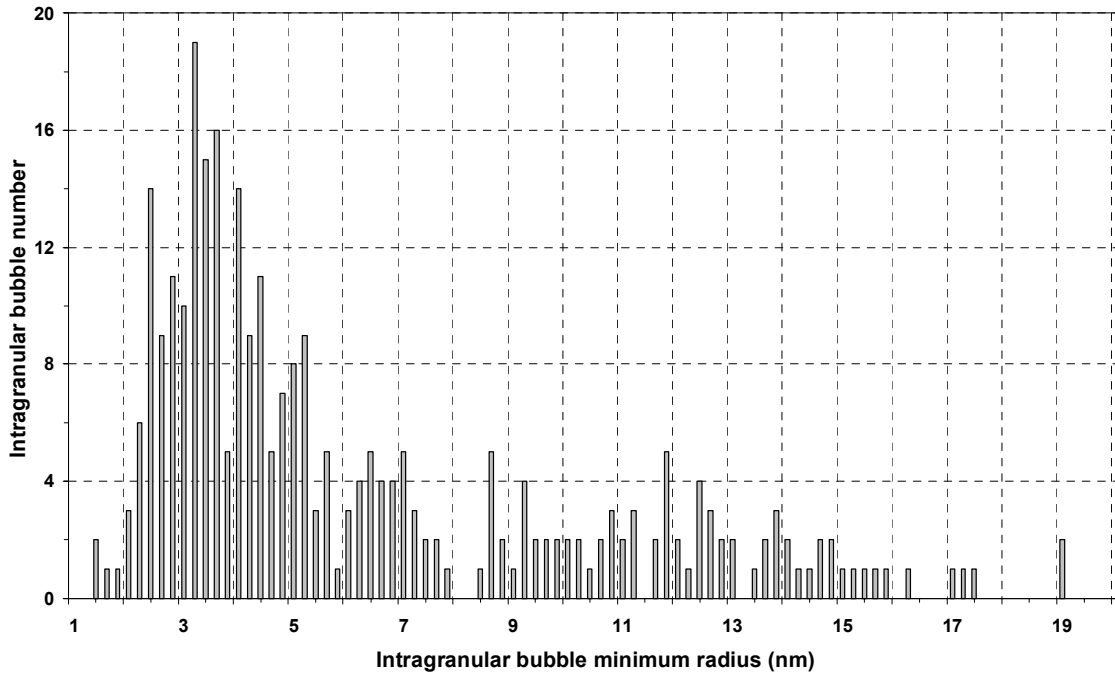
Fig. 2-30   Distribution of intragranular bubble radii in pebbles from the BERYLLIUM irradiation, after out-of-pile heating to 1000 K, from the quantitative analysis of the TEM micrograph in Fig. 2-21a [Rab03c]. Since bubbles are round section ellipsoids, here the minimum radius is considered. On a sample of 300 bubbles, the average radius r_i is 6.2 nm and the average bubble concentration N_i 7.2·10^{20} bubbles m^{-3}. The related intragranular sink strength k_{sc} is 7.5·10^6 m^{-1}; intragranular swelling 0.11%.

The characteristic diffusion length has been assessed as:

$$\alpha \approx 100 \;\; \mu m \tag{2.10}$$

Such value approximately corresponds, as expected, to the average grain size in the material examined and can be assumed also for the reference pebbles for the HCPB blanket.

2.5.3 The intragranular sink strength

In order to assess the intragranular sink strength:

$$k_{sc} = \sqrt{4\pi \; r_i N_i} \tag{2.11}$$

a quantitative analysis of intragranular bubble population parameters (average radius r_i and concentration N_i) has been performed. In principle, as well as bubble radius and concentra-
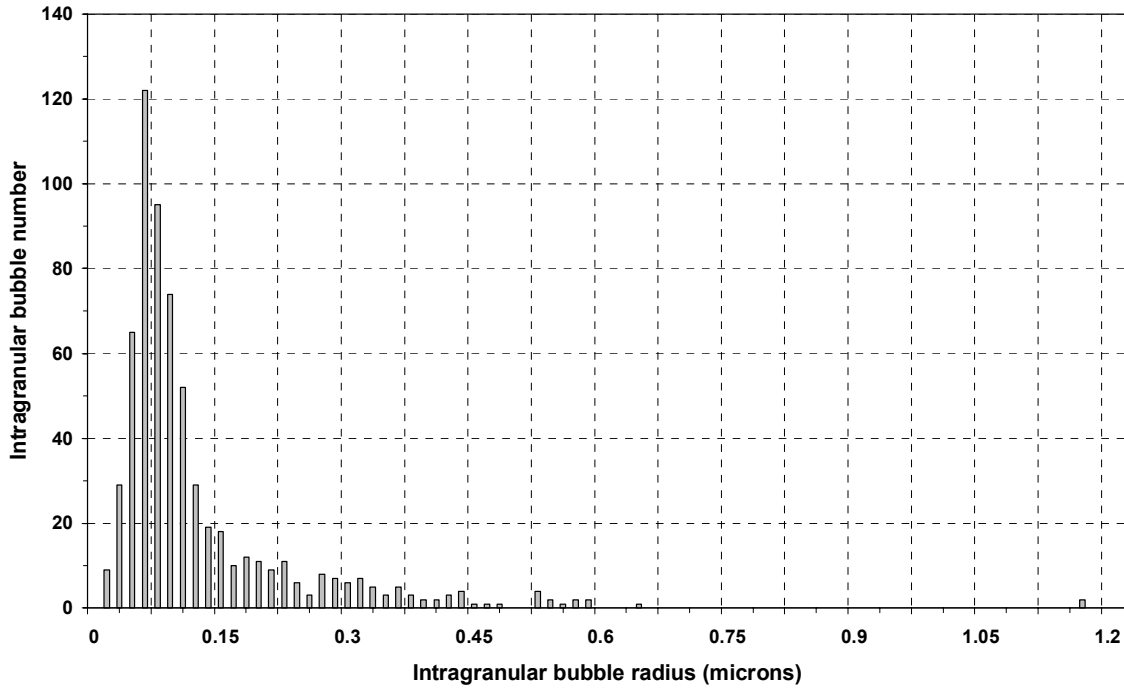
Fig. 2-31   Distribution of intragranular bubble radii in pebbles from the BERYLLIUM irradiation, after out-of-pile heating to 1340 K, from the quantitative analysis of the STEM micrograph in Fig. 2-23b [Rab03c]. On a sample of 520 bubbles, the average radius r_i is 0.13 μm and the average bubble concentration N_i is $8.9 \cdot 10^{18}$ bubbles m^{-3}. The related intragranular sink strength k_{sc} is $3.8 \cdot 10^6$ m^{-1}, intragranular swelling 44.6%.

tion, also k_{sc} depends on temperature. The analysis has been carried out at two reference temperatures during an out-of-pile heating at 10 K/min, i.e. at the beginning and at the end of the precipitation stage, respectively at 1000 K and at 1340 K. The TEM micrographs in Fig. 2-21a and Fig. 2-23b have been considered. The statistical distribution of bubble radii (Fig. 2-30, Fig. 2-31) is typically logarithmic-normal, as expected for particles, the growth rate of which increases with size.

Since a TEM micrograph is a projection of a 3D volume, the depth of which is the thickness of the TEM layer, in order to assess bubble concentration, an assessment of the TEM layer thickness is necessary. On the basis of the theory for the determination of extinction distance of fringes [Ame64] and of observations of the development in depth of grain boundary bubble chains (Fig. 2-21b), the thickness of the TEM layer has been assessed as about 300 nm.

It has been observed that, though both bubble radius and concentration change dramatically between 1000 K and 1340 K, *their product maintains the same order of magnitude*. As a consequence, the intragranular sink strength can be considered to remain constant during the transient, with the average value of $5.6 \cdot 10^6$ m^{-1}. The constancy of the product $r_i N_i$ implies that, between the two temperatures, intragranular swelling has occurred: as a matter of fact, from 0.11% at 1000 K (Fig. 2-30) it evolves to 44.6% at 1340 K (Fig. 2-31).

^{4}He DIFFUSION AND PRECIPITATION PARAMETERS						
Knudsen-cell experiment	Temperature ramp (K/min)	$\dfrac{Q_D}{k}$ (K)	$\dfrac{\Delta Q_D}{k}$ (K)	$\overline{\sqrt{\chi}k_{sc}}$ (m^{-1})	$\Delta\left(\overline{\sqrt{\chi}k_{sc}}\right)$ (m^{-1})	$\overline{\chi}$
028bei	10	$2.95\cdot10^4$	$3.69\cdot10^2$	$9.33\cdot10^2$	$1.24\cdot10^2$	$2.74\cdot10^{-4}$
114bei	10	$2.94\cdot10^4$	$5.12\cdot10^2$	$9.21\cdot10^2$	$9.79\cdot10^1$	$2.67\cdot10^{-4}$
159bei	10	$2.87\cdot10^4$	$6.75\cdot10^1$	$7.37\cdot10^2$	$1.36\cdot10^2$	$1.71\cdot10^{-4}$
231bei	10	$2.91\cdot10^4$	$3.39\cdot10^2$	$1.18\cdot10^3$	$8.41\cdot10^1$	$4.39\cdot10^{-4}$
116bei	30	$2.96\cdot10^4$	$9.30\cdot10^2$	$4.74\cdot10^3$	$1.31\cdot10^3$	$7.08\cdot10^{-3}$*
160bei	30	$3.01\cdot10^4$	$2.56\cdot10^3$	$4.49\cdot10^3$	$1.29\cdot10^3$	$6.35\cdot10^{-3}$*
233bei	30	$3.00\cdot10^4$	$5.14\cdot10^2$	$4.18\cdot10^3$	$2.38\cdot10^3$	$5.49\cdot10^{-3}$*
Logarithmic average at 10 K/min	10					$2.72\cdot10^{-4}$
Logarithmic average at 30 K/min	30					$6.28\cdot10^{-3}$
Logarithmic average						**$1.04\cdot10^{-3}$**

* in the assumption that $k_{sc}=\sqrt{4\pi\ r_i N_i}$ is the same at 10 and at 30 K/min

Tab. 2-2   Activation energies for diffusion and hindered intragranular sink strengths for ^{4}He, calculated by the EFFUSX code as a result of the fitting of the experimental gas release curves from the BERYLLIUM irradiation, with their errors. The corresponding average values for the precipitation hindering factor are also shown.

2.5.4 The precipitation hindering factor

The value of the intragranular sink strength k_{sc}, calculated from the pure random capture theory, is remarkably higher than the product $\sqrt{\chi}k_{sc}$ calculated by the EFFUSX code. The discrepancy, since it amounts to some orders of magnitude, cannot be explained in terms of uncertainties in the assessment of bubble population parameters. Besides, the value of k_{sc} remains of the same order of magnitude during the transient. The only reasonable explana-

^{3}H DIFFUSION AND PRECIPITATION PARAMETERS						
Knudsen-cell experiment	Temperature ramp (K/min)	$\dfrac{Q_D}{k}$ (K)	$\dfrac{\Delta Q_D}{k}$ (K)	$\overline{\sqrt{\chi}k_{sc}}$ (m^{-1})	$\Delta\left(\overline{\sqrt{\chi}k_{sc}}\right)$ (m^{-1})	$\overline{\chi}$
114bei	10	$2.11\cdot10^4$	$2.73\cdot10^2$	$3.73\cdot10^1$	$8.74\cdot10^0$	$4.39\cdot10^{-7}$
155bei	10	$2.01\cdot10^4$	$1.34\cdot10^2$	$1.67\cdot10^1$	$1.69\cdot10^0$	$8.75\cdot10^{-8}$
159bei	10	$2.07\cdot10^4$	$4.84\cdot10^2$	$3.17\cdot10^1$	$1.31\cdot10^1$	$3.16\cdot10^{-7}$
231bei	10	$2.08\cdot10^4$	$5.31\cdot10^2$	$4.51\cdot10^1$	$2.16\cdot10^0$	$6.41\cdot10^{-7}$
116bei	30	$2.17\cdot10^4$	$3.37\cdot10^1$	$1.62\cdot10^2$	$4.31\cdot10^0$	$8.27\cdot10^{-6}$*
156bei	30	$2.48\cdot10^4$	$6.08\cdot10^1$	$4.39\cdot10^2$	$2.62\cdot10^1$	$6.07\cdot10^{-5}$*
157bei	30	$2.03\cdot10^4$	$2.25\cdot10^3$	$3.19\cdot10^1$	$6.01\cdot10^1$	$3.21\cdot10^{-7}$*
160bei	30	$1.92\cdot10^4$	$7.09\cdot10^2$	$1.81\cdot10^1$	$1.08\cdot10^1$	$1.03\cdot10^{-7}$*
233bei	30	$1.92\cdot10^4$	$8.82\cdot10^2$	$1.94\cdot10^1$	$1.45\cdot10^1$	$1.18\cdot10^{-7}$*
Logarithmic average at 10 K/min	10					$5.92\cdot10^{-7}$
Logarithmic average at 30 K/min	30					$3.11\cdot10^{-6}$
Logarithmic average						**$1.49\cdot10^{-6}$**

* in the assumption that $k_{sc} = \sqrt{4\pi\ r_i N_i}$ is the same at 10 and at 30 K/min

Tab. 2-3   Activation energies of diffusion and hindered intragranular sink strengths for ^{3}H, calculated by the EFFUSX code as a result of the fitting of the experimental gas release curves from the BERYLLIUM irradiation, with their errors. The corresponding average values of the precipitation hindering factor are also shown.

tion is that, indeed, a precipitation hindering factor exists, and, furthermore, it is much smaller than 1. From the average value of the hindered intragranular sink strength, obtained from the fitting of the experimental gas release curves, and considering that the intragranular sink strength is practically constant it is possible to assess an average value of the precipitation hindering factor during the transient as:

$$\chi = \frac{\left(\sqrt{\chi}k_{sc}\right)^2_{EFFUSX}}{k^2_{sc}} = \frac{\left(\sqrt{\chi}k_{sc}\right)^2_{EFFUSX}}{4\pi\,r_i N_i} \tag{2.12}$$

The values for the different experiments are shown in Tab. 2-2 for ^{4}He and in Tab. 2-3 for ^{3}H: the logarithmic average for the complete set of experiments is equal to about $1.0\cdot10^{-3}$ for ^{4}He and $1.5\cdot10^{-6}$ for ^{3}H.

This study has proven that a model of gas diffusion and precipitation is indeed able to describe out-of-pile gas release from irradiated beryllium pebbles, *provided that a strong bias in the gas precipitation rate with respect to the pure random capture theory is taken into account*. If one assumes zero solubility of gas-in-solid, the bias factor is equal to the unit only for precipitation on external surfaces, whilst it is much lower for precipitation at the surface of pressurised bubbles. If this phenomenon is neglected, the precipitation term in the reaction rate equations is overestimated with respect to the boundary loss term of a factor of $1/\sqrt{\chi}$ (Eq. 2-7). Since gas at grain boundaries can be much more easily released than gas trapped in intragranular bubbles, the final consequence of this is a dramatic underestimation of macroscopic gas release in the out-of-pile experiments considered.

Furthermore, the bias is not the same for ^{4}He and ^{3}H, since it depends from the type of atom. In particular, for tritium it is stronger (Tab. 2-3). A lower precipitation hindering factor for tritium than for helium explains the faster migration of tritium atoms to grain boundaries observed also in the out-of-pile gas release experiments from highly irradiated beryllium from BR2 moderator (Fig. 2-12, paragraph 2.3.4.2). This phenomenon cannot be due to a higher mobility of tritium atoms, since the ratio H/K in Eq. 2-7 does not depend on the diffusion coefficient. As a matter of fact, a higher mobility enhances both precipitation and migration to grain boundaries at the same time.

The relevant lowering of the precipitation rate observed in this study in beryllium has been previously observed also for fission gases in nuclear fuels. In disagreement with the pure random capture theory, the presence of bubbles does not prevent long range migration of gas atoms. In other words, the effectiveness of bubbles as sinks for gas atoms is lower that expected on the basis of their size and concentration. This has been attributed to the fact that very small bubbles at the beginning of the precipitation stage are highly pressurised (in the range of some hundreds MPa to 1 GPa internal pressure, paragraph 3.5) and create in their vicinity a strong elastic strain field. The energy barrier around the bubble prevents gas atoms from falling into it. The effect is particularly strong if precipitation is quick, starting from a supersaturated solution. Taking this phenomenon into account, in the case where gas mobility is much larger than vacancy mobility, the precipitation term in Eq. 2-5 has to be modified as follows [Ron87a]:

$$Kc = 4\pi\,r_i N_i \left(CD_g D_{self}\right)^{1/2} c^{1/2} \tag{2.13}$$

C is a constant. The precipitation rate is controlled by the geometrical average of the gas diffusivity D_g and of the self-diffusion coefficient of the material D_{self}, and its dependence on c has changed from linear to parabolic. As a consequence, the precipitation rate is less dependent on the concentration of gas in solution than it would be in a linear model. By comparing Eq. 2.13 with Eq. 2.5, the following expression of the precipitation hindering factor is obtained:

$$\chi = \sqrt{\frac{C\, D_{self}}{D_g c}}$$

(2.14)

In case the gas solubility is not negligible, Eq. 2-13 has to be multiplied by the solubility factor $(1 - c_S / c)$ and, after comparison with Eq. 2-5a, the following expression for the precipitation hindering factor is obtained:

$$\chi = \left(1 - \frac{c_S}{c}\right)\sqrt{\frac{C\, D_{self}}{D_g c}}$$

(2.14a)

Since it contains the gas diffusion coefficient and the self-diffusion coefficient of the solid, the precipitation hindering factor is also thermally activated and it is lower if the mobility of the gas and its concentration are higher, in agreement with the experimental observation for helium and tritium in beryllium, described above. In case the solubility of the gas plays an important role, the precipitation hindering factor is further reduced and tends to 0 if the concentration of gas in solution approaches the solubility limit. The values of χ measured for ^{4}He in Tab. 2-2 and for ^{3}H in Tab. 3-3 are comprehensive of the effect of both the stress field around bubbles and the solubility.

In extending the conclusions of this study on precipitation hindering to the description of in-pile behaviour, it has to be taken into account that in-pile precipitation occurs on a longer time scale than in fast out-of-pile temperature transients and approaches equilibrium conditions, therefore a weaker precipitation hindering is in principle expected.

2.5.5 The thermally activated atomic diffusion coefficients

From the analysis described above (Tab. 2-2, Tab 2-3), the thermally activated atomic diffusion coefficients for ^{4}He and for ^{3}H can be assessed as:

$$D_{4He}\left[m^2 s^{-1}\right] \approx 10^{-4} \exp\left(-\frac{29380 \pm 760}{T}\right) = 10^{-4} \exp\left(-\frac{2.532 \pm 0.065\ eV}{kT}\right)$$

(2.15)
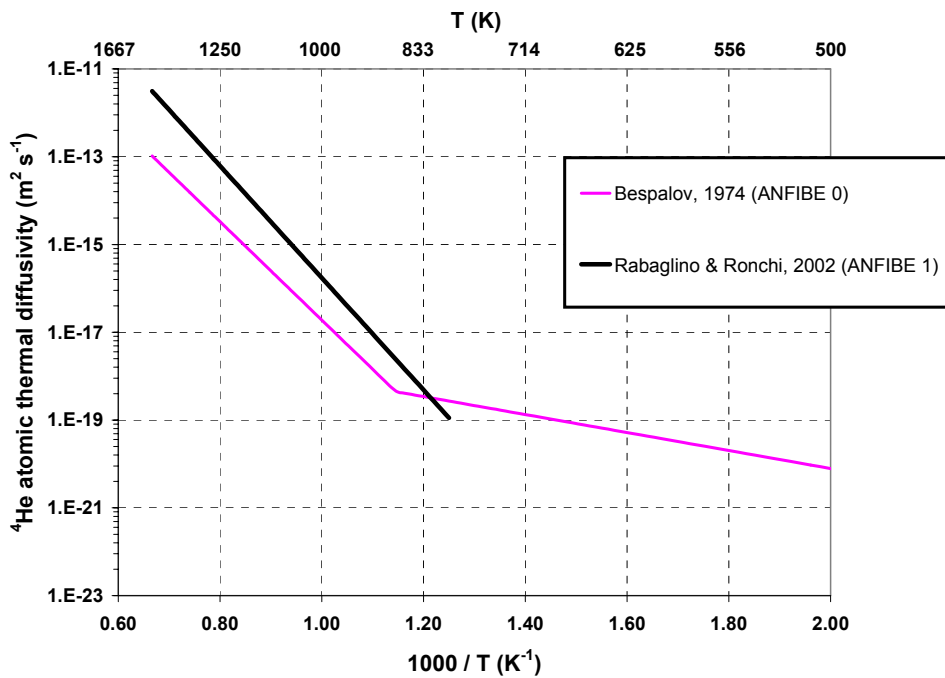
Fig. 2-32   Atomic diffusivities of ^{4}He in beryllium [Sca95] [Sca98].
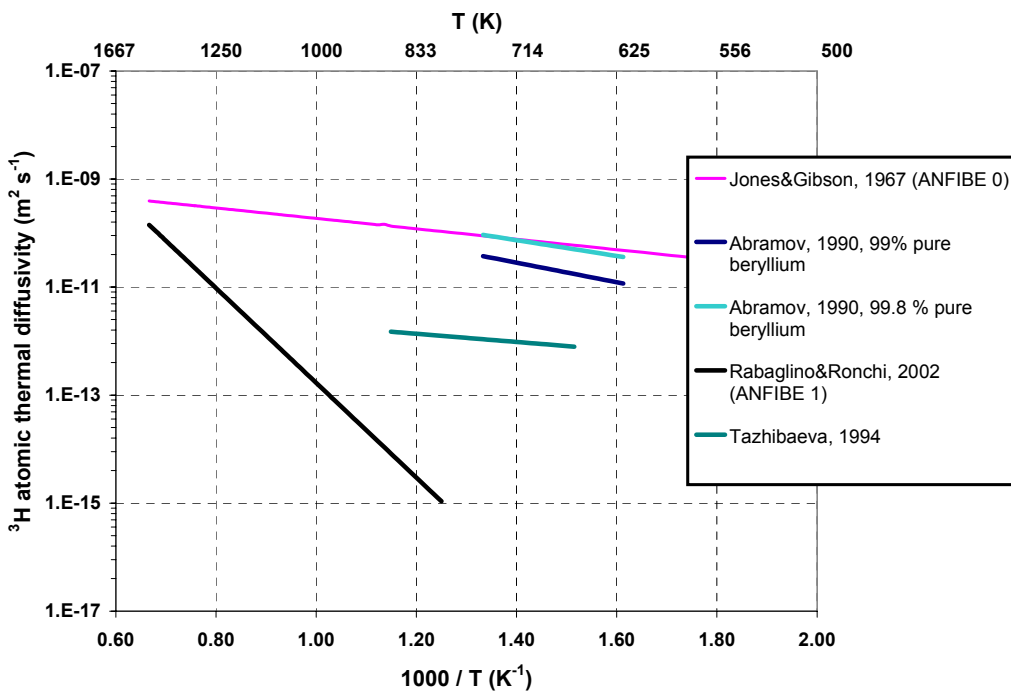
Fig. 2-33   Atomic diffusivities of ^{3}H in beryllium [Cau02] [Jon67b][Abr90] [Taz94].

$$D_{3H}\left[m^2 s^{-1}\right] \approx 10^{-4} \exp\left(-\frac{20200 \pm 690}{T}\right) = 10^{-4} \exp\left(-\frac{1.740 \pm 0.059 \ eV}{kT}\right) \qquad (2.16)$$

These expressions are valid for irradiated beryllium pebbles from the BERYLLIUM experiment (about 480 appm [4]He, 8 appm ^{3}H), in the range where atomic diffusion-controlled gas release is observed, i.e. from 800 to 1500 K for both gases.

The activation energies with their error are an output of the inverse analysis of the gas release curves, therefore they are precisely assessed. The pre-exponential factor is an input datum of the EFFUSX code and it is approximately assessed by trial and error, consequently only the order of magnitude can be given. The reported value is the one which enables to perform the best fittings. Due to the presence of the precipitation hindering factor in the analytical model, which is also thermally activated since it contains the self-diffusion coefficient of beryllium, the reported activation energy of the diffusivity includes the activation energy of the precipitation hindering factor.

It is here assumed that the diffusion coefficients are independent of the gas-in-solid concentration. There is no indication in the literature that enthalpy and entropy of diffusion are concentration-dependent with such a low gas inventory as in the samples from the BERYLLIUM irradiation. Nevertheless, at much higher helium and tritium concentrations, like in the samples from BR2 moderator examined in paragraph 2.3.4, the effect might become relevant.

In Fig. 2-32 and 2-33 the values measured in this study are compared to previous studies in the literature. For [4]He, the version 0 of the ANFIBE code contains Bespalov's correlation [Sca98] [Bes74]; for ^{3}H, Jones & Gibson's correlation [Sca98] [Jon67a] [Jon67b].

The scatter of experimental data is generally large, due to the use of different methods and different type of materials. The values measured in this study, if considered together with the precipitation hindering factor, are the most suitable for implementation in the ANFIBE code, because they are part of a coherent and integrated model to describe gas diffusion and precipitation in irradiated beryllium pebbles.

2.5.6 Additional considerations on the precipitation hindering factor

If the precipitation hindering factor for both [4]He and ^{3}H depended only on the elastic strain field surrounding overpressurised bubbles, it could be described by Eq. 2-14. In this case, on the basis of the measured values of [4]He and ^{3}H diffusivities in Eq. 2-15 and 2.16, the ratio between the precipitation hindering factors of ^{3}H and [4]He would have the following expression:

$$\frac{\chi_{3H}}{\chi_{4He}} = \sqrt{\frac{D_{4He}c_{4He}}{D_{3H}c_{3H}}} = \sqrt{\frac{c_{4He}}{c_{3H}}} \exp\left(-\frac{4590}{T}\right) \qquad (2.17)$$

For the temperature transients considered, an average value of such ratio in the range 800 K – 1500 K can be calculated on the basis of the evolutions of ^{4}He and ^{3}H concentrations in solution predicted by the EFFUSX code as a function of temperature and it turns out to be of the order of 0.01. This is a further confirmation that the precipitation hindering factor for tritium is much lower than for helium. Nevertheless, the ratio which can be derived from the average values of χ in Tab. 2-2 and Tab. 2-3 is an order of magnitude lower, about 0.001. This suggests that the effect of the solubility in delaying the precipitation of tritium is not negligible and the precipitation hindering factor for tritium could be better described by Eq. 2-14a. The low values for the tritium precipitation hindering factor measured in this study may be an indirect confirmation that tritium is soluble in beryllium.

2.6 Summary of the experimental results

The characterisation of pebbles from the BERYLLIUM irradiation, in all its different parts previously described, enables an integrated macroscopic/microscopic validation of the gas atomic diffusion and precipitation model in the ANFIBE code, as well as some important improvements of the gas kinetics model. In Tab. 2-4 the experiments, the techniques and the main conclusions of the studies presented in this chapter are collected, with their impact on the improved version 1 of ANFIBE, described in Chapter 3, and beyond.

As far as the samples from the EXOTIC 8 irradiation and from BR2 moderator are concerned, although the characterisation performed up to now (Tab. 2-5 and Tab. 2-6) is limited to helium and tritium release experiments, the qualitative results obtained are relevant in order to understand general trends of diffusion phenomena in different samples. As far as the fragments from BR2 moderator are concerned, a full quantitative microstructure characterisation and an inverse analysis of gas release curves, by the same methodology that was applied for the pebbles from the BERYLLIUM experiment, is needed in the near future in order to confirm the conclusions of this study, in particular on the gas precipitation theory, at very high fluence.

2.7 Discussion

The study of out-of-pile helium and tritium release from 2 types of weakly irradiated pebbles and from highly irradiated fragments during out-of-pile heating to the melting point has been performed. The study has made it possible to better understand the basic microscopic mechanisms of diffusion, precipitation into bubbles and bubble venting which are responsible for gas release in beryllium and to examine how they are affected by grain size and irradiation conditions.

In particular, for pebbles from the BERYLLIUM irradiation, a full characterisation of the microstructure has been performed, at different temperatures during a reference temperature transient of 10 K/min, corresponding to different gas release stages. The relationship between gas release modes and microstructure evolution has been identified. For the same material, an inverse analysis of measured gas release curves has been carried out, on the basis of a model taking into account atomic gas diffusion, precipitation into intragranular

CHARACTERISATION OF WEAKLY IRRADIATED BERYLLIUM PEBBLES FROM THE *BERYLLIUM* IRRADIATION			
Study 1. Gas release during out-of-pile annealing in a vacuum to the melting point (Knudsen cell / mass spectrometry)			
Measured quantities	*Performed experiments*	*Relevant quantities or phenomena for ANFIBE 1*	*Relevant quantities or phenomena for further developments*
^{4}He release rate	4 at 10 K/min, 3 at 30 K/min	^{4}He integral release	
^{3}He release rate	4 at 10 K/min, 3 at 30 K/min	^{3}He integral release	
^{3}H release rate	3 at 10 K/min, 4 at 30 K/min	^{3}H integral release	
Study 2. Microstructure characterisation and related quantitative analyses.			
Conditions	*Techniques*	*Relevant quantities or phenomena for ANFIBE 1*	*Relevant quantities or phenomena for further developments*
As-fabricated	OM, SEM, TEM	Grain size, shape and grain microstructure.	
After irradiation	SEM, TEM	Absence of bubbles.	Interaction between gas and irradiation-induced dislocation kinetics
After irradiation and out-of-pile heating, at 10 K/min, to:			
1000 K	SEM, TEM	Average bubble size, bubble 3D distribution, bubble concentration, swelling. Intragranular sink strength, precipitation hindering factor. Verification of the gas precipitation stage. Pressure inside the bubbles, verification of the Equation of State of helium.	Dislocation density. Interaction between gas precipitation and irradiation-induced dislocation kinetics
1350 K	OM, SEM, STEM	Average bubble size, bubble 3D distribution, bubble concentration, swelling. Intragranular sink strength, precipitation hindering factor, characteristic gas migration range. Verification of bubble growth and coalescence at grain boundaries.	
1500 K	SEM, Computer Aided Microtomography by synchrotron radiation	3D structure of percolation paths. Verification of the bubble venting stage.	Gas percolation model.

Study 3. Inverse analysis of the gas release curves (EFFUSX code)			
	Analysed experiments	Relevant quantities for the validation of ANFIBE 1	Relevant quantities or phenomena for further developments
	7 of ^{4}He release, 9 of ^{3}H release	^{4}He and ^{3}H thermal diffusion coefficient:. Precipitation hindering factor (average value)	Bubble venting model, model of the precipitation hindering factor

Tab. 2-4   Summary of the characterisation of pebbles from the BERYLLIUM irradiation performed in this study, with the impact of the results on ANFIBE and beyond.

bubbles, atom migration to grain boundaries and bubble venting. Bubble venting has been described as a thermally activated phenomenon due to material creep under the influence of pressurized bubbles. It has been demonstrated that such a model is able to describe all observed stages of gas release, both for helium and for tritium. Fundamental parameters in the model have been assessed, specifically for the material considered: the characteristic length of gas atom migration to grain boundaries and helium and tritium thermally activated atomic diffusivities.

The quantitative analysis of bubble size and concentration and of their evolution during the reference temperature transient has been performed, in order to compare the gas precipitation rate observed to the capture section of bubbles. The most important result of this study is the confirmation that also in irradiated beryllium, like in nuclear fuels, a strong bias effect in gas precipitation with respect to the classical random capture theory exists. In particular, gas precipitation rate is much lower than expected and it is for tritium even lower than for helium. If such precipitation hindering phenomenon is neglected, gas migration to grain boundaries and, correspondingly, macroscopic gas release are dramatically underestimated.

The results of these studies have a large impact of the possibility of improvement and validation of the ANFIBE code, in view to enable a reliable extrapolation to the HCPB blanket. In some key material properties, the pebbles from the BERYLLIUM irradiation are similar to the

CHARACTERISATION OF WEAKLY IRRADIATED BERYLLIUM PEBBLES FROM THE *EXOTIC 8* IRRADIATION			
Study 1. Gas release during out-of-pile annealing in a vacuum to the melting point (Knudsen cell / mass spectrometry)			
Measured quantities	*Performed experiments*	*Relevant quantities for the validation of ANFIBE 1*	*Relevant quantities or phenomena for further developments*
^{4}He release rate	1 at 10 K/min, 1 at 30 K/min		Confirmation of the assessment of precipitation hindering

Tab. 2-5   Summary of the characterisation of pebbles from the EXOTIC 8 irradiation performed in this study, with the impact of the results on ANFIBE and beyond.

CHARACTERISATION OF HIGHLY IRRADIATED BERYLLIUM FRAGMENTS FROM BR2 MODERATOR, 2nd MATRIX, CHANNEL B120			
Study 1. Gas release during out-of-pile annealing in a vacuum to the melting point (Knudsen cell / mass spectrometry)			
Measured quantities	*Performed experiments*	*Relevant quantities for ANFIBE 1*	*Relevant quantities or phenomena for further developments*
^{4}He release rate	1 at 10 K/min, 1 at 30 K/min	^{4}He integral release	Confirmation of the assessment of precipitation hindering
^{3}He release rate	1 at 10 K/min, 1 at 30 K/min		
^{3}H release rate	1 at 10 K/min, 1 at 30 K/min	^{3}H integral release, qualitative confirmation of the much higher migration of tritium atoms to grain boundaries with respect to helium atoms	Confirmation of the assessment of precipitation hindering

Tab. 2-6   Summary of the characterisation of highly irradiated beryllium samples from the disposed moderator of BR2 performed in this study, with the impact of the results on ANFIBE and beyond.

reference material for the blanket and they have been examined in a range of temperatures including the blanket operating conditions (above 700 K). The data provided by the characterisation of gas release and corresponding microstructure evolution enable to validate single parts of the gas kinetics model separately and from a microscopic point of view and to check the links between microscopic and macroscopic quantities, e.g. between gas precipitated and gas released. In particular, the identification and assessment of gas precipitation hindering enables a remarkable improvement of the description of gas release for beryllium pebbles.

Some open issues remain. Typical in-pile phenomena (e.g. irradiation induced bubble resolution) cannot be characterised in out-of-pile studies and are of fundamental importance. Nevertheless, some relevant information on in-pile precipitation can be indirectly derived from the analysis performed at End Of Irradiation. The effect of high dose is only partially characterised in this study and for a very different material from the reference pebbles. Nevertheless, the behaviour of weakly irradiated pebbles at high temperature is in some aspects similar to the expected behaviour of the same material at lower temperatures but high dose: in particular, gas release at high dose is expected to obey to the same mechanisms (formation of percolation paths with a defined structure) as observed in weakly irradiated pebbles at high temperature. Finally, the very low values of the precipitation hindering factor for tritium found in this study suggest that tritium is soluble in beryllium and that tritium solubility plays a relevant role in determining the precipitation rate.

3 Model development and validation - The version 1 of the ANFIBE code

3.1 Introduction

The ANFIBE code was developed in the years 1992-1995 in order to predict helium and tritium retention and swelling in beryllium under fast neutron irradiation in the Helium Cooled Pebble Bed (HCPB) blanket for fusion reactors. At that time the experimental database for the calibration and validation of the code was very limited and only partially relevant in respect of the foreseen application. The early version of the code, ANFIBE 0, could be calibrated only on the basis of macroscopic swelling and gas release data, since evidence on microscopic gas diffusion phenomena was not available yet. Furthermore, the material type considered was very different from the beryllium pebbles and the irradiation conditions very far from those foreseen for the HCPB blanket. The need for a revision and a more detailed validation of the code rose in the latest years, as it was observed that a remarkable quantity of tritium is produced in beryllium during irradiation in a fusion power reactor up to End-Of-Life (EOL) of the blanket modules. In case tritium were not continuously released in-pile, tritium inventory might be a killing point for the HCPB blanket, therefore tritium release from beryllium has to be reliably predicted. In spite of the continuous enlargement and improvement of the available experimental database, model extrapolation is still necessary to describe EOL conditions: in order to make the extrapolation more reliable, models have to be improved and validated with higher effectiveness and detail than in the past.

The full characterisation of irradiated beryllium and the related theoretical study of gas diffusion, precipitation and release, presented in Chapter 2, provide a detailed and coherent database for a re-calibration of ANFIBE. The characterisation of beryllium pebbles from the COBRA-1A irradiation, reported in the literature, gives a further significant contribution for the improvement and validation of the code. In the following paragraphs, the main improvements implemented in the version 1 of ANFIBE are described, with particular attention to the effect of a change in the modelling of microscopic phenomena on the prediction of macroscopic gas release. A detailed validation procedure, concerning the relationship between microscopic and macroscopic quantities, is then defined and applied. Finally, the issues which have been raised by the experimental studies and could not be solved in the frame of the present work are critically discussed in order to show the way towards a further improvement of the code.

3.2 The validation database

The benchmarks for the validation and improvement of ANFIBE, presented in the next paragraphs, are a number of transients, where the irradiation history of beryllium samples is followed in most cases by post-irradiation heating. For all benchmarks, an extended database has been made available by measurements of the actual values of a number of microscopic and macroscopic quantities described by the model, so that a direct comparison between the

measured values and the theoretical predictions is possible. The selection of the benchmarks is also based on the need to consider different types of materials and as relevant as possible for the HCPB blanket. On the basis of the experimental study presented in Chapter 2 and of other relevant studies in the literature, the following benchmarks have been selected:

From the BERYLLIUM irradiation (1994, 92 days, 780 K, 480 appm ^{4}He)*:*

1. Irradiation of BrushWellmann Fluoride Reduction Process (FRP) 2 mm diameter pebbles (mixture of capsules 5 and 8) and out-of-pile thermal ramp annealing in a vacuum at about 10 K/min (Knudsen-cell ^{4}He / ^{3}H release experiment *159bei*).

2. The same, but with out-of-pile thermal ramp annealing at about 30 K/min (Knudsen-cell ^{4}He / ^{3}H release experiment *233bei*).

The material and the related available database have been presented in Tab. 2-1 and 2-4 in Chapter 2.

From the COBRA-1A irradiation (1992-1994, 669 days, 652 K):

3. Irradiation of BrushWellmann 1 mm pebbles (C03 capsule, 2723 appm ^{4}He) and stepped annealing (^{4}He release experiment *cobraC031* and ^{3}H release experiment *cobraC033*)

4. Irradiation of NGK 1 mm pebbles (D03 capsule, 2662 appm ^{4}He) and stepped annealing (^{4}He release experiment *cobraD031* and ^{3}H release experiment *cobraD033*)

5. Irradiation of Brush Wellmann 3 mm pebbles (3165 appm ^{4}He)

The materials and the related available database are presented in Tab. 3-1 and 3-2 [Gel97] .

From the disposed moderator of Belgian Reactor 2 (BR2), 2nd matrix (1980-1995, 15 years, 19200 appm ^{4}He, 316 K):

6. Irradiation of Vacuum Hot Pressed (VHP) bricks and out-of-pile heating of fragments in a vacuum at about 10 K/min (Knudsen-cell ^{4}He / ^{3}H release experiment 232bei, Fig. 2-11)

7. The same, but with out-of-pile thermal ramp at about 30 K/min (Knudsen-cell experiment 234bei, Fig. 2-13).

The material and the related available database have been presented in Tab. 2-1 and Tab. 2-6 in Chapter 2.

Irradiation conditions	COBRA-1A 1-mm pebbles C03 capsule	COBRA-1A 3-mm pebbles C03 capsule	COBRA-1A 1-mm pebbles D03 capsule	*HCPB blanket*
Material type	Brush Wellmann pebbles, 1 mm diameter	Brush Wellmann pebbles, 3 mm diameter	NGK pebbles, 1 mm diameter	*NGK REP pebbles, 1 mm diameter*
Grain size	40 to 200 µm	40 to 200 µm	40 to 200 µm	*40 to 200 µm*
Major impurities	940 ppm BeO, 750 ppm Mg, 565 ppm Fe	200 ppm Be0, 2400 ppm Mg, 370 ppm Fe	15100 ppm BeO, 170 ppm Mg, 1100 Fe	*2300 ppm BeO, 300 ppm Mg, controlled ratios between impurities*
Irradiation time	669 days	669 days	669 days	*40000 hours (≈ 4.5 years)*
Neutron spectrum	Fast fission	Fast fission	Fast fission	*fusion*
Irradiation fluence	$5.04 \cdot 10^{26}$ m^{-2} (E > 0.1 MeV) $1.35 \cdot 10^{26}$ m^{-2} (E > 1 MeV)	$5.38 \cdot 10^{22}$ m^{-2} (E > 0.1 MeV) $1.48 \cdot 10^{26}$ m^{-2} (E > 1 MeV)	$4.98 \cdot 10^{22}$ m^{-2} (E > 0.1MeV) $1.32 \cdot 10^{26}$ m^{-2} (E > 1 MeV)	*Up to $3 \cdot 10^{26}$ m^{-2} (E > 1 MeV)*
Irradiation temperature	652 K	652 K	651 K	*770 – 1030 K*
^{4}He content	2723 appm	3164 appm	2662 appm	*Up to 25700 appm at EOI*
^{3}H content	14.9 appm at EOI (1994) 13.1 appm in 1997 (*)	16.8 appm at EOI (1994) 14.8 appm in 1997 (*)	14.6 appm at EOI (1994) 12.9 appm in 1997 (*)	*Up to 640 appm at EOI*
(*) at the time of the characterisation				

Tab. 3-1   Main material characteristics and irradiation conditions of beryllium pebbles from the COBRA-1A irradiation in EBR-II [Gel97], compared to the reference material for the solid blanket [Pia02] [Che02].

CHARACTERISATION OF IRRADIATED BERYLLIUM PEBBLES

FROM THE *COBRA-1A* IRRADIATION

1-mm Brush Wellmann pebbles, capsule C03

Measured quantitiy	*Techniques*	*Relevant quantities for the validation of ANFIBE 1*	*Relevant quantities or phenomena for further developments*
^{4}He content at EOI	Vaporisation after stepped anneal	^{4}He in-pile release	
^{3}H content at EOI		^{3}H in-pile release, pebble size effect	
Out-of-pile ^{4}He release	Stepped anneal (two different techniques)	^{4}He integral release	
Out-of-pile ^{4}He release	Vaporisation	^{4}He content, 4He in-pile release	

1-mm NGK pebbles, capsule D03

Measured quantitiy	*Techniques*	*Relevant quantities for the validation of ANFIBE 1*	*Relevant quantities or phenomena for further developments*
^{4}He content at EOI	Vaporisation after stepped anneal	^{4}He in-pile release	
^{3}H content at EOI	Melting after stepped anneal	^{3}H in-pile release, pebble size effect on gas release	
Out-of-pile ^{4}He release	Stepped anneal (two different techniques)	^{4}He out-of-pile release	
Out-of-pile ^{3}H release	Stepped anneal	^{3}H out-of-pile release	

3-mm Brush Wellmann pebbles, capsule D03

Analysis	*Techniques*	*Relevant quantities for the validation of ANFIBE 1*	*Relevant quantities or phenomena for further developments*
Density measurements at EOI		Swelling at EOI	
Microstructure at EOI	TEM	Average bubble size, bubble 3D distribution, bubble concentration, swelling.	Dislocation density. Interaction between gas precipitation and irradiation-induced dislocation kinetics
^{3}H content at EOI	Melting	^{3}H in-pile release, pebble size effect on gas release	

Tab. 3-2   Summary of the characterisation of pebbles from the COBRA-1A irradiation [Gel97], with the impact of the results on ANFIBE and beyond.

To sum up, a total of 9 in-pile and out-of-pile transients, related to 3 irradiation experiments and 5 different materials, of which 4 are pebbles, have been considered. The benchmarks from BERYLLIUM and COBRA-1A, due to the similarity of the material to the reference peb-

bles for the HCPB blanket, have been taken as a reference for model improvement. The database available for COBRA-1A is much less complete than for BERYLLIUM, but it is essential in view to the extrapolation of models because a much higher dose was reached in pebbles with different sizes.

The benchmarks from BR2, in spite of the lack of a systematic microstructure characterisation, are relevant to assess the uncertainty of the improved gas kinetics models in respect of their extrapolation to a different material at very high dose. The set of benchmarks proposed includes different materials and different irradiation temperatures and neutron fluence ranges, therefore it is suitable to verify if the improvements implemented in the models on the basis of one material are also applicable to a completely different one.

3.3 Needs for improvement of the gas precipitation model in ANFIBE 1

For the various benchmarks considered, in the description of both in-pile irradiation and out-of-pile thermal annealing, ANFIBE 0 generally underestimates macroscopic gas release. By examining in detail the prediction of the gas balance (gas in dynamic solution, in intragranular bubbles, in grain boundary bubbles, paragraph 3.10), such trend has been explained as the consequence of a general overestimation of gas precipitation into intragranular bubbles. In ANFIBE 0 gas precipitation into intragranular bubbles is described according to the classical random capture theory. The gas precipitation rate is linearly dependent on the concentration of gas in solution and no bias to the linear behaviour is considered, since the precipitation hindering factor and the gas solubility are, respectively, 1 and 0, both for helium and for tritium. The study presented in Chapter 2 (paragraph 2.5.4) has confirmed that the dependence of the precipitation rate on the concentration of gas in solution is non linear and should be described by Eq. 2-13. If linearity is maintained, a precipitation hindering factor, depending on temperature and gas concentration in dynamic solution, has to be introduced: the inverse analysis of gas release presented in Chapter 2 has shown that the precipitation hindering factor is on average much smaller than 1 and much lower for tritium than for helium. By neglecting precipitation hindering, gas precipitation is dramatically overestimated. For tritium, also in-solid solubility might play a role in reducing the precipitation rate.

The above described effects delay gas precipitation both in-pile and out-of-pile in the same way, but they are not sufficient to explain the remarkable overestimation of gas precipitation in ANFIBE 0 in the in-pile case. In the presence of a neutron flux, atom recoils, by colliding with single gas atoms trapped in intragranular bubbles, can re-inject them into the lattice and they can also destroy very small bubbles. Such radiation re-solution effects, which were not taken into account in ANFIBE 0, contribute significantly to lowering the net gas precipitation rate in-pile.

The overestimation of gas precipitation can also be related to an imprecise equation of state for helium in overpressurised bubbles, especially during their nucleation of early growth phase. For the same bubble population (average concentration N_i and radius r_i), i.e. the same intragranular sink strength $k_{sc} = \sqrt{4\pi\ r_i N_i}$, different equations of state lead to different predictions of the gas inventory in bubbles.

3.4 Solubility of helium and tritium in beryllium

3.4.1 Helium

Similarly to all other rare gases [Fas76], helium shows an extremely low solubility in metals [Lae89]. For beryllium, helium solubility has not been measured. Nevertheless, in the frame of fission reactor fuel studies also for actinide transmutation purposes, it has been seen that helium, due to its relatively small size, has a different behaviour than other rare gases produced under irradiation [Ron04b], in particular it is much more mobile. On the basis of the very low average values of the precipitation hindering factor for helium in beryllium found in the study of helium release from the pebbles from the BERYLLIUM irradiation in Chapter 2 (paragraph 2.5.4), it cannot be excluded that in the presence of very small bubbles with an internal pressure up to about 1 GPa (Chapter 2, Fig. 2-21a), helium solubility might play a non negligible role. As a matter of fact, assuming that helium solubility is described by Sievert's law, the dependence on pressure is linear, because helium gas is monoatomic:

$$c_{SHe} = S(T)p_{He} \qquad\qquad (3.1)$$

According to Eq. 3-1, between atmospheric pressure and the pressures typical of the beginning of the gas precipitation stage in beryllium, helium solubility is expected to increase up to 10000 times and even though at atmospheric pressure it is negligible, at very high pressures it could become significant.

In the absence of experimental studies on this phenomenon, in ANFIBE 1 helium solubility has been included in the precipitation hindering factor, without a separate analytical description:

$$\chi_{He} = \chi'_{He}\left(1 - \frac{c_{SHe}}{c_{He}}\right) \qquad\qquad (3.2)$$

3.4.2 Tritium

The dissolution of hydrogen from a hydrogen-enriched atmosphere into beryllium lattice is a thermally activated process and can be described by Sievert's law:

$$c_{SH} = S(T)\sqrt{p_{H_2}} = S_0\, exp\left(\frac{Q}{kT}\right)\sqrt{p_{H_2}} \qquad\qquad (3.3)$$

The solubility increases with the square root of the partial pressure of H_2 in the surrounding atmosphere p_{H2}, which implies that hydrogen dissolves in the atomic form. Among the various correlations proposed in the literature for $S(T)$, the ones by Jones & Gibson [Jon67b],
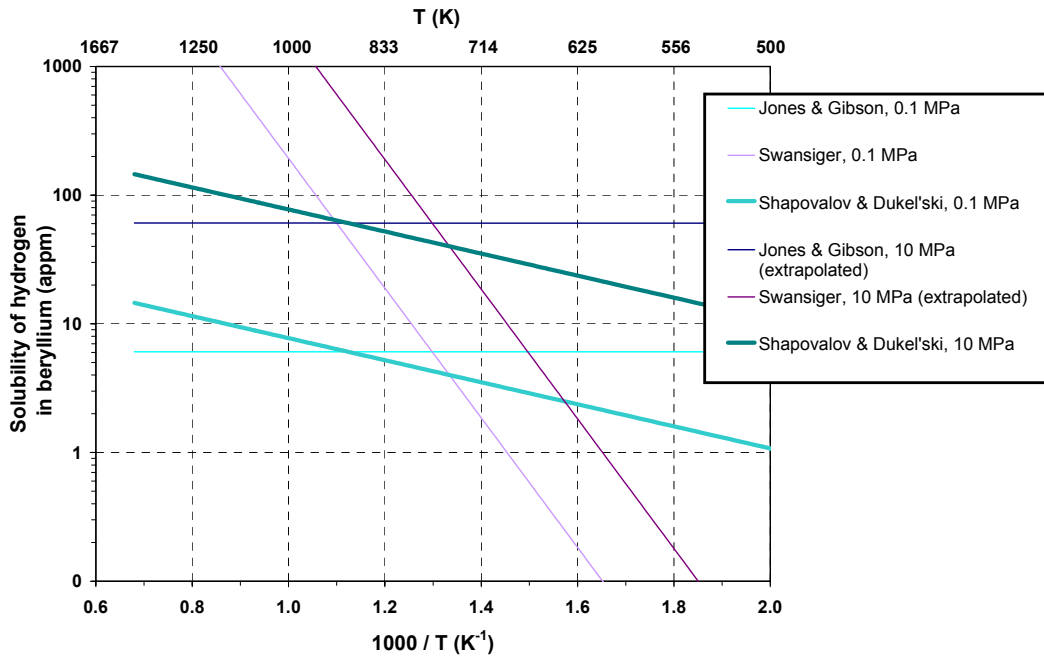
Fig. 3-1   Hydrogen solubility in α-beryllium at 0.1 and 10 MPa hydrogen partial pressure, from room temperature up to 1473 K. At 0.1 MPa, the validity range of Jones & Gibson's correlation is 673 < T< 1173 K, of Swansiger's correlation 558 < T < 783 K, of Shapovalov and Dukel'ski's correlation 673 < T < 1473 K. At 10 MPa, the correlations of Jones & Gibson and Swansinger are extrapolated.

Swansiger [Swa86] and Shapovalov & Dukel'ski [Sha88] are the most significant and often cited [Cau02] (Fig. 3-1). The last one is part of a more general study of the beryllium-hydrogen phase diagram up to 12 MPa. According to Shapovalov & Dukel'ski, the solubility of hydrogen in the hcp α-phase of beryllium, between 673 and 1473 K and up to a hydrogen partial pressure of 12 MPa, is given by the following expression:

$$c_{SH}[appm] = S(T)\sqrt{p_{H_2}} = 0.176\,exp\left(-\frac{1973}{T}\right)\sqrt{p_{H_2}\,[Pa]} \qquad \begin{array}{l} 673 < T < 1473\ K \\ \\ p_{H_2} < 12\ MPa \end{array} \qquad (3.4)$$

For the bcc β-phase, above its stability limit (1542 K at 0.1 MPa for pure beryllium), hydrogen solubility is:

$$c_{SH}[appm] = S(T)\sqrt{p_{H_2}} = 0.341\,exp\left(-\frac{2552}{T}\right)\sqrt{p_{H_2}\,[Pa]} \qquad \begin{array}{l} T_{\beta\ stable} < T < T_m \\ \\ p_{H_2} < 12\ MPa \end{array} \qquad (3.5)$$

Hydrogen solubility in beryllium increases with temperature and pressure and is higher in the bcc β-phase of beryllium than in the hcp α-phase. This is due to the fact that hydrogen atoms in the gas-in-solid phase are in interstitial positions and the number of octahedral interstices

which accommodate hydrogen atoms is 3 times higher in β-beryllium than in α-beryllium [Fas76].

In irradiated beryllium, p_{H2} is the equilibrium partial pressure of di-tritium gas $^3H_2$ in intragranular bubbles, mainly filled with helium. On the basis of the ideal gas equation of state, p_{H2} can be expressed as a function of the concentration of atomic tritium in bubbles b_H and of the average intragranular bubble concentration N_i and radius r_i :

$$c_{SH} = S(T) \sqrt{\frac{3RT}{8\pi \ N_i r_i^3}} \sqrt{b_H} \tag{3.6}$$

According to Eq. 3.6, the solubility can be calculated in principle as a function of the unknowns of the set of reaction-rate equations representing the tritium kinetics model in ANFIBE (Annex 1), provided that a separate analytical description of the precipitation hindering factor, without including the solubility effect, (i.e. of the quantity χ` in Eq. 2-5a) is possible. At present only the assessment of an averaged value of the global precipitation hindering factor, including the solubility effect, is available from the inverse analysis of tritium release performed in paragraph 2.5 for the pebbles from the BERYLLIUM irradiation. Therefore, also in order to maintain a model fully coherent with the one applied to measure key diffusion and precipitation parameters in Chapter 2, in ANFIBE 1 tritium solubility has been included in the precipitation hindering factor :

$$\chi_{3H} = \chi'_{3H} \left(1 - \frac{c_{S3H}}{c_{3H}} \right) \tag{3.7}$$

Some qualitative remarks are nevertheless possible. In the reference gas release experiments from the pebbles from the BERYLLIUM irradiation in Chapter 2, taking into account the theoretical prediction of the concentration of tritium in bubbles, the partial pressure of tritium in intragranular bubbles is some kPa. According to Eq. 3-4, tritium solubility is of the order of some appm, to be compared with the tritium inventory in the samples (about 8 appm). According to Sievert's law, an increase in the partial pressure of tritium in bubbles of 2 orders of magnitude leads in any case to an increase in the solubility of 10 times: it can be concluded that, if in the initial precipitation phase tritium solubility is negligible, it might become relevant as precipitation goes further, with the final effect of limiting or lowering the precipitation rate. Such remarkable effect of the solubility might explain the extremely low values found in Chapter 2 for the precipitation hindering factor of tritium.

3.5 The Equation Of State for helium in small bubbles

At the beginning of the gas precipitation stage, during irradiation or during out-of-pile annealing, microscopic bubbles are formed, in the range of some nanometres (Fig. 2-21a). They
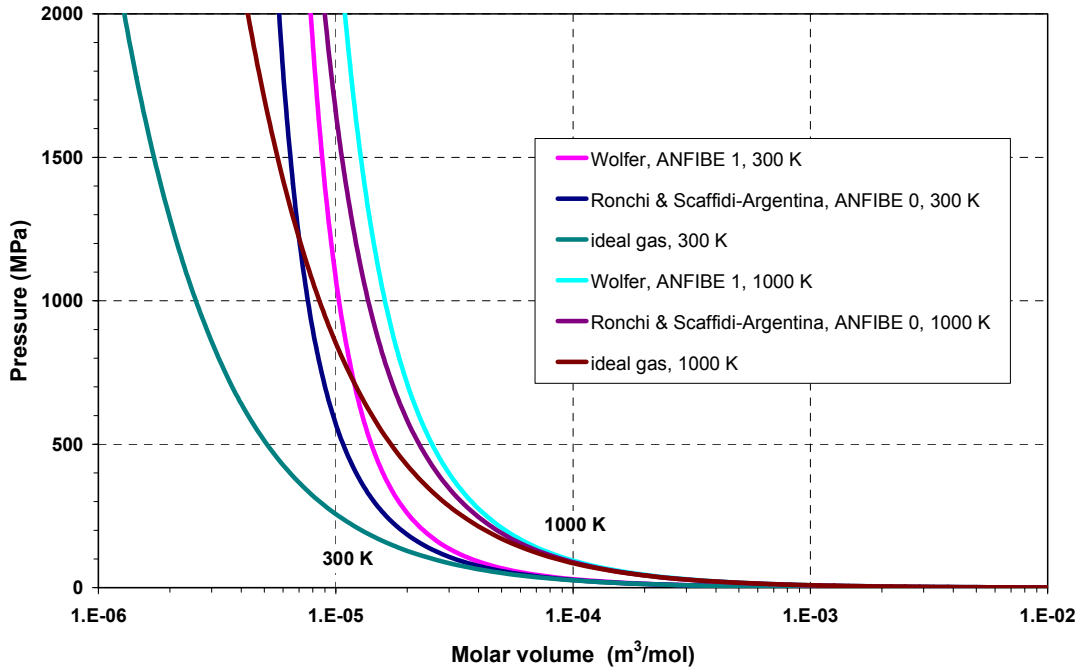
Fig. 3-2   Different Equations Of State for helium in small bubbles, compared at 300 K and 1000 K.

contain essentially helium and a very small amount of tritium. Assuming mechanical equilibrium, gas internal pressure can be assessed as:

$$p = \frac{2\sigma}{r_i} + p'$$ (3.8)

where σ is the surface tension of beryllium, r_i the bubble radius and p' the isotropic stress at the bubble surface. The surface tension is around 1 N m^{-1} [Sca98]; if the radius is of some nm, then helium pressure reaches many hundreds of MPa.

At such high pressures helium does not behave like an ideal gas, therefore a specific Equation Of State (EOS) has to be developed. The high-density EOS implemented in ANFIBE 0 was developed by Ronchi for argon, xenon and krypton [Ron81] and then modified for helium by Scaffidi-Argentina [Sca95c]. A different EOS, specifically developed for small helium bubbles in beryllium by Wolfer [Wol81] [Ver72a] [Ver72b] on the basis of Beck's helium-helium interaction potential, has been implemented in ANFIBE 1. Wolfer's EOS has the following expression:

$$\frac{p}{\rho \, kT} = z(p,T)$$ (3.9)

The compressibility z is a function of the effective hard-sphere diameter of the helium atom, computed on the basis of Beck's potential and of the gas density ρ : the detailed analytical expression and iterative calculation procedure are reported in [Wol81]. Wolfer's EOS has been implemented in a subroutine called HELEOS, which substitutes in ANFIBE 1 the subroutine EOSCOM of ANFIBE 0.

In Wolfer's EOS the effective helium atom diameter decreases with increasing temperature and pressure, whilst in Van der Waals' law helium diameter is fixed, therefore pressure in Wolfer's EOS is lower than in Van der Waals' EOS. A further consequence of Wolfer's model is that the number of helium atoms in a small bubble with a certain equilibrium radius is nearly independent of temperature.

Wolfer's EOS is 'harder' than the one implemented in ANFIBE 0 (Fig. 3-2), therefore a certain population of bubbles (e.g. in Fig. 2-21a) contains a smaller gas amount, with the following consequence: for the same intragranular sink strength (i.e. the same bubble radius and concentration) the amount of gas precipitated is lower. This is in agreement with the experimental observations in Chapter 2.

3.6 Precipitation hindering

The inverse analysis of gas release presented in Chapter 2 has confirmed that gas precipitation into intragranular bubbles is significantly slower than predicted by the linear model in Eq. 2-1. In other words, the assumption of a linear dependence of gas precipitation on the concentration of gas in solution leads to the overestimation of gas precipitation and correspondingly to a dramatic underestimation of gas release. In order to maintain a linear model, a precipitation hindering factor, depending on concentration and temperature, has to be introduced. The analysis presented in Chapter 2 has made it possible to assess an average value of the precipitation hindering factor for helium and for tritium, for pebbles from the BERYLLIUM irradiation, during a certain class of out-of-pile temperature transients (thermal ramp annealing at 10 or 30 K/min): such average values have been introduced in the ANFIBE code separately in the helium kinetics model and in the tritium kinetics model (Annex A):

$$\chi_{4He} = 1.0 \cdot 10^{-3} \tag{3.10}$$

$$\chi_{3H} = 1.5 \cdot 10^{-6} \tag{3.11}$$

In the absence of data allowing for a full analytical description of the dependence of χ on temperature and concentration of gas atoms in solution, as well as on solubility, the assumption of a constant precipitation hindering in ANFIBE 1 is the most reasonable analytical approach that can be attempted at present. In the past no description of precipitation hindering was possible, due to the lack of a proper experimental characterisation of microscopic gas diffusion phenomena.

3.7 Radiation re-solution

Solubility of gas-in-solid defines the equilibrium concentration of single gas atoms in the lattice in the lowest possible energetic configuration and in the presence of a precipitated gas phase in the form of bubbles. Since, however, the gas pressure in bubbles, and hence the gas free energy, is not pre-fixed, but rather defined by the strong capillarity restraints acting on the bubble surface, the equilibrium concentration of gas-in-solid depends in a complex way on the mechanical equilibrium in the bulk. Since the concept of solubility is implicitly associated to diffusion phenomena in solid, any diminution of the capillarity pressure due to diffusion effects (for instance, bubble random coalescence) leads to a decrease in the free energy of the gas in bubbles and hence to a lower equilibrium concentration of the gas-in-solid with a consequent augmentation of the amount precipitated. Thus, strictly speaking, a solid subjected to self-diffusion processes containing oversaturated gas, will only reach thermodynamic and mechanical equilibrium when all the gas is expanded to the ambient pressure. Due to the very low density of gas, this would entail an enormous swelling of the solid. In most cases, this does not occur since gas porosity grows anisotropically to form vented channels through which gas escapes to the ambient; however, in some plastic materials gas swelling may lead to foam-like structures with large porosities and high gas retention. Though self-diffusion in solid is normally very slow, any crystal containing oversaturated gas does significantly expand only over very long times. This is, for instance, the case of beryllium pebbles in the blanket of a fusion reactor, since they are irradiated for several years.

An in-pile effect, however, increases the apparent solubility limits of gas-in-solid, due to elastic or inelastic collisions of lattice atoms with fast neutrons. The recoils created directly or through nuclear reactions spend their energy in collisions leading to ionisation and lattice displacement cascades. The first losses are converted into heat, whilst the latter create point defects as well as an effective radiation-enhanced self-diffusion. Since the lattice atoms are displaced by collision energies far above the thermal levels, radiation enhanced diffusion produces homogenisation effects, including re-solution of precipitated phases, and, particularly, gas bubbles. These effects are well known in nuclear fuels, where the displacement rate is very high and the residence time of a fission gas atom in bubbles is of the order of only a few hours at fission rates of the order of 10^{19} m^{-3} s^{-1}. Thus, a re-solution rate of the gas precipitated in bubbles can be calculated from the dpa rate (or, as an alternative, from the nuclear reaction or recoil atom generation rate) and validated experimentally by measuring the dynamic solubility of the gas, i.e., the concentration of gas frozen in the lattice under conditions of low thermal diffusion. The re-solution rate frequency η (s^{-1}), which is the inverse of the average residence time of gas atoms in a bubble, is described in ANFIBE [Sca95c] as proportional to the generation rate of recoil helium atoms from nuclear reactions β, which is an input datum for the code, in particular:

$$\eta = \frac{\eta_0}{\beta_0}\beta = \frac{1.36 \cdot 10^{-7}}{4.2 \cdot 10^{-6}}\beta \tag{3.12}$$

According to Eq. 3-12, at a helium generation rate β_0 of $4.2 \cdot 10^{-6}$ mol m^{-3} s^{-1} in beryllium, the residence time of a helium atom in an intragranular bubble $1/\eta_0$ is about 2000 hours. Such value has proved to give good predictions of the gas precipitated at End-Of-Irradiation for all irradiation histories considered in the validation of ANFIBE 1(Tab. 3-3).

Furthermore, recoil atoms can completely destroy intragranular bubbles below a certain critical size and consequently affect their concentration (Eq. A-5, Annex A). The bubble destruction frequency η^* (s^{-1}) is described in ANFIBE [Sca95c] as proportional to the resolution frequency (i.e. to the helium generation rate) and to the inverse of the bubble radius:

$$\eta^* = 10 \; \eta \frac{r_0}{r_i} = 10 \; \eta \frac{3.8 \cdot 10^{-10}}{r_i} \tag{3.13}$$

According to Eq. 3-13, the bubble destruction frequency η^* is 10 times the gas atom re-solution frequency η if the average radius of bubbles r_i is about 0.4 nm. The influence of radiation re-solution on gas release and swelling in beryllium is expected to be important only at intermediate temperatures, where atomic mobility is sufficiently high to produce precipitation, and sufficiently low to prevent migration to the grain boundary.

From the point of view of the general gas kinetics model in ANFIBE 1 (Annex A), in the presence of radiation re-solution, the term ηb appears in-pile as a sink in the equation which describes the concentration of helium or tritium in intragranular bubbles b (Eq. A-2) and correspondingly as a source in the equation for the concentration of gas-in-solid c (Eq. A-1). The bubble destruction term - $\eta^* N_i$ appears as a sink in the equation which describes the concentration intragranular bubbles N_i (Eq. A-5).

3.8   Effect of free surfaces on gas release

The measurement of tritium inventory after irradiation in 1-mm and 3-mm pebbles from CO-BRA-1A irradiation [Gel97] provided quantitative evidence that gas release is affected by the pebble size: smaller pebbles have higher release (Tab. 3-3, Chapter 3). This trend was confirmed also out-of-pile by the comparison of tritium release from 2 mm and 0.1-0.2 mm pebbles from the BERYLLIUM irradiation [Sca97c].

Considering that pebbles, independently from size and production method, always have coarse grains (40 –200 micron), an explanation of this phenomenon in agreement with the general gas release model in ANFIBE can be attempted.

Assuming spherical grains and the absence of open porosity inside the pebble, the release probability due to free surfaces P_{fs} is:

$$P_{fs} = \frac{free \; surface}{grain \; boundary \; surface} \approx \frac{4\pi \; R^2}{4\pi \; \alpha^2 N_g} \tag{3-14}$$

R is the pebble radius, α the average grain radius and N_g the number of grains in the pebble, which can be assessed as follows:

$$N_g \approx \frac{pebble\ volume}{grain\ volume} = \frac{R^3}{\alpha^3} \tag{3-15}$$

From Eq. 3-14 and Eq. 2-15 it can be concluded that:

$$P_{fs} \approx \frac{\alpha}{R} \tag{3-16}$$

In the assumption that grain size in pebbles of any radius is similar, in the absence of percolation paths the ratio of gas release is the inverse ratio of pebble radii. In materials with fine grains, P_{fs} tends to 0: as a matter of fact for such materials the free surface effect is not relevant and gas can be released only in the presence of percolation paths inside the grains.

Nevertheless, in Eq. 3-16, beside the pebble size, also the grain size plays a role. Since pebbles are melting products, it is reasonable to expect that smaller pebbles tend also to have smaller grains because the cooling is faster. As a matter of fact, it has been recently observed that in NGK pebbles of different diameter the grains frequently extend to the centre of the pebble [Moe03].

In the version 1 of the ANFIBE code, in order to keep a model coherent with the one adopted for the inverse analysis of the experimental gas release curves presented in paragraph 2.5.1, the percolation probability is assumed to be always 1, i.e. gas atoms are supposed to be released as soon as they reach grain boundaries. Such assumption would be exact if a pebble consisted in only one grain and, on the basis of the results of paragraph 2.5, it has been proven to be satisfactory for small pebbles with large grains.

3.9   Validation of ANFIBE 1

3.9.1 The validation procedure

For the ANFIBE code version 1 an *integrated macroscopic/microscopic validation procedure* has been defined and applied, which is presented in Fig 3-3. The method considers in parallel macroscopic (gas release) and microscopic quantities which appear in the differential equations of the analytical model (e.g. precipitation rate, gas balance, bubble population characteristics), thus enabling a direct comparison and understanding of the relationship between the global effect and a number of individual phenomena which contribute to it. Such a
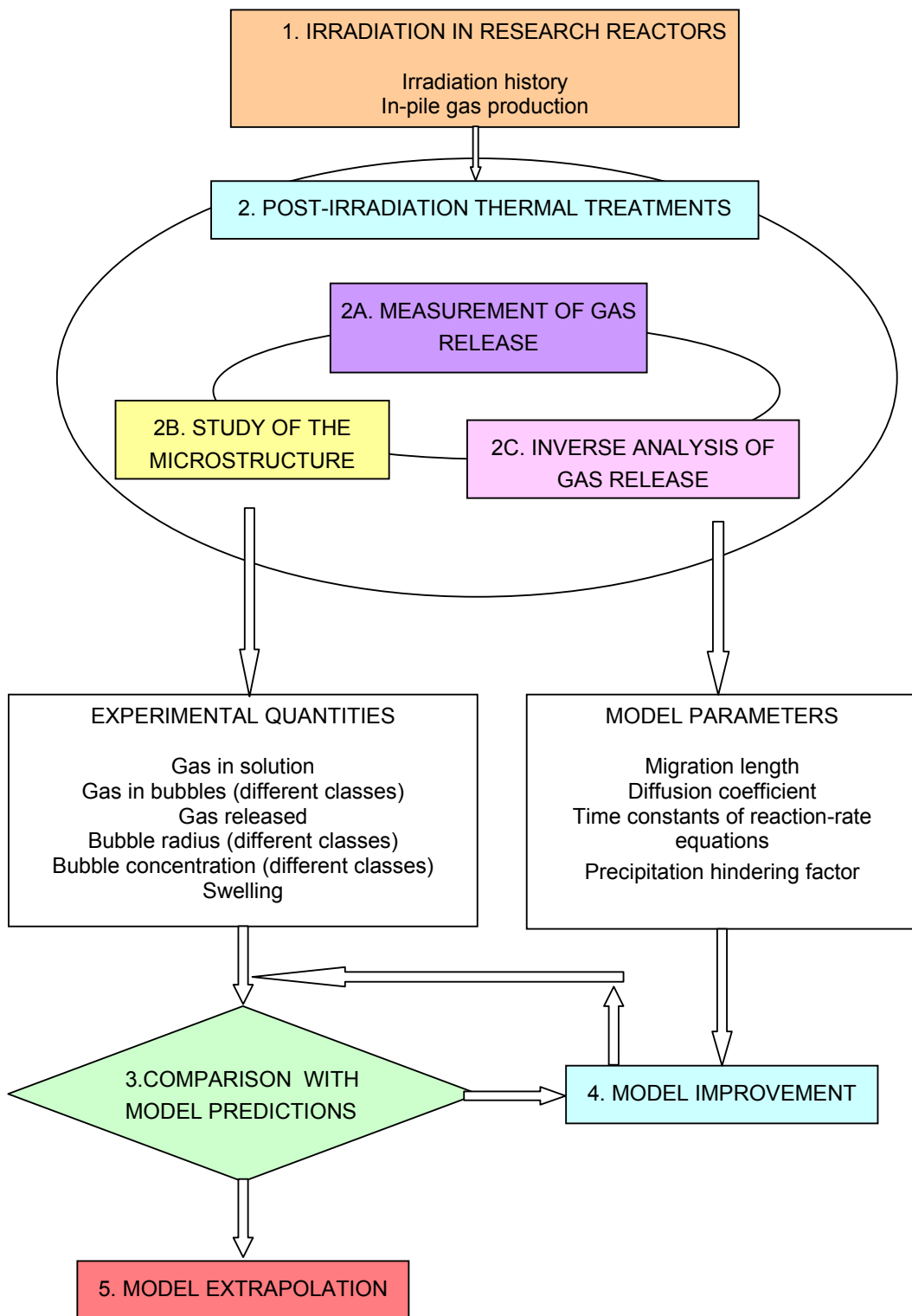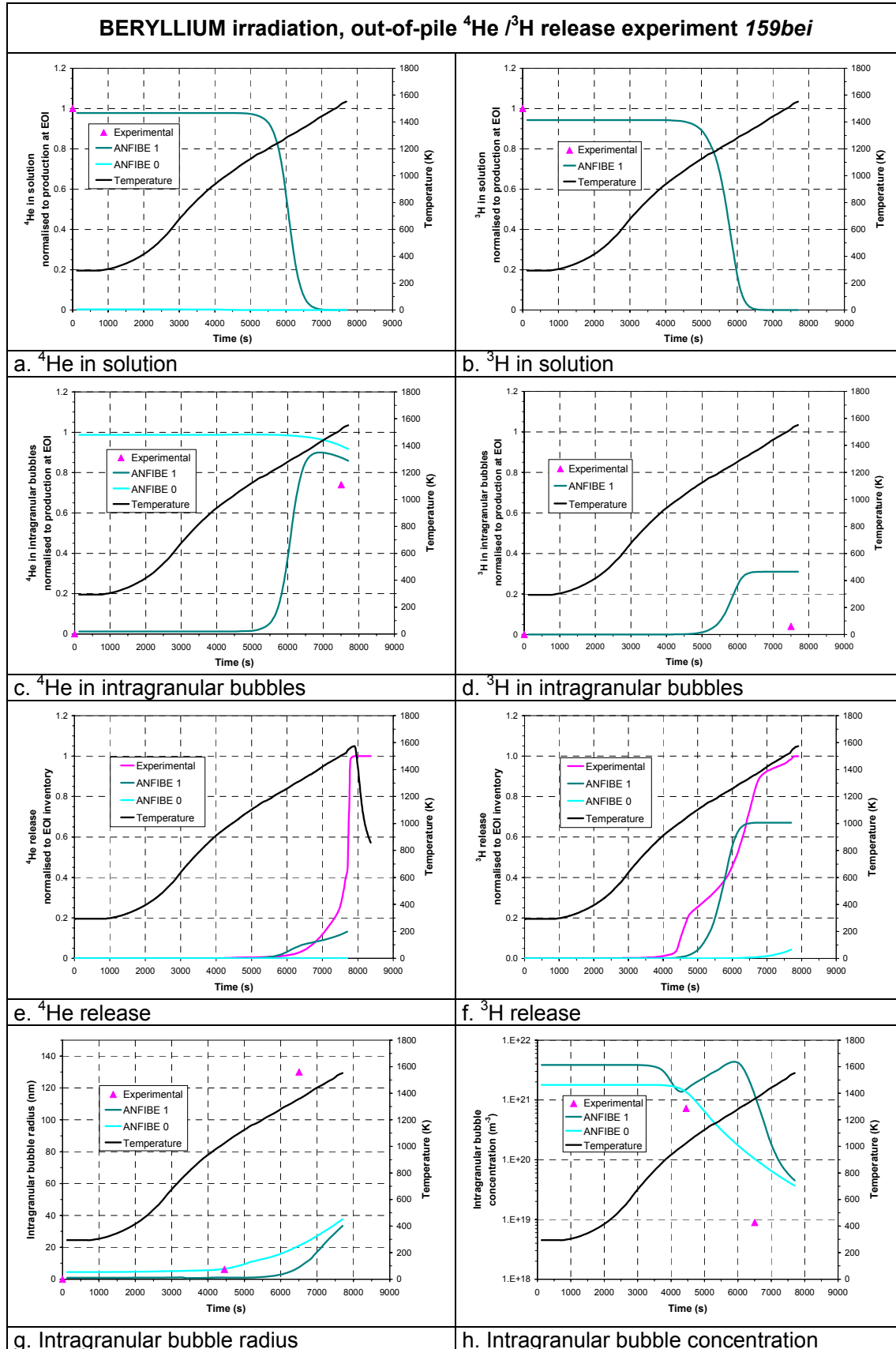
Fig. 3-3   The integrated macroscopic/microscopic validation procedure applied in this work
            for the development of the version 1 of the ANFIBE code.

Quantity		BERYLLIUM	COBRA-1A C03 3-mm pebbles	COBRA-1A C03 1-mm pebbles	COBRA-1A D03 1-mm pebbles	BR2 moderator 2nd matrix, channel B120
^{4}He in solution (% of production)	Experimental	≈100 % (*)	n.q.	n.q	n.q.	n.a.
c_{4He}	ANFIBE 0	0.27 %	0.05 %	0.05 %	0.05 %	0 %
	ANFIBE 1	97.9 %	83.3 %	83.9 %	84.0 %	98.9 %
^{4}He in intragranular bubbles (% of production)	Experimental	≈ 0 (*)	n.a.	n.a.	n.a.	n.a.
b_{4He}	ANFIBE 0	98.7 %	99.4%	99.4%	99.4 %	99.8 %
	ANFIBE 1	1.25 %	13.1 %	12.7 %	12.7 %	0.71 %
^{4}He in-pile release (% of production)	Experimental	≈ 0 %	≈ 0 %	≈ 0 %	≈ 0 %	≈ 0 %
	ANFIBE 0	≈ 0 %	≈ 0 %	≈ 0 %	≈ 0 %	≈ 0 %
(= ^{4}He at grain boundaries g_{4He} in ANFIBE 1)	ANFIBE 1	0.88 %	3.55 %	3.26 %	3.24 %	0.3 %
^{3}H in solution (% of production)	Experimental	≈100 % (*)	n.a.	n.a.	n.a.	n.a.
c_{3H}	ANFIBE 0	n.a.	n.a.	n.a.	n.a.	n.a.
	ANFIBE 1	94.3 %	98.1 %	98.1 %	98.3 %	100 %
^{3}H in intragranular bubbles (% of production)	Experimental	≈ 0 (*)	n.q.	n.q.	n.q.	n.a.
b_{3H}	ANFIBE 0	n.a.	n.a.	n.a.	n.a.	n.a.
	ANFIBE 1	0.002 %	≈ 0 %	≈ 0 %	≈ 0 %	≈ 0 %
^{3}H in-pile release (% of production)	Experimental	n.a.	7 %	27 %	29 %	n.a.
	ANFIBE 0	0.16 %	0.08 %	0.09 %	0.5 %	0.12 %
(= ^{3}H at grain boundaries g_{3H} in ANFIBE 1)	ANFIBE 1	5.70 %	1.95 %	1.88 %	1.73 %	0 %
Intragranular bubble radius (nm)	Experimental	≈ 0 (*)	11.9	n.a.	n.a.	n.a.
r_i	ANFIBE 0	4.5	6.9	6.9	6.9	1.44
	ANFIBE 1	1.1	2.8	2.2	2.2	0.2
Intragranular bubble concentration (m^{-3})	Experimental	n.q. (*)	$2.0 \cdot 10^{22}$	n.a.	n.a.	n.q. (*)
N_i	ANFIBE 0	$1.78 \cdot 10^{21}$	$3.3 \cdot 10^{21}$	$3.3 \cdot 10^{21}$	$3.2 \cdot 10^{21}$	$1.4 \cdot 10^{24}$
	ANFIBE 1	$2.1 \cdot 10^{21}$	$3.6 \cdot 10^{22}$	$3.1 \cdot 10^{22}$	$3.0 \cdot 10^{22}$	$4.0 \cdot 10^{24}$
Intragranular sink strength (m^{-1})	Experimental	Finite (*)	$5.5 \cdot 10^7$	n.a.	n.a.	n. a.
$k_{sc} = (4\pi r_i N_i)^{0.5}$	ANFIBE 0	$1.0 \cdot 10^7$	$1.7 \cdot 10^7$	$1.7 \cdot 10^7$	$1.7 \cdot 10^7$	$1.6 \cdot 10^7$
	ANFIBE 1	$5.6 \cdot 10^6$	$3.2 \cdot 10^7$	$2.9 \cdot 10^7$	$2.9 \cdot 10^7$	$1.1 \cdot 10^8$
Swelling (%)	Experimental	≈ 0 %	1.45 % (1% due to intragranular bubbles)	n.a.	n.a.	n.a.
	ANFIBE 0	0.07 %	0.5 %	0.5 %	0.4 %	1.75 %
	ANFIBE 1	0.0013 %	0.17 %	0.13 %	0.13 %	0.02 %

(*) Gas atoms trapped in the vicinity of dislocations, which act as nucleation sites

n.a. = not available, n. q. = not quantifiable

Tab. 3-3   *ANFIBE validation in-pile.* The available experimental data at End-Of-Irradiation ([Gel97], this study) are compared to the predictions of ANFIBE 0 and 1.

BERYLLIUM irradiation, out-of-pile ^{4}He /^{3}H release experiment *159bei*

a. ^{4}He in solution

b. ^{3}H in solution

c. ^{4}He in intragranular bubbles

d. ^{3}H in intragranular bubbles

e. ^{4}He release

f. ^{3}H release

g. Intragranular bubble radius

h. Intragranular bubble concentration

| i. Intragranular sink strength | j. Swelling |
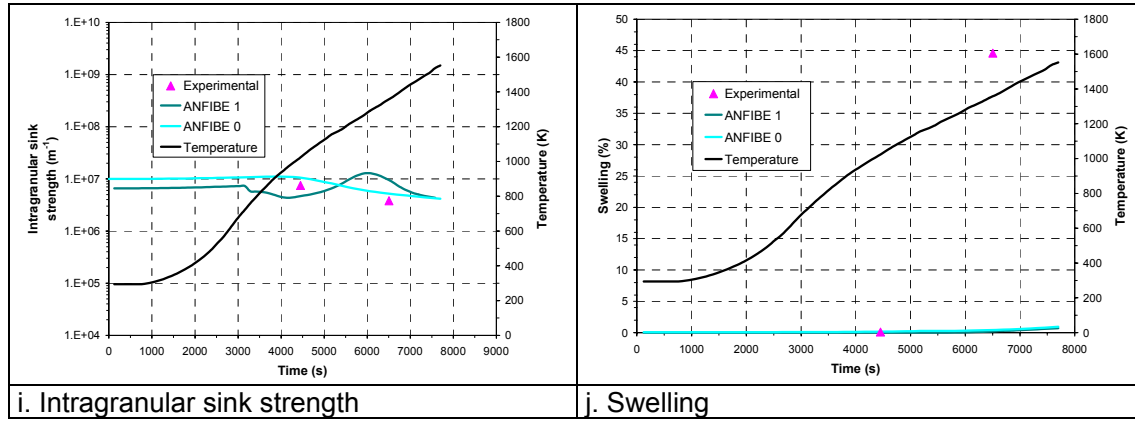
Fig. 3-4   *ANFIBE validation out-of-pile. BERYLLIUM irradiation, benchmark 159bei.* The predictions of ANFIBE 0 and 1 of gas balance, gas release and microstructure are compared to the available experimental data (from Chapter 2 of this study).

detailed validation methodology, which has a general validity in the field of modelling of gas retention and release in nuclear materials, is applied here for the first time.
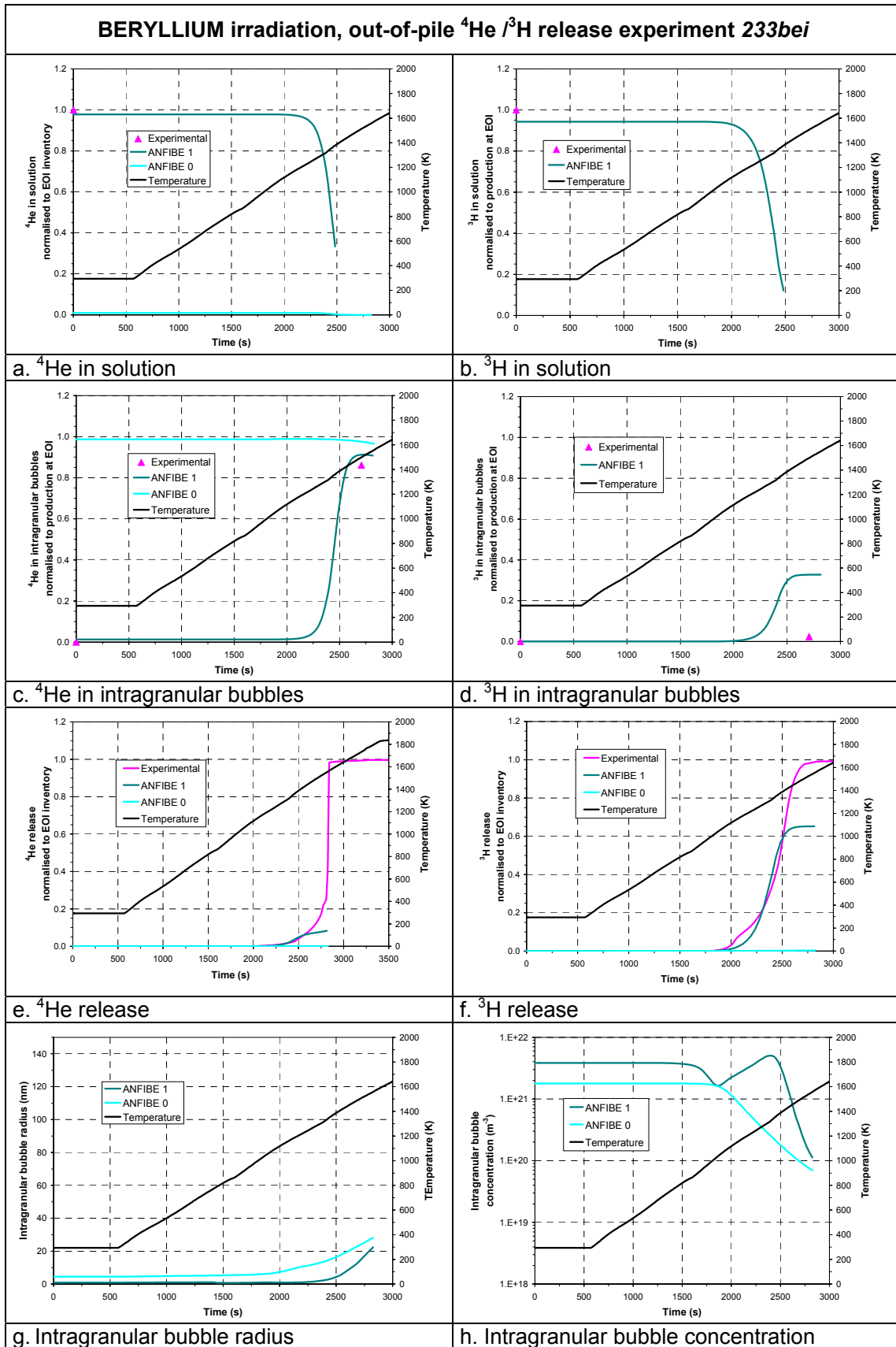
The high level of detail and coherency of the method increase the reliability in the extrapolation of the models and make it also possible to identify necessary theoretical improvements and the experiments needed to validate them.

Though the procedure is in this study applied only to a limited set of quantities and model parameters, which is not exhaustive of the whole analytical model of helium and tritium kinetics and swelling in the ANFIBE code (Annex A), the progress allowed in the prediction of some key quantities as helium and tritium release is remarkable.

3.9.2 Results

In the next pages the predictions of the ANFIBE code version 1 are compared to the available experimental data and, where possible due to the very different output subroutines, to the predictions of ANFIBE 0, for the different benchmarks listed in paragraph 3.2, for helium and tritium kinetics, bubble population and swelling. Tab. 3-3 sums up the available results in-pile (at End-Of-Irradiation, EOI) and Figs. 3-4 to 3-11 collect those during out-of-pile annealing in form of viewgraphs. In particular, gas release is presented in relation with other gas balance quantities (gas in dynamic solution, in intragranular bubbles, at grain boundaries) and with the evolution of the intragranular bubble population. The prediction of the intragranular sink strength, which is proportional to the gas precipitation rate into intragranular bubbles since the precipitation hindering factor has been taken as constant (1 in ANFIBE 0, the values measured in paragraph 2.5.4 in ANFIBE 1), is also shown.

All gas release values have been normalised to the inventory at the beginning of the out-of-pile annealing, with the exception of tritium release experiments cobraC033 and cobraD033,

BERYLLIUM irradiation, out-of-pile ^{4}He /^{3}H release experiment *233bei*

a. ^{4}He in solution

b. ^{3}H in solution

c. ^{4}He in intragranular bubbles

d. ^{3}H in intragranular bubbles

e. ^{4}He release

f. ^{3}H release

g. Intragranular bubble radius

h. Intragranular bubble concentration

| i. Intragranular sink strength | j. Swelling |
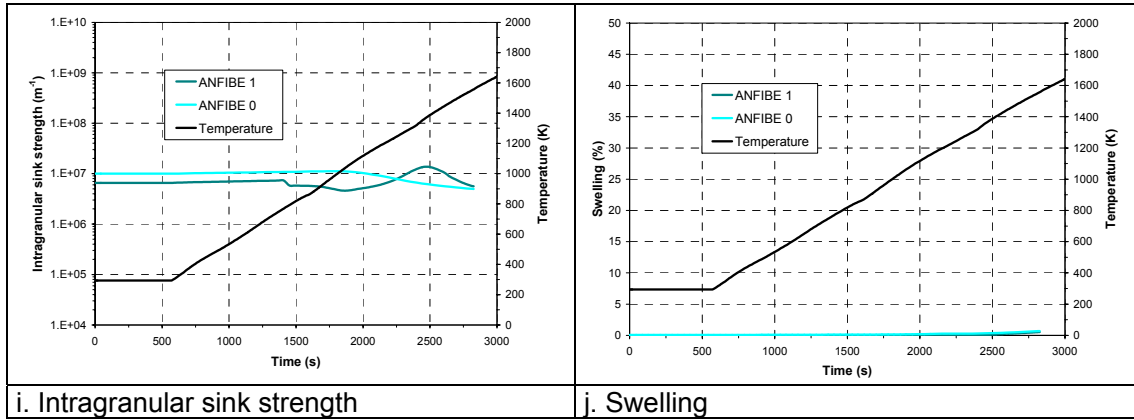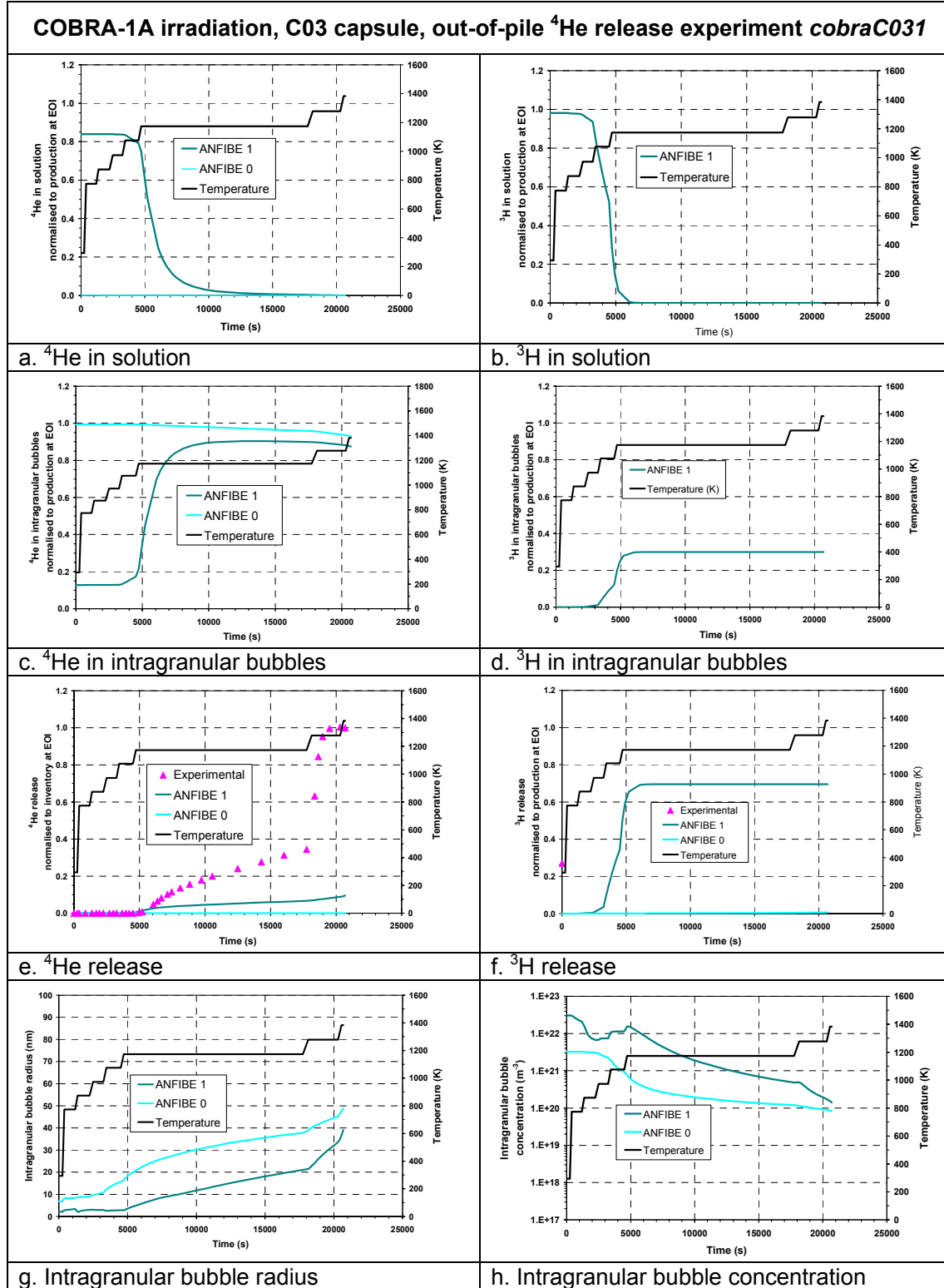
Fig. 3-5   *ANFIBE validation out-of-pile. BERYLLIUM irradiation, benchmark 233bei.* The predictions of ANFIBE 0 and 1 of gas balance, gas release and microstructure are compared to the available experimental data (from Chapter 2 of this study).

where the measurement of tritium inventory at EOI (Tab. 3-3) made it possible to compare predicted and measured tritium release, normalised to the production during irradiation.

3.9.2.1 BERYLLIUM

For the BERYLLIUM irradiation, an absolute measurement of the inventory of helium and tritium in the samples at EOI (related to the in-pile release) is not available, therefore in Fig. 3-4 and Fig. 3-5 the experimental values of the gas balance quantities are normalised to the inventory at the beginning of the thermal ramp, measured as the integral of the experimental gas release curve, whilst ANFIBE predictions are normalised to the calculated inventory at the beginning of the thermal ramp, which depends on in-pile production, in-pile release and, for tritium, following out-of-pile decay. Since ANFIBE predicts a negligible in-pile release, the results of the two normalisations can be directly compared.

It can be observed that already during irradiation but even more during the thermal ramp annealing, the predictions of ANFIBE 0 and ANFIBE 1 are remarkably different. According to ANFIBE 0 practically the whole gas inventory precipitates already in-pile into intragranular bubbles (Tab. 3-3), as a consequence, during the thermal ramp, release is extremely low, in contrast with the experimental observations, because intragranular bubbles are little mobile. The small gas release at high temperature appears to be due not to atom migration to grain boundaries, but to intragranular bubble migration, which is responsible for a decrease of the inventory of gas in bubbles (Fig. 3-4c). After the correction of the in-pile and out-of-pile pre-cipitation model, ANFIBE 1 presents a much better prediction capability: it correctly predicts that at EOI most part of the gas inventory is still in dynamic solution in the lattice, therefore it can be easily released, as soon as the temperature increases, by atom migration to grain boundaries. For both helium and tritium, a fast precipitation into intragranular bubbles occurs at the same time, of the order of the experimental observations: this phenomenon limits the release at high temperature, since the intragranular bubble venting observed at 1500 K

77

COBRA-1A irradiation, C03 capsule, out-of-pile ^{4}He release experiment *cobraC031*

a. ^{4}He in solution

b. ^{3}H in solution

c. ^{4}He in intragranular bubbles

d. ^{3}H in intragranular bubbles

e. ^{4}He release

f. ^{3}H release

g. Intragranular bubble radius

h. Intragranular bubble concentration

| i. Intragranular sink strength | j. Swelling |
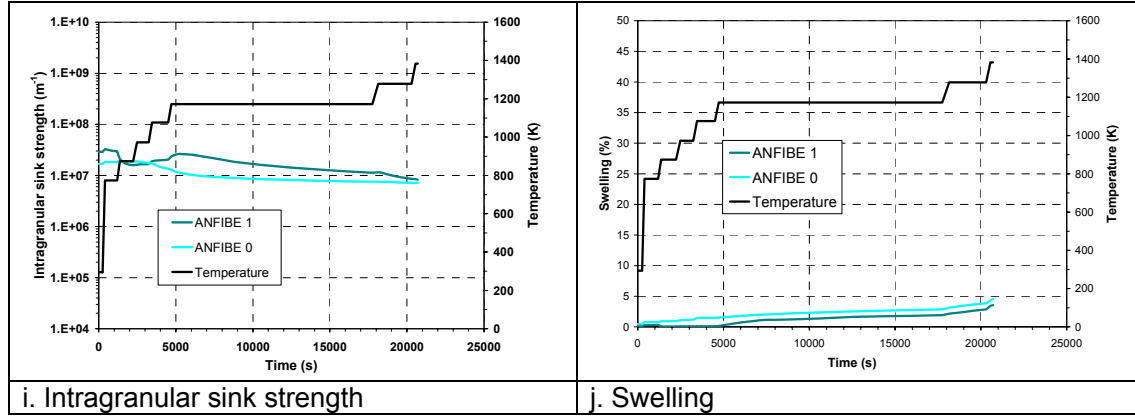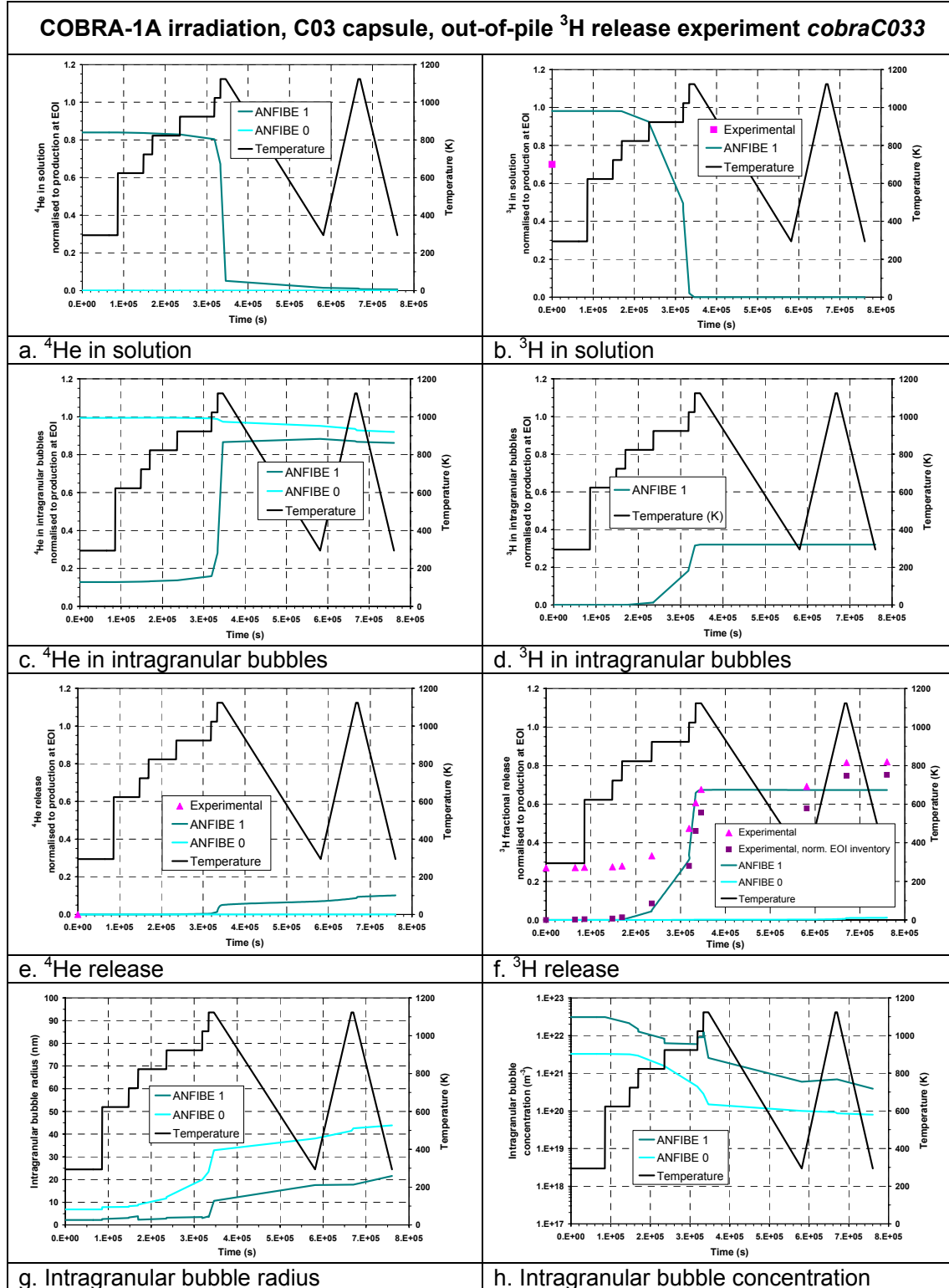
Fig. 3-6   *ANFIBE validation out-of-pile. COBRA-1A irradiation, benchmark cobraC031.* The predictions of ANFIBE 0 and 1 of gas balance, gas release and microstructure are compared to the available experimental data from [Gel97].

(paragraph 2.3.2, Fig. 2-3) is not included in the model. For tritium ANFIBE 1 correctly predicts that precipitation is much slower than for helium, but it is in absolute terms still too fast in respect of the experimental data: the limit value is about 30% instead of the some percent observed. The excessive tritium precipitation (Fig. 3-4d) corresponds to the defect in the prediction of tritium release in the same range of temperatures (Fig. 3-4f). In respect of the extrapolation to reactor conditions, this implies that tritium release is not overestimated by ANFIBE 1.

As far as the bubble population characteristics (radius and concentration) are concerned, ANFIBE 1 gives better predictions at EOI, since the bubbles of 5 nm diameter predicted by ANFIBE 0 (Tab. 3-3) are not experimentally observed (Fig. 2-19b). Nevertheless, during the thermal ramp ANFIBE 1 underestimates bubble growth (Fig. 3-4g) and coalescence (Fig. 3-4h). This is related to the prediction of a high concentration of gas in solution c, which implies a high bubble nucleation rate, since this is proportional to c^2 (Eq. A-5, Annex A). Therefore, with a lower inventory of gas precipitated, much smaller bubbles and much lower swelling than in ANFIBE 0 are predicted. The model of bubble nucleation, growth and coalescence in ANFIBE 1 needs to be re-calibrated. At 1500 K both ANFIBE 0 and 1 dramatically underestimate bubble growth and swelling, probably due to fact that the creep law implemented in the code does not take into account the deterioration of beryllium mechanical properties at such temperatures.

As far as the intragranular sink strength is concerned, which is proportional to bubble radius and concentration, both ANFIBE 0 and ANFIBE 1 predict that, in spite of the large change in bubble radius and concentration during the thermal ramp, their product remains of the same order of magnitude. Such prediction is in agreement with the experimental observation in paragraph 2.5.3, which had enabled to assess an average value of the precipitation hindering factor, and provides a further confirmation of it. The constancy of the intragranular sink strength implies that, without precipitation hindering, the precipitation rate would remain roughly constant during the thermal ramp and that intragranular swelling occurs. Since the

COBRA-1A irradiation, C03 capsule, out-of-pile ^{3}H release experiment *cobraC033*

a. ^{4}He in solution

b. ^{3}H in solution

c. ^{4}He in intragranular bubbles

d. ^{3}H in intragranular bubbles

e. ^{4}He release

f. ^{3}H release

g. Intragranular bubble radius

h. Intragranular bubble concentration

| i. Intragranular sink strength | j. Swelling |
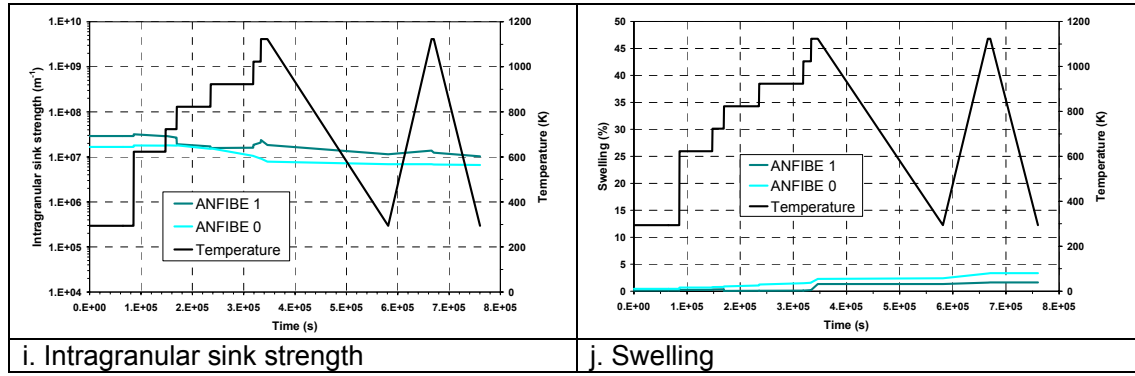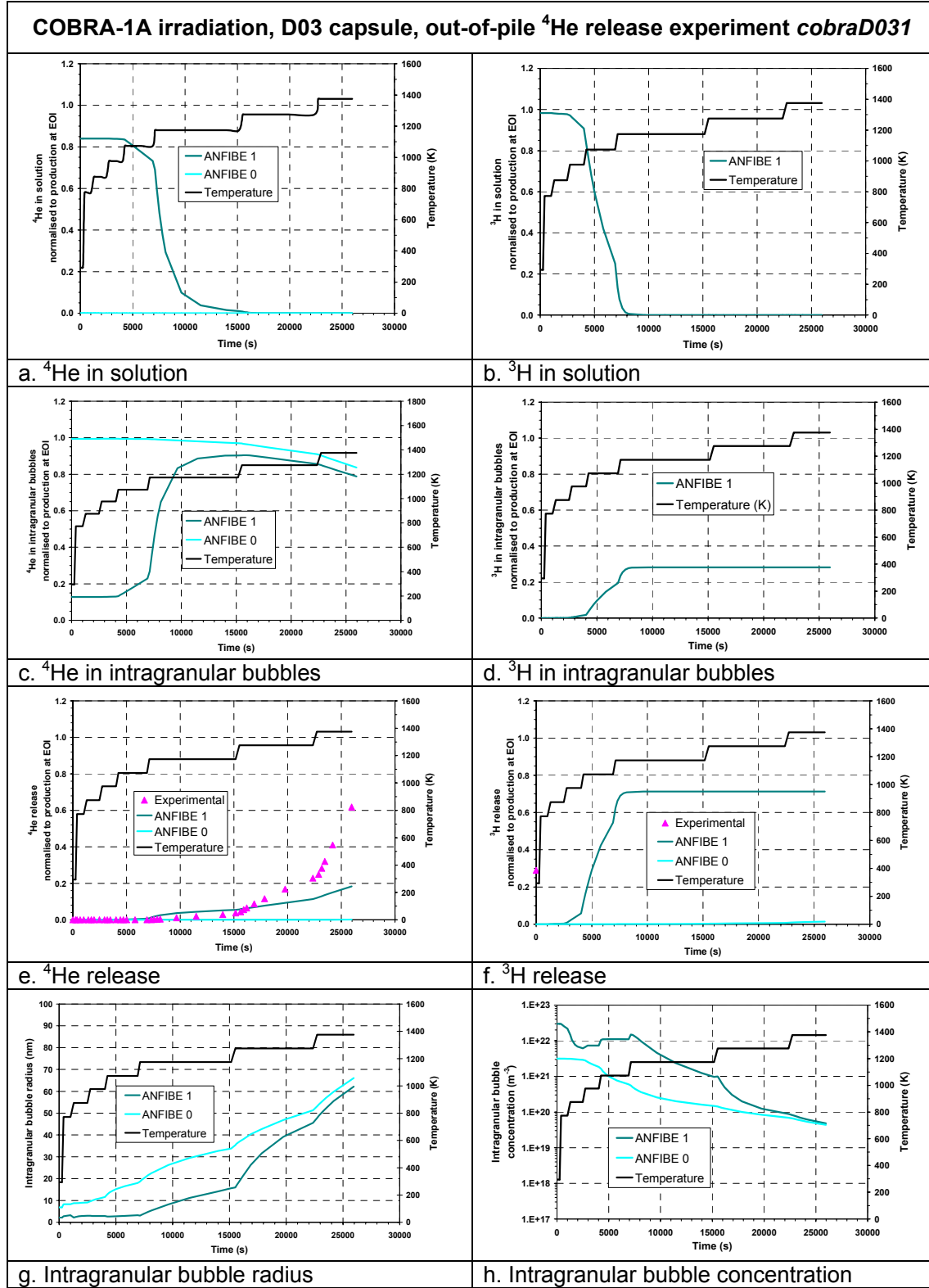
Fig. 3-7　　*ANFIBE validation out-of-pile. COBRA-1A irradiation, benchmark cobraC033. The predictions of ANFIBE 0 and 1 of gas balance, gas release and microstructure are compared to the available experimental data from [Gel97].*

intragranular sink strength is correctly predicted and in ANFIBE the calculation of bubble parameters follows from the calculation of gas balance, it is not expected that the prediction of gas balance is much affected by the unsatisfactory description of bubble growth and coalescence.

By comparing the benchmark 233bei (Fig. 3-5) with the benchmark 159bei (Fig. 3-4), the effect of a faster heating transient on ANFIBE predictions can be judged. All macroscopic and microscopic quantities and their trends remain qualitatively similar, but the prediction of helium and tritium release by ANFIBE 1 further improves, e.g. tritium release is no longer underestimated for temperatures lower than 1200 K (Fig. 3-4f and Fig. 3-5f).

3.9.2.2 COBRA-1A

For the pebbles irradiated in COBRA-1A, the average grain size has not been measured in the Post Irradiation Examinations (PIE) [Gel97]; therefore ANFIBE predictions are based on the assumption that the microstructure of both BrushWellmann and NGK pebbles is similar to the pebbles from the BERYLLIUM irradiation, i.e. the characteristic migration length is 100 microns. The PIE of COBRA-1A are not exhaustive for the application of the integrated microscopic/macroscopic validation procedure, because helium and tritium release were measured separately in very different annealing experiments and the corresponding microstructure evolution was not examined. Nevertheless, since EOI fluence and gas production in COBRA-1A are much larger than in BERYLLIUM (3000 appm ^{4}He instead of 480), COBRA-1A provides the opportunity to check the possibility to extrapolate ANFIBE 1 to higher fluence for pebbles similar to the reference material for the blanket, also in out-of-pile release experiments with a different heating transient (step instead of thermal ramp annealing). Furthermore, for COBRA-1A the only available data on in-pile tritium release for 1-mm pebbles were obtained, by measuring the tritium inventory at EOI and comparing it to the calculated in-pile production (Tab. 3-1). Such datum is a starting point to assess the reliability of ANFIBE predictions of tritium release also in-pile for pebbles, though many other data would be needed to prove it definitely.

COBRA-1A irradiation, D03 capsule, out-of-pile ^{4}He release experiment *cobraD031*

a. ^{4}He in solution

b. ^{3}H in solution

c. ^{4}He in intragranular bubbles

d. ^{3}H in intragranular bubbles

e. ^{4}He release

f. ^{3}H release

g. Intragranular bubble radius

h. Intragranular bubble concentration

| i. Intragranular sink strength | j. Swelling |
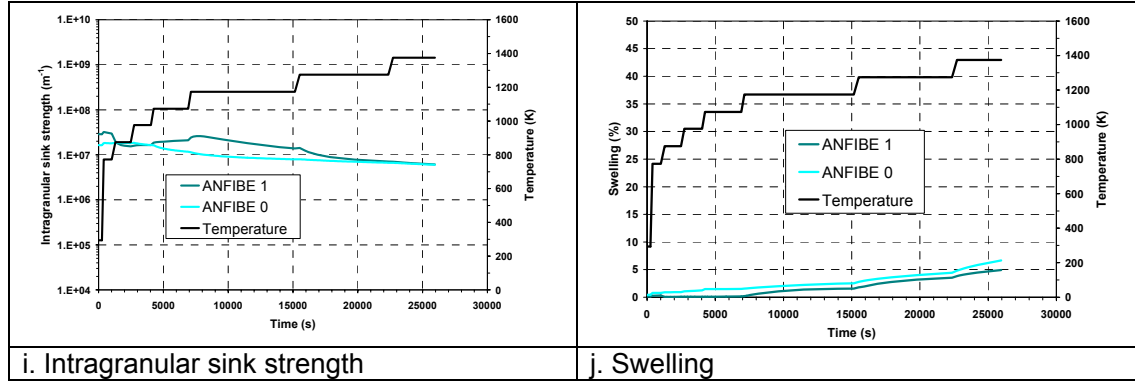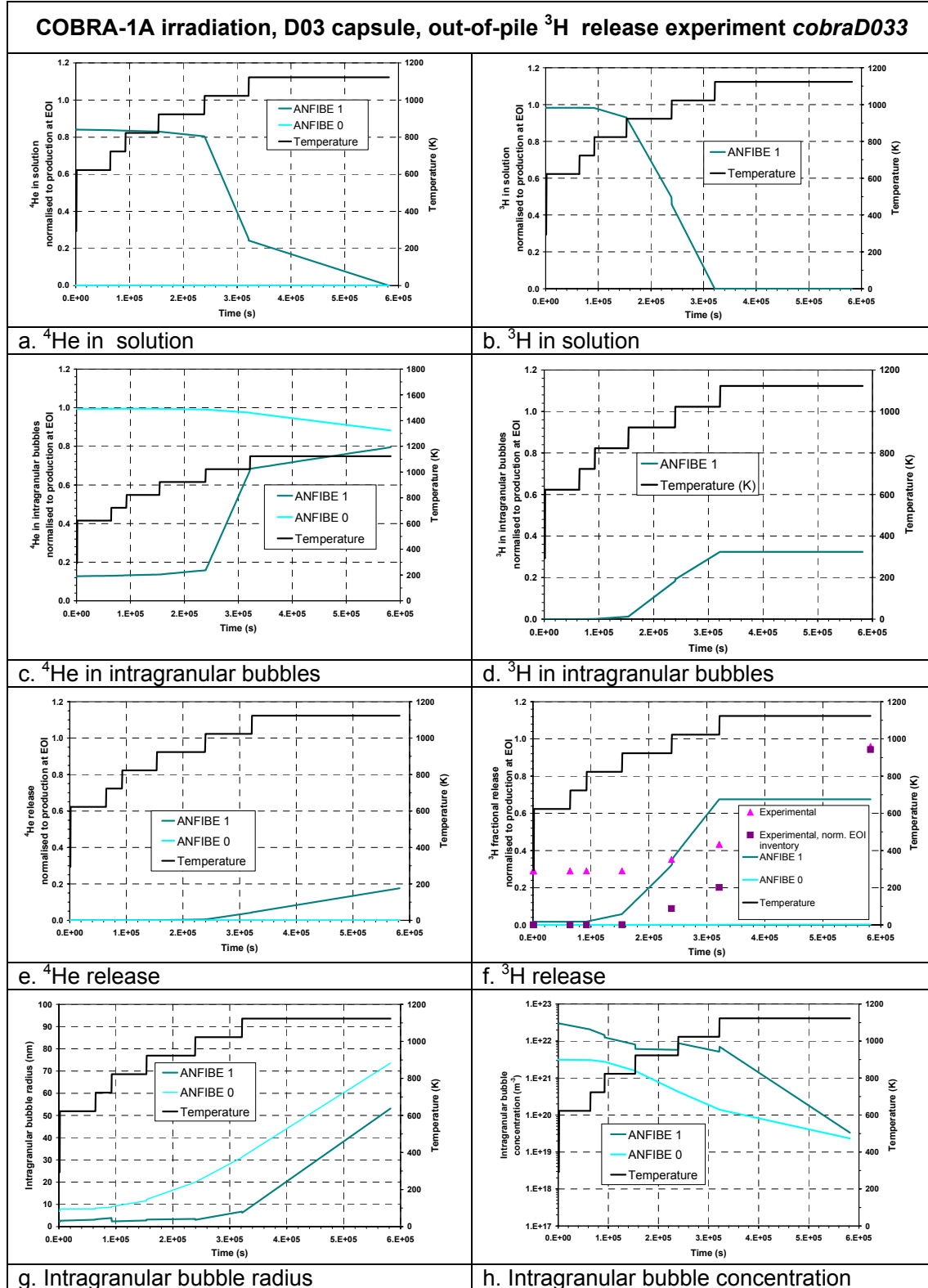
Fig. 3-8   *ANFIBE validation out-of-pile. COBRA-1A irradiation, benchmark cobraD031. The predictions of ANFIBE 0 and 1 of gas balance, gas release and microstructure are compared to the available experimental data from [Gel97].*

In Figs. 3-6, 3-7, 3-8, 3-9 the experimental gas release and ANFIBE predictions are always normalised to gas production at EOI. Similarly to the pebbles from the BERYLLIUM irradiation, also for COBRA-1A an excessive gas precipitation into intragranular bubbles since the early beginning of the irradiation history leads in ANFIBE 0 to an extremely low helium and tritium release during out-of-pile annealing. In ANFIBE 1 the prediction is remarkably improved, though gas precipitation is still overestimated. In particular the experimental in-pile tritium release is in the range of 10 to 30%, whilst the prediction is remarkably lower (order of a few %) (Tab. 3-3). This can be explained either by a limited extrapolation possibility of the simplified gas precipitation model adopted in ANFIBE 1 or by an overestimation of the characteristic migration length in the material (i.e. the grain size), which can also be responsible of the underestimation of helium release during the step annealings. In any case, for the experiment cobraC031 (1 mm BrushWellmann pebbles) ANFIBE 1 correctly predicts that helium release starts at about 1100 K (Fig. 3-6e), though in the experiment cobraD031 (1 mm NGK pebbles) helium release starts later than foreseen by the code (Fig. 3.8e).

As far as the out-of-pile tritium release measurements cobraC033 (1 mm Brush Wellmann pebbles) and cobraD033 (1 mm NGK pebbles) are concerned, in Figs. 3-7f and 3-9f the experimental data have been normalised to both tritium production at EOI (triangles) and tritium inventory at EOI (squares): such representation makes it possible to assess the ability of the code to describe tritium release kinetics during the out-of-pile temperature transient independently of the irradiation history. Though the two transients are similar in duration and temperatures, the BrushWellmann pebbles are better described than the NGK pebbles. For the first material, if in-pile release is taken into account (Fig. 3.7f, triangles), ANFIBE 1 gives a very satisfactory prediction of tritium behaviour starting from 900 K; below this limit the release is underestimated, but the out-of-pile kinetics is correctly described (squares). For the NGK pebbles, below 1000 K ANFIBE 1 predicts a too fast release kinetics (Fig. 3.9, squares), which causes an overestimation of tritium release above 900 K. At lower temperature, ANFIBE 1 appears in any case to be conservative in respect of fusion blanket applications (triangles). The TEM examination of NGK 3-mm diameter pebbles after irradiation in

COBRA-1A irradiation, D03 capsule, out-of-pile ^{3}H release experiment *cobraD033*

a. ^{4}He in solution

b. ^{3}H in solution

c. ^{4}He in intragranular bubbles

d. ^{3}H in intragranular bubbles

e. ^{4}He release

f. ^{3}H release

g. Intragranular bubble radius

h. Intragranular bubble concentration

| i. Intragranular sink strength | j. Swelling |
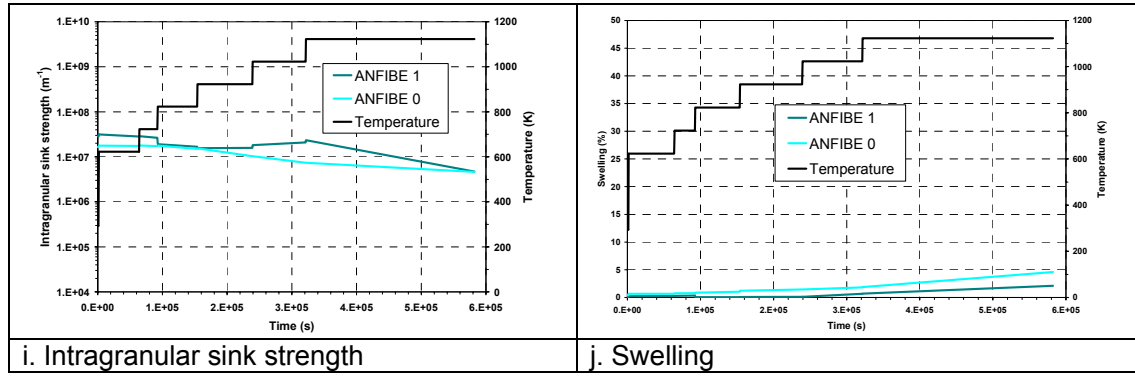
Fig. 3-9 *ANFIBE validation out-of-pile. COBRA-1A irradiation, benchmark cobraD033.* The predictions of ANFIBE 0 and 1 of gas balance, gas release and microstructure are compared to the available experimental data from [Gel97].
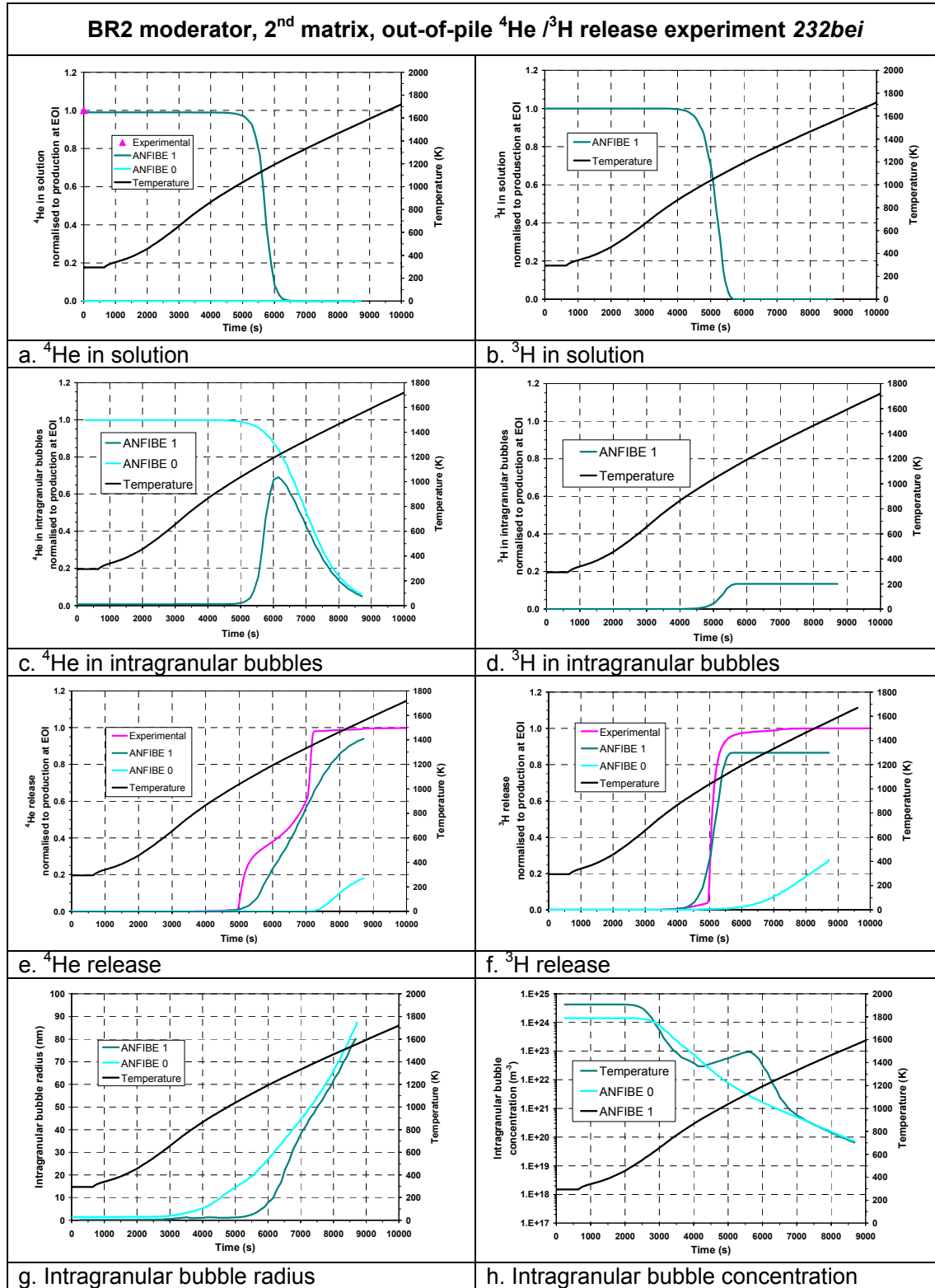
COBRA-1A provided also one valuable set of data on the pebble microstructure at EOI for the validation of the model of in-pile bubble nucleation, growth and coalescence (Eq. A-5, Annex A) and swelling up to 3000 appm ^{4}He production for pebbles. Such data show that, similarly to the BERYLLIUM irradiation, ANFIBE 1 underestimates intragranular bubble radius, though the prediction of bubble concentration is acceptable (Tab.3-3).

In conclusion, though in COBRA-1A benchmarks ANFIBE 1 is remarkably extrapolated, the trends observed in the BERYLLIUM irradiation in-pile and out-of-pile are confirmed and the same limitations appear. Furthermore, for 1 mm pebbles tritium release is generally underestimated below 900 K, i.e. in a temperature range relevant for the HCPB blanket. This implies that the extrapolation of ANFIBE 1 for the reference pebbles foreseen for the blanket is reasonable until 3000 appm ^{4}He production and that it probably gives conservative predictions of helium and tritium release.

3.9.2.3 BR2 disposed moderator, 2nd matrix

For these benchmarks it has to be pointed out that ANFIBE 1 is applied far outside its validation range, because the gas precipitation model was developed and adapted for pebbles from the BERYLLIUM irradiation and the material from BR2 moderator is very different in terms of grain size and irradiation conditions. Furthermore, the assumption of a complete percolation in ANFIBE 1 is for fine grains less applicable. On the contrary, ANFIBE 0 is for this material applied in his original validation range, though in the validation procedure only macroscopic phenomena were considered.

In general the prediction capability of ANFIBE 1 in terms of helium and tritium release and balance is also for the benchmarks from BR2 moderator much higher than in ANFIBE 0 (Figs. 3-10 and 3-11). Like for weakly irradiated pebbles from BERYLLIUM and COBRA-1A, ANFIBE 0 overestimates in-pile and out-of-pile gas precipitation into intragranular bubbles and therefore remarkably underestimates gas release. This proves that in-pile and out-of-pile precipitation hindering plays a fundamental role in all material types and irradiation conditions, which is a further confirmation of the validity of the methodology applied in this study in

BR2 moderator, 2nd matrix, out-of-pile ^{4}He /^{3}H release experiment *232bei*

a. ^{4}He in solution

b. ^{3}H in solution

c. ^{4}He in intragranular bubbles

d. ^{3}H in intragranular bubbles

e. ^{4}He release

f. ^{3}H release

g. Intragranular bubble radius

h. Intragranular bubble concentration

| i. Intragranular sink strength | j. Swelling |
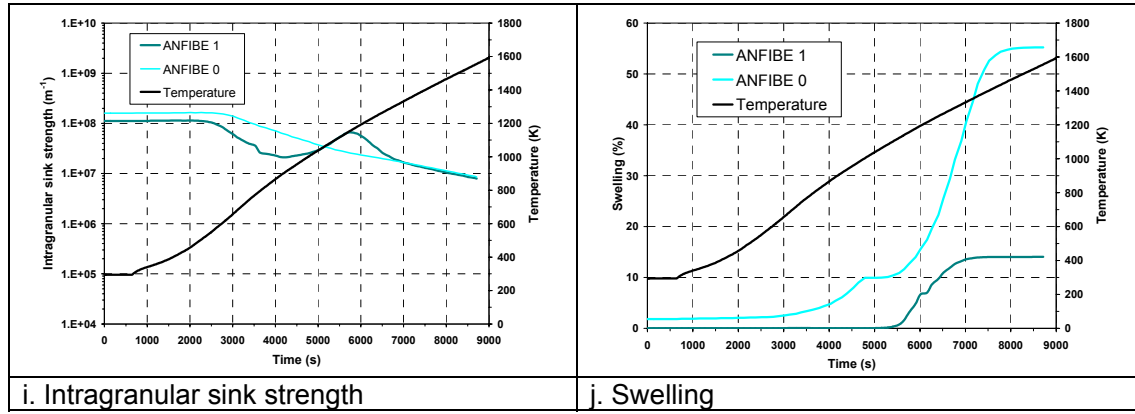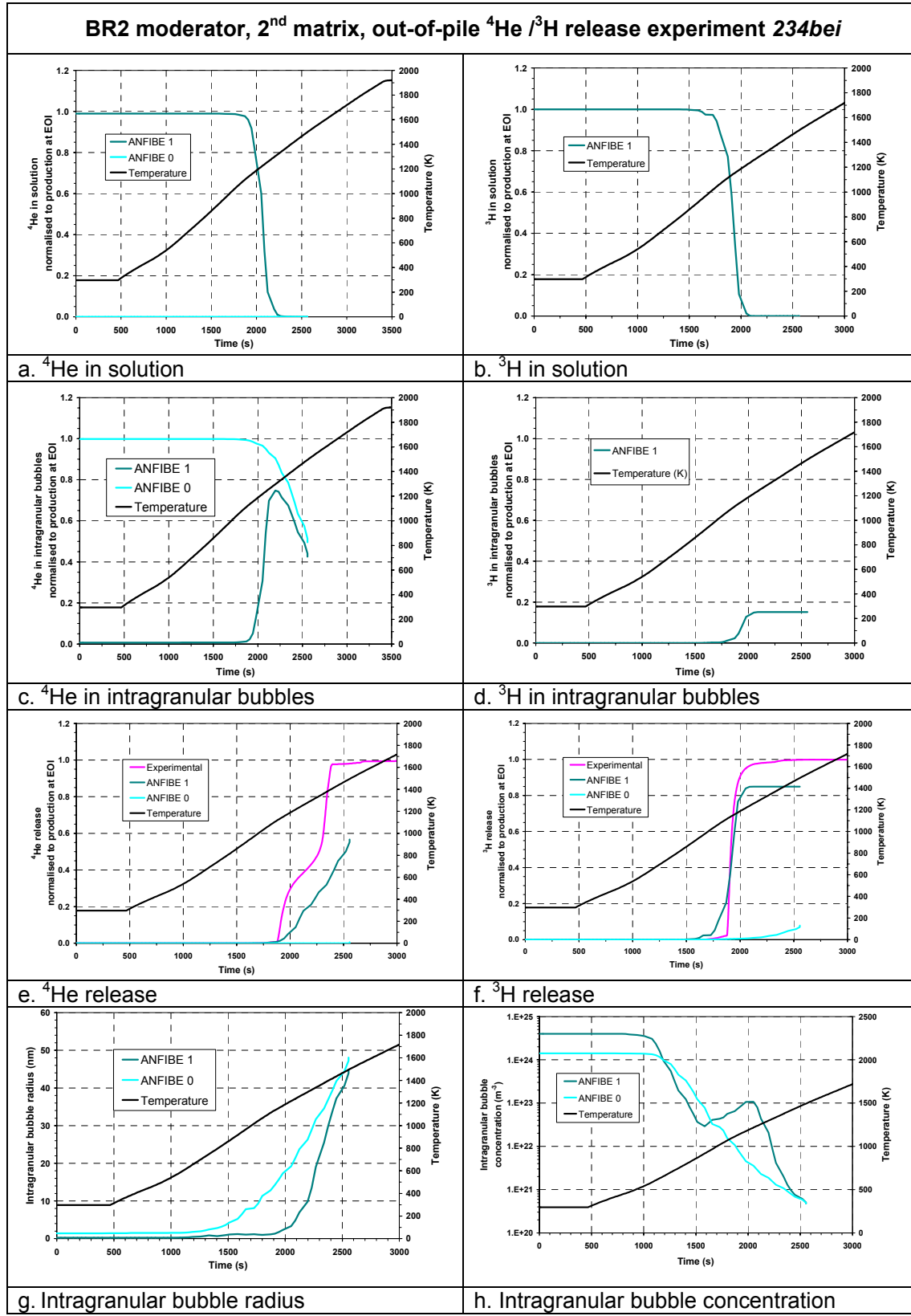
Fig. 3-10   *ANFIBE validation out-of-pile. BR2 moderator 2nd matrix, benchmark 232bei. The predictions of ANFIBE 0 and 1 of gas balance, gas release and microstructure are compared to the available experimental data (from Chapter 2 of this study).*

order to enable model extrapolation. The main issue in ANFIBE 1 for the material from BR2 moderator, and in general for any material with small grains, is the assumption of a percolation probability of 1, i.e. that gas which reaches grain boundaries is immediately released to the outside. With fine grains the fraction of porosities at grain boundaries connected to the outside is much smaller than 1 at low temperature and fluence and the ratio of free surface to grain boundary surface is also negligible, therefore for such material the assumption of complete percolation leads to an initial overestimation of gas release, until percolation paths are actually formed. In Fig. 3-10 and Fig. 3-11 helium and tritium release are overestimated in the early diffusion stage, but at about 1000 K, when a burst release begins (paragraph 2.3.4), ANFIBE 1 prediction starts to be in very good agreement with the experimental data. As a matter of fact, the release peak is due to the formation of percolation channels at grain boundaries and corresponds to the abrupt increase of the percolation probability to 100%. Therefore, before that peak, the prediction of ANFIBE 1 does not correspond to gas release but to gas at grain boundaries, after the peak to the actual gas release.

In conclusion, ANFIBE 1 can describe in a rather satisfactory way helium and tritium release and the gas balance also in highly irradiated beryllium with small grains, *in all conditions where percolation paths are already formed*. In all other conditions, ANFIBE 1 is able to predict gas at grain boundaries, but a further development and validation of the percolation model is needed to assess which fraction of the gas trapped at grain boundaries is actually released to the outside.

3.10 Comparison of ANFIBE 0 and ANFIBE 1

After applying the integrated macroscopic/microscopic validation procedure on the benchmarks considered, some general conclusions on the respective prediction capabilities of ANFIBE 0 and 1 can be drawn.

BR2 moderator, 2nd matrix, out-of-pile ^{4}He /^{3}H release experiment *234bei*

a. ^{4}He in solution

b. ^{3}H in solution

c. ^{4}He in intragranular bubbles

d. ^{3}H in intragranular bubbles

e. ^{4}He release

f. ^{3}H release

g. Intragranular bubble radius

h. Intragranular bubble concentration

| i. Intragranular sink strength | j. Swelling |
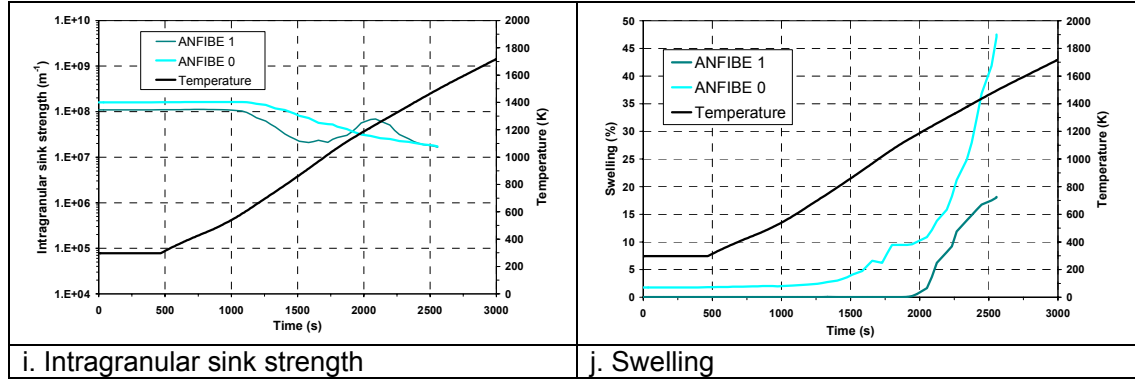
Fig. 3-11   *ANFIBE validation out-of-pile. BR2 moderator 2nd matrix, benchmark 234bei.*
The predictions of ANFIBE 0 and 1 of gas balance, gas release and microstruc-
ture are compared to the available experimental data (from Chapter 2 of this
study).

ANFIBE 0 appears in general not suitable to describe helium and tritium kinetics and bal-
ance, especially in a fusion relevant material, i.e. beryllium pebbles with coarse grains, where
the characteristic migration distance of gas atoms to grain boundaries is of the order of 100
microns. Helium and tritium release during out-of-pile heating are dramatically underesti-
mated. By considering the detail of the gas balance in all benchmarks considered, such in-
correct gas release prediction can always be explained as a consequence of an overestima-
tion of in-pile and out-of-pile gas precipitation into intragranular bubbles. ANFIBE 0 predicts
that the whole gas inventory precipitates already during irradiation: as a consequence, at the
beginning of the thermal ramp annealing, the whole gas is immobilised and cannot be re-
leased because the duration of the temperature transient is much shorter than the time nec-
essary for migration of intragranular bubbles to grain boundaries. The intragranular sink
strength is in ANFIBE 0 not corrected by the precipitation hindering factor: also bubble reso-
lution, which contributes to lowering the in-pile gas precipitation rate, is not taken into ac-
count.

As a consequence of the improvement of the gas precipitation model performed on the basis
of the experimental studies in Chapter 2 and of the application of the integrated macro-
scopic/microscopic validation procedure, the prediction of helium and tritium release appears
in general to be remarkably improved in ANFIBE 1 for all benchmarks considered. In particu-
lar for tritium, after introducing precipitation hindering, the same analytical model as for he-
lium (Eq. A-1, Eq. A-2, Eq. A-3, Eq. A-4, Annex A) can be applied in-pile and out-of-pile with
the same numerical solver.

If only the range of operating temperatures of beryllium in the HCPB blanket is considered
(700 – 1050 K) the prediction of ANFIBE 1 is always reasonable, with a trend to underesti-
mate tritium release, especially in-pile. At higher temperatures, gas release is always re-
markably underestimated, because intragranular bubble venting phenomena are not yet in-
cluded in the model.

As far as the extrapolation of the models to higher fluence, different irradiation temperatures and different microstructure is concerned, ANFIBE 1 gives also acceptable results for pebbles, though in-pile tritium release is underestimated, and also for fine grain material, *in all conditions where the assumptions adopted for the models are realistic.*

On the contrary, ANFIBE 1 appears to give a less satisfactory prediction of bubble characteristics than ANFIBE 0, though their product, related to the precipitation rate, is in the two versions of the code similar. Though ANFIBE 1 predicts gas balance in a much more reasonable way than ANFIBE 0, the bubble nucleation, growth and coalescence model (which is described in Eq. A-5, Annex A) still has to be calibrated by measuring the respective governing parameters.

It has been proven that the integrated microscopic/macroscopic validation procedure defined and applied in this study is very effective in identifying key phenomena, in measuring model parameters and finally in enabling model improvement with the aim of extrapolating them.

3.11 Comparison of EFFUSX and ANFIBE 1 predictions for the BERYLLIUM irradiation

Some key parameters of the helium and tritium kinetics model in ANFIBE 1, such as gas atomic diffusivities, precipitation rate, characteristic migration length, have been measured on the basis of an inverse analysis of the gas release curves from the BERYLLIUM irradiation, performed by means of the EFFUSX code and presented in paragraph 2.5.

The gas kinetics model applied to perform the inverse analysis, described in paragraph 2.5.1, is similar to the one in ANFIBE, still there are some differences between the direct calculation of gas release by ANFIBE and the fitting by EFFUSX, as follows after comparison, respectively, of Fig. 3-4e, Fig. 3-5e, Fig. 3-4f, Fig. 3.5f with Fig. 2-26, Fig. 2-27, Fig. 2-28, Fig. 2-29. In general, the inverse analysis provides better predictions than ANFIBE. This is due to the fact that ANFIBE, in addition to the simple diffusion and precipitation model of EFFUSX, contains some additional terms related to the in-pile behaviour (e.g. bubble resolution, correction of the in-pile diffusivities due to irradiation induced diffusion). ANFIBE, before calculating the out-of-pile thermal ramp annealing, calculates the irradiation history, whilst EFFUSX starts from the beginning of the out-of-pile transient with the assumption that the whole helium and tritium are in dynamic solution. A further difference for temperatures above 1500 K is that the empirical model of bubble venting especially developed for the EFFUSX code in paragraph 2.5.1 has not been included in ANFIBE.

3.12 Open issues of ANFIBE 1 and needed developments in the near future

3.12.1 The bubble kinetics and swelling models

This study was focussed on the improvement of the model for gas atom precipitation into intragranular bubbles in ANFIBE, in-pile and out-of-pile. Although the experimental studies performed in Chapter 2 and the results presented in the previous paragraphs show that such

part of the model is fundamental for a correct prediction of gas release, the whole analytical model in ANFIBE (see the equations in Annex A) is in principle able to provide a very comprehensive description of all other diffusion phenomena which play a role, of the microstructure evolution (bubble kinetics) and of swelling. It is necessary in the near future to extend the integrated macroscopic/microscopic validation procedure, applied in this study only for improving the diffusion and precipitation model, to re-calibrate the bubble kinetics model (nucleation, growth and coalescence of intragranular bubbles, Eq. A-5 in Annex A, and of grain boundary bubbles, Eq. A-6 and A-7), which is strictly related to the swelling model and to the gas percolation model.

3.12.2 The precipitation model

The measurement of the precipitation hindering factors for helium and tritium and their introduction into ANFIBE enabled a remarkable improvement of the gas balance and release predictions. Nevertheless, the assumption of a constant precipitation hindering factor during all possible irradiation histories and out-of-pile temperature transients is only a first approximation. Such assumption will have soon to be confirmed by similar measurements on different materials (e.g. the highly irradiated beryllium from BR2 disposed moderator and, in the longer term, the pebbles from the HIDOBE irradiation). As a matter of fact, precipitation hindering is a function of temperature and of the concentration of gas in solution c (Eq. 2.14a, Chapter 2) and represents the fact that the precipitation rate depends on the square root of c, as well as including the solubility. In some of the benchmarks used to validate the code, it appears that precipitation is still overestimated, especially in-pile and at high temperature and this may be due to an incorrect precipitation model. A further step in the development of ANFIBE will be the direct introduction of a non linear precipitation model and its calibration by an inverse analysis of gas release curves: for such improvement the measurement of the self-diffusion coefficient and of the solubility is necessary.

3.12.3 Effect of radiation damage on gas diffusion

In the frame of the study of gas precipitation in pebbles from the BERYLLIUM irradiation (paragraph 2.4.4), a certain interaction between gas precipitation and irradiation-induced dislocations has been observed. In the presence of a network of dislocations which act as sinks for gas atoms, gas diffusion phenomena are related to dislocation loop growth. The development of a model for such interaction would also be an important step towards the further improvement of the gas precipitation and diffusion model in ANFIBE 1.

3.12.4 The percolation model

Another issue of ANFIBE 1, especially for beryllium with fine grains at low temperatures, is the absence of a percolation model which also takes into account the presence of free surfaces. It has been observed in paragraph 3.10 that such assumption plays for pebbles with large grains a minor role, whilst it leads to a remarkable and undesired overestimation of gas release from beryllium with fine grains in a temperature range typical of the HCPB blanket operating conditions. Assuming that the description of gas migration to grain boundaries is

correct, as suggested by the results in paragraph 3.10, the next step is the development of an analytical percolation model, based on the structure of percolation paths in the material considered, in order to describe the evolution of grain boundary bubble towards an interconnected network reaching the outer surface. In order to validate such model, a 3D characterisation of such structures is needed: this can be obtained only by the further development and application of the microtomography technique presented in paragraph 2.4.1.

3.12.5 High burn-up effects

The extrapolation of ANFIBE to high fluence is based on the assumption that no additional phenomena play a role in determining gas release at high fluence than those acting a low fluence, i.e. essentially gas diffusion, precipitation and formation of percolation paths. Still, in UO_2, a remarkable increase of gas release occurs at high burn-up correspondingly to a restructuring of the grains (the rim effect, or High Burn-up Structure formation) [Lee00] [Las95]. As the lattice damage increases during irradiation, dislocations tend to fragment grains, until a limit value of damage in the lattice is reached. At this limit the grain undergoes a full restructuring, with the final effect to expel abruptly the gas trapped inside. Experimental evidence on this phenomenon in beryllium is not available, but since the maximum damage in beryllium in the HCPB blanket reaches 80 dpa, it cannot be excluded that rim formation might occur as the End-Of-Life is approached. Such phenomenon would play a positive role in enhancing gas release from beryllium in-pile, therefore, if it is not taken into account in the models, like in ANFIBE version 1, the prediction of gas release is underestimated and conservative in respect of blanket applications, since a release as high as possible is desired.

As far as the influence of grain size on High Burnup Structure formation is concerned, for UO_2 pellets it has been experimentally proved [Une00] that larger grains, which already show lower gas release due to their largest migration distance, also have a higher resistance to rim formation, which implies a lower decrease of grain size at high burn-up and, correspondingly, a lower beneficial effect of high burn-up on gas release. In extrapolating these results to beryllium pebbles, it has nevertheless to be taken into account that pebbles with large grains also have a high "free surface effect" (paragraph 3.8) which is not present in UO_2 pellets and which enhances gas release. In order to optimise the grain size of pebbles with the aim of enhancing gas release, the influence of such opposed effects has to be quantified.

3.13 Discussion

In the previous paragraphs the development and validation of the version 1 of the ANFIBE code and its comparison with the previous version 0 has been presented.

On the basis of the experimental characterisation, carried out in Chapter 2 for some types of irradiated beryllium, a particular validation procedure for the gas kinetics models has been defined and applied for the first time, the so-called *integrated microscopic/macroscopic validation*, where the relationship between gas release and microscopic diffusion phenomena is considered. The procedure has been successfully applied to identify issues in the model and to improve it consequently. The main effect of such methodology has been to enable the

correction of the gas precipitation model, by introducing a precipitation hindering factor for helium and tritium and in-pile re-solution effects.

A number of benchmarks, consisting in an irradiation history followed by out-of-pile thermal ramp or stepped annealing, for pebbles from the BERYLLIUM and COBRA-1A irradiations and for highly irradiated fragments from the disposed moderator of Belgian Reactor 2, have been considered. The samples cover a wide range of material type and irradiation parameters and the out-of-pile experiments a wide range of temperatures, therefore the set of benchmarks considered are significant in view of assessing the extrapolation capability of ANFIBE 1. For pebbles, ANFIBE 1 gives reasonable predictions of gas balance and release in the range of blanket operating temperatures, with a trend to underestimate out-of-pile helium and tritium release and, according to the only set of in-pile tritium release data available for pebbles from the COBRA-1A irradiation, also in-pile tritium release. As a result of the validation procedure, ANFIBE 1 is expected to give reasonable projections of helium and tritium retention for pebbles in the HCPB blanket, with the additional consideration that gas release is probably underestimated. For beryllium with fine grains, ANFIBE 1 predictions are also significant, as soon as interconnected porosities or cracks at grain boundaries are formed.

As far as the prediction of bubble nucleation, growth, coalescence and swelling is concerned, ANFIBE 1 needs further improvements from the analytical point of view. Furthermore, the development and calibration of a percolation model is needed to be able to describe gas release at low fluence and low temperature for a material with fine grains.

4 Model application - Assessment of tritium retention in beryllium in the blanket of a fusion power reactor

4.1 The HCPB blanket in the European Power Plant Conceptual Study

The European Power Plant Conceptual Study (PPCS) was launched in 1999 in order to assess the attractiveness of fusion power plants as an option for electricity production in the second half of the 21st century. Four reference commercial fusion power plant types of 1.5 GW electric power are analysed in the PPCS, with different tritium breeding blanket types, of which two are based on technologies with a limited extrapolation from the presently available ones, two more advanced. In the first group, model B reactor has a blanket of the Helium Cooled Pebble Bed (HCPB) type, which has been developed in Europe since the beginning of the 90s [Dal94] [Her01]. The HCPB blanket is since 1995 one of the two European reference blankets for the DEMO reactor, a prototype fusion power reactor of about 600 MW electric power, to be build after ITER around 2035. In the HCPB blanket tritium breeder is in a ceramic form (lithium orthosilicate Li_4SiO_4 or lithium metatitanate Li_2TiO_3), therefore beryllium
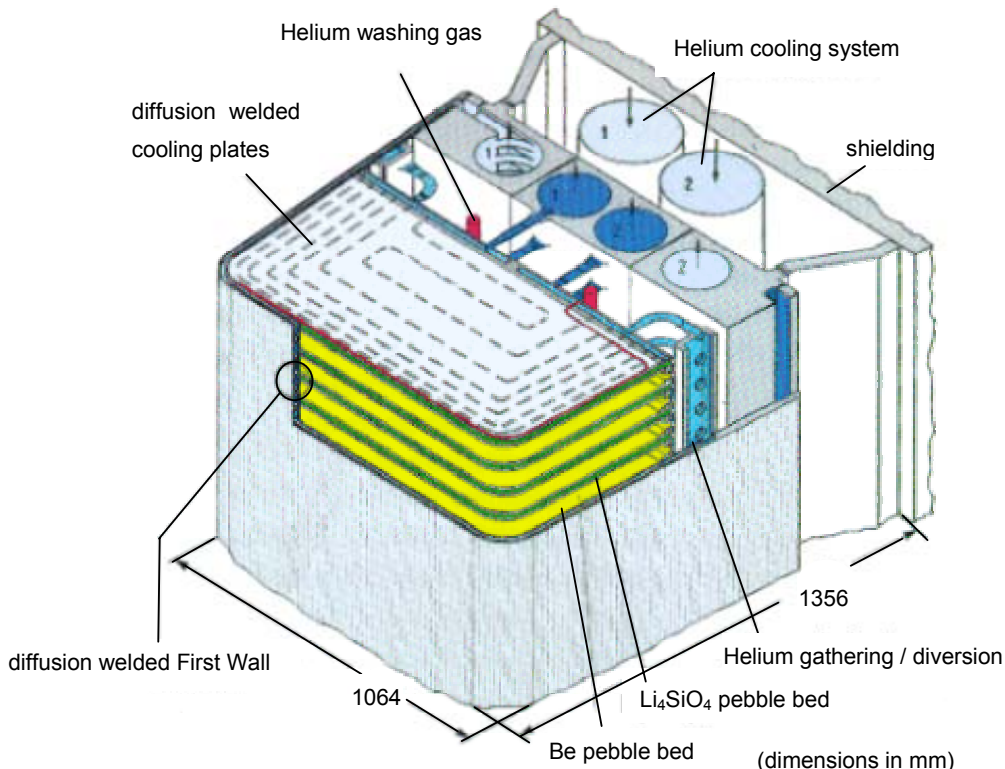
Fig. 4-1   The European Helium Cooled Pebble Bed (HCPB) blanket module, 1995 design [Her01], considered in this study as a reference for the calculation of End-Of-Life tritium inventory in beryllium.

94
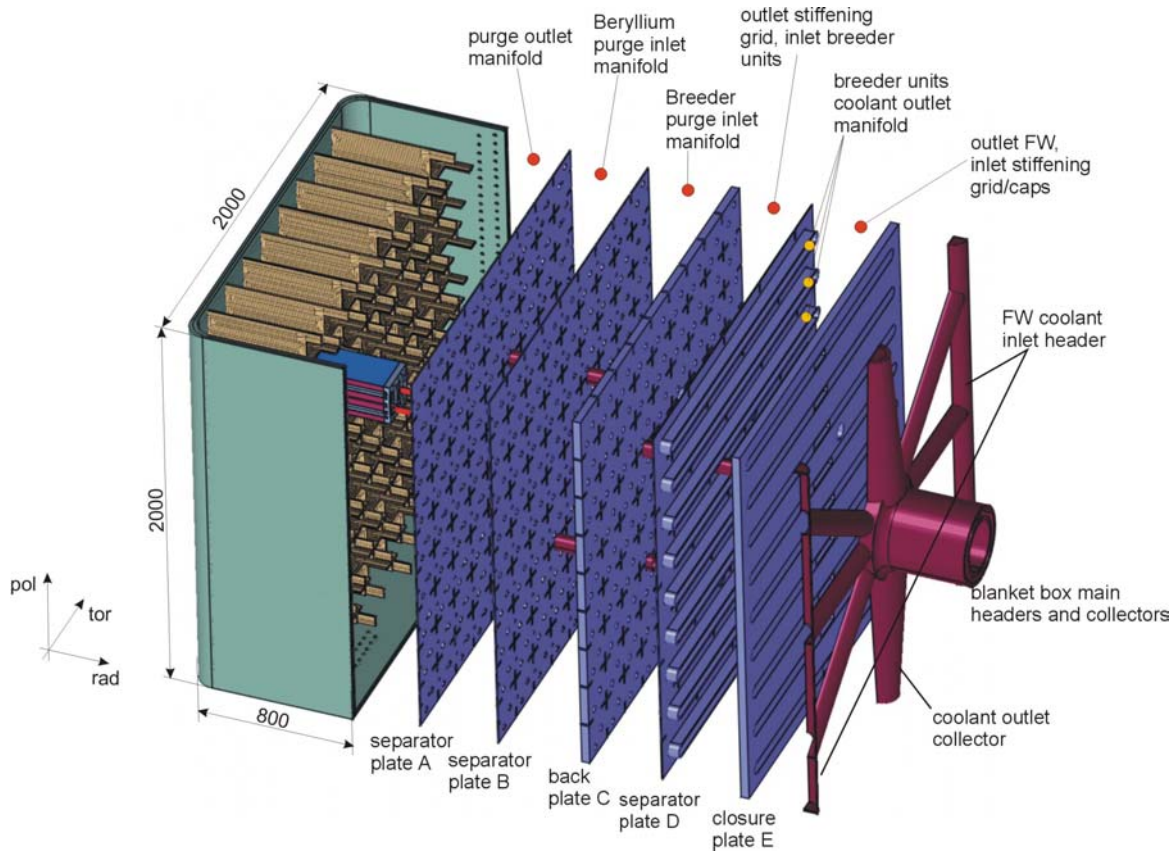
Fig. 4-2   Exploded view of the components of the Helium Cooled Pebble Bed blanket module, 2003 design. The module consists of a box, a stiffening grid, which contains the breeding units, and four rear plates to distribute and collect the helium flow [Her03].

as a neutron multiplier is needed, in a ratio of at least 4 beryllium volume parts per ceramic breeder volume part [Fis88]. In order to avoid material cracking during irradiation, to keep a good contact of ceramic breeder and neutron multiplier with the helium cooled steel walls and to improve gas release, both ceramic breeder and beryllium are in the form of small pebbles (0.25-0.6 mm diameter for the ceramic breeder, 1 mm for beryllium). In the EXOTIC 7 irradiation programme it has been seen [Kley99] that ceramic breeder pebbles and beryllium pebbles are incompatible under irradiation, because energetic tritium atoms produced in the breeder are implanted into beryllium and BeO at the beryllium surface interacts with Li_4SiO_4 and forms Li_2BeSiO_4; therefore breeder and beryllium pebble beds have to be separated by steel plates. As far as the cooling of the beds and of the first wall of the blanket module is concerned, this is achieved by high pressure (8 MPa) helium flowing in channels machined in the walls, with inlet and outlet temperatures of 300°C and 500°C respectively, which have since a long time been established as allowing a suitable balance of pressure drop, heat transfer and primary stress in blanket cooling plates. All structures are in reduced activation ferritic-martensitic steel EUROFER. Pebble bed purging for removal of tritium is provided by independent helium at atmospheric pressure flowing through the beds.

As far as the bed layout is concerned, the HCPB blanket design has been recently evolving from a box with horizontal plates (Fig. 4-1) to a more advanced and complex solution shown in Fig. 4-2 [Her03]. The need for a major revision of the module layout comes from the PPCS [Coo03], where maintenance, and thus mainly economic, considerations led to the development of a HCPB reactor model with a radial segmentation into consumable blanket boxes with a limiting weight of about 24 tons each.

The revised HCPB blanket module consists in a box with dimensions up to 4 x 2 x 0.8 m^3 (toroidal x poloidal x radial), with a stiffening grid inside, which has structural functions and is filled with independent breeding units, in a similar way as fuel elements in fission reactors. The single unit (Fig. 4-3) contains two ceramic breeder pebble beds surrounded by beryllium pebbles.

4.2   Issues of the behaviour of pebble beds under irradiation

In order to assess the safety and attractiveness of a fusion power plant with a HCPB blanket, it is fundamental to be able to predict the behaviour of pebble beds during irradiation, in particular up to End-Of-Life (EOL) conditions (40000 hours normal operation). Two are the main issues: the thermomechanical behaviour of beryllium and ceramic breeder pebble beds and gas retention/release in beryllium. The first issue presents different aspects: pebble bed expansion, creep, mechanical interaction with the box walls, which have an influence on thermal conductivity and on the pressure drop in the purging flow. Tritium release in the ceramic breeder has been shown to be practically 100%, therefore it can be assumed that all bred
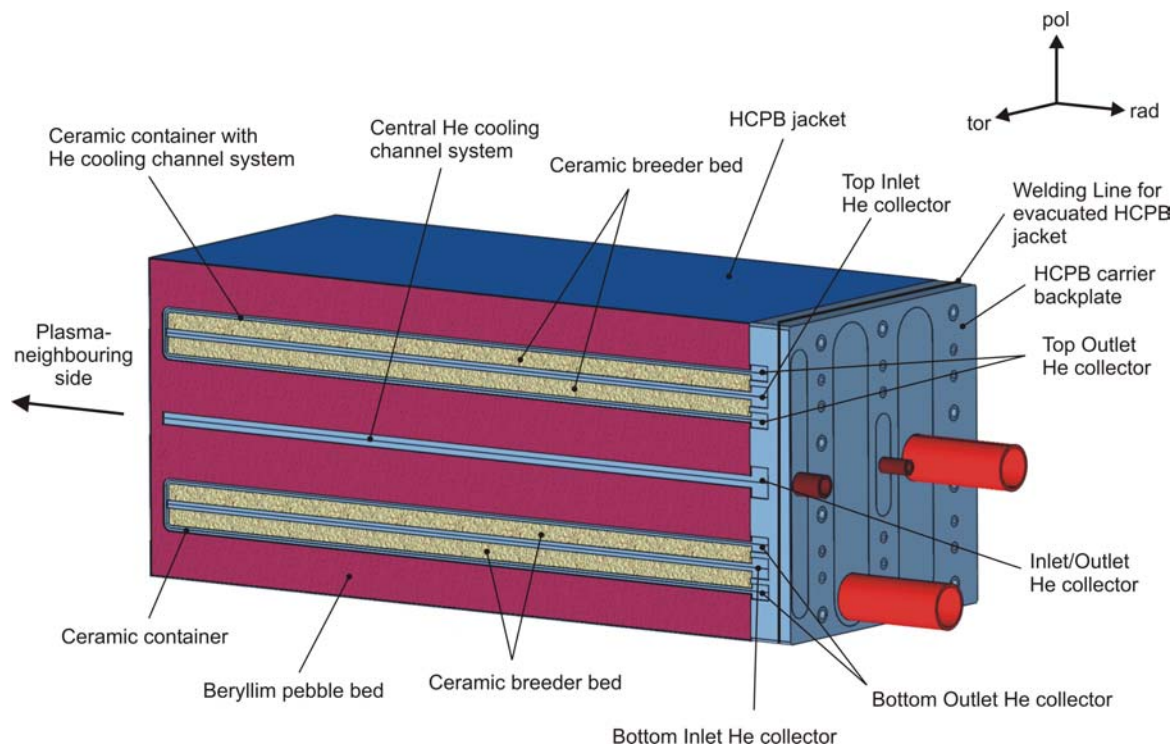
Fig. 4-3   Breeding unit of the Helium Cooled Pebble Bed blanket module in Fig. 4-2 [Her03].
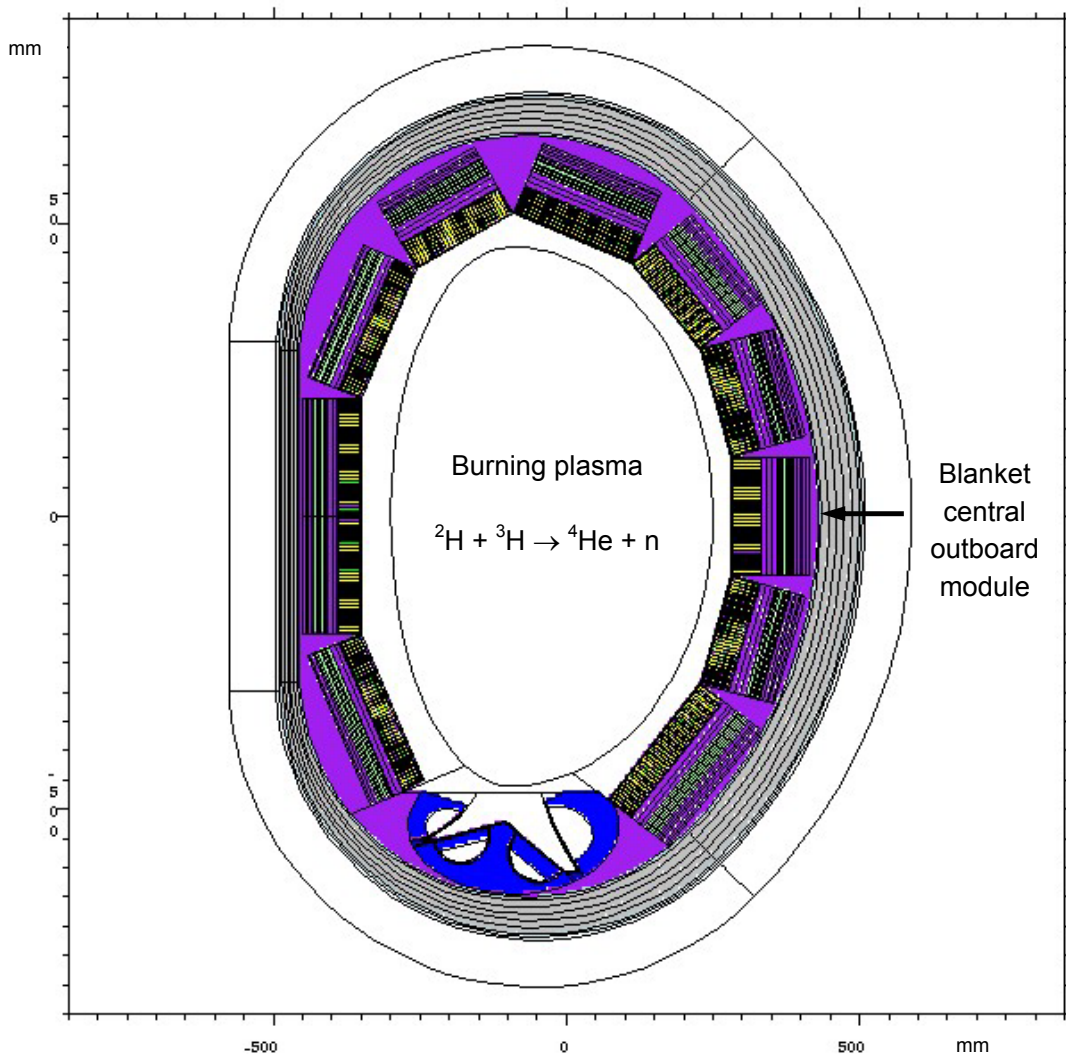
Fig. 4-4   Poloidal cross section of the vacuum chamber of the fusion power reactor Model B in Fig. 1-1, showing the layout of Helium Cooled Pebble Bed blanket modules.

tritium can be extracted by the purging flow and that the remaining inventory is negligible. As far as beryllium is concerned, the problem of gas retention, in particular tritium retention, has to be addressed with a high priority. Gas retention induces swelling, with an effect on the bed mechanical and thermal behaviour: a volume increase of the pebble bed, in the presence of wall constraints and in the range of high operating temperatures, might induce a load increase and creep phenomena, which modify the contact area between pebbles, therefore the thermal conductivity of the bed. In its turn, the temperature profile has an influence on gas release kinetics. From the point of view of safety, a high inventory of tritium trapped in beryllium is unacceptable, because it could be abruptly released in case of an accidental temperature transient and make the plant site evacuation necessary.

In the frame of the studies of the behaviour of pebble beds under irradiation, the development of analytical models (the ANFIBE code) for the prediction of swelling and helium and tritium release/retention in beryllium represents a necessary step, though not the conclusive one. On the basis of the experimental studies and model developments presented in Chapters 2 and 3 of this study and in particular after the application of the integrated macroscopic/microscopic validation procedure and the improvement of the gas precipitation model, ANFIBE 1 can be extrapolated, in the limit of the assumptions adopted, to give a provisional projection of tritium release in beryllium pebbles at EOL of a blanket module. Such analysis is still very simplified, because it considers the beryllium material behaviour independently of the pebble bed behaviour, i.e. it neglects the fact that changes in the material under irradiation induce changes in the pebble bed and that those, in their turn, affect the code input parameters for the prediction of material behaviour.

4.3 Assessment of tritium inventory in beryllium at End-Of-Life of the HCPB blanket central outboard module

4.3.1 Model and assumptions

The blanket module with the highest neutron load has been considered, i.e. the central outboard module (Fig. 4-4), in the reference power plant Model B of the PPCS, whose main characteristics are: 1.5 GW electric power, 3.3 GW fusion thermal power, 2.24 MW m^{-2} midplane neutron wall load, 0.5 MW m^{-2} surface heat flux on the first wall [Mar02]. The reference layout of the blanket module is the 1995 design (Fig. 4-1). The module occupies a 20 degree sector of the torus and contains about 3.1 tons of beryllium pebbles, to be compared with 390 tons in the whole blanket. For the horizontal beds in the module, neutronics calculations have been performed [Che02], in order to assess helium and tritium production and neutron flux profiles in beryllium, as a function of the radial distance from the first wall. For each value of radius and neutron flux, the temperature profile in a poloidal plan between two opposite helium cooled plates has been assessed by a finite element calculation, by means of the code FIDAP, on the basis of a continuum model of the pebble bed [Bue02] with a constant thermal conductivity of 7.5 W m^{-1} K^{-1} during the whole 40000 hours lifetime of the module. The thermal conductivity of non irradiated beryllium pebble beds in helium up to 450 ºC lies between 2 and 12 W m^{-1} K^{-1} depending on the bed compaction [Pia03] [Rei02] and is significantly lower than the one of beryllium metal (around 200 W m^{-1} K^{-1} up to 400 K). The heat transfer coefficient at the helium cooled plate as been assumed constant and equal to 2 kW m^{-2} K^{-1}. The whole volume of beryllium in the module has been subdivided into a number of cells and to each cell a set of values of neutron flux, helium and tritium production (from the neutronic calculation) and temperature (from the thermal calculation) has been associated, which are input data needed for ANFIBE. In the neutronic calculation 16 radial zones have been considered, at increasing distance from the first wall. In every radial zone and each pebble layer the temperature profile is parabolic in a poloidal plan and three average values from the helium cooled plate to the centre of the bed have been calculated, corresponding each to 1/3 of the layer (1/6 and 1/6 on opposite sides of the temperature profile maximum). Since all layers are in the same thermal conditions, such subdivision into 48 cells (16 radial x

3 poloidal) describes the whole module, after appropriate mass weighing. The material is the reference one presently foreseen for the blanket, i.e. 1 mm diameter beryllium pebbles produced by NGK by REP (Fig. 1-4); such pebbles have coarse grains, therefore the characteristic migration length can be assumed similar to the pebbles from the BERYLLIUM irradiation and studied in Chapter 2, i.e. 100 microns. The reference operation time is 40000 hours, corresponding to the EOL conditions of the blanket module. The calculated values of tritium production already take into account in-pile tritium decay and the in-pile equilibrium:

$$^3He + n \leftrightarrow {^3H} + p \tag{4.1}$$

For every cell of the bed (corresponding to a set of values of irradiation temperature, helium and tritium production and neutron flux as input data) both ANFIBE 0 and ANFIBE 1 have been applied to assess tritium release and the related tritium inventory at EOL, in the assumption that the temperature profile does not change during irradiation. Actually, if pebble swelling and creep phenomena are significant, it cannot be excluded that, due to an increase in the contact area of the pebbles, the thermal conductivity of the bed increases: such effect is higher in the zones with higher neutron flux and temperature; therefore it tends to act against a further increase of temperature. An assessment of the change in pebble bed thermal conductivity and temperature profile at EOL due to pebble swelling was attempted in [Sca95] [Sca97b] on the basis of the ANFIBE code version 0. Nevertheless, it has to be also taken into account that during irradiation, due to the accumulation of gas atoms and point defects in the lattice, the thermal conductivity of the material itself (independently from the bed behaviour) tends to decrease. Such phenomenon occurs in UO_2 [Ron04] and has been recently characterised in Russian works [Sys02] also for beryllium: it has been seen that beryllium thermal conductivity drops to 1/5 of the original value after irradiation at 70 °C up to a fluence of $6.0 \cdot 10^{26}$ m^{-2} (neutron energy > 0.1 MeV). The reduction is related to radiation damage in combination with gas trapping in defects, therefore it is larger if the irradiation occurs at lower temperatures and it is partially recovered after annealing.

The two irradiation effects on the bed thermal conductivity, the first related to bed compaction due to swelling and the second to the decrease of the material thermal conductivity, act in opposite directions. No models or experimental data are presently available to quantify each of them, in order to assess which is dominating. For the sake of simplicity, the bed temperature profile for the calculation of tritium release from beryllium in this study has been assumed constant during the whole lifetime of the blanket module.

4.3.2 Results

Fig. 4-5 shows the assessment, performed by 3D MNCP (Monte Carlo N-Particle) transport models and the FISPACT inventory code, of the profiles of helium and tritium production at different radial positions in the central outboard module of the reference HCPB blanket in the PPCS [Che02], at End-Of-Life conditions. The related temperature profile and ANFIBE predictions of tritium release are shown in Fig. 4-6.
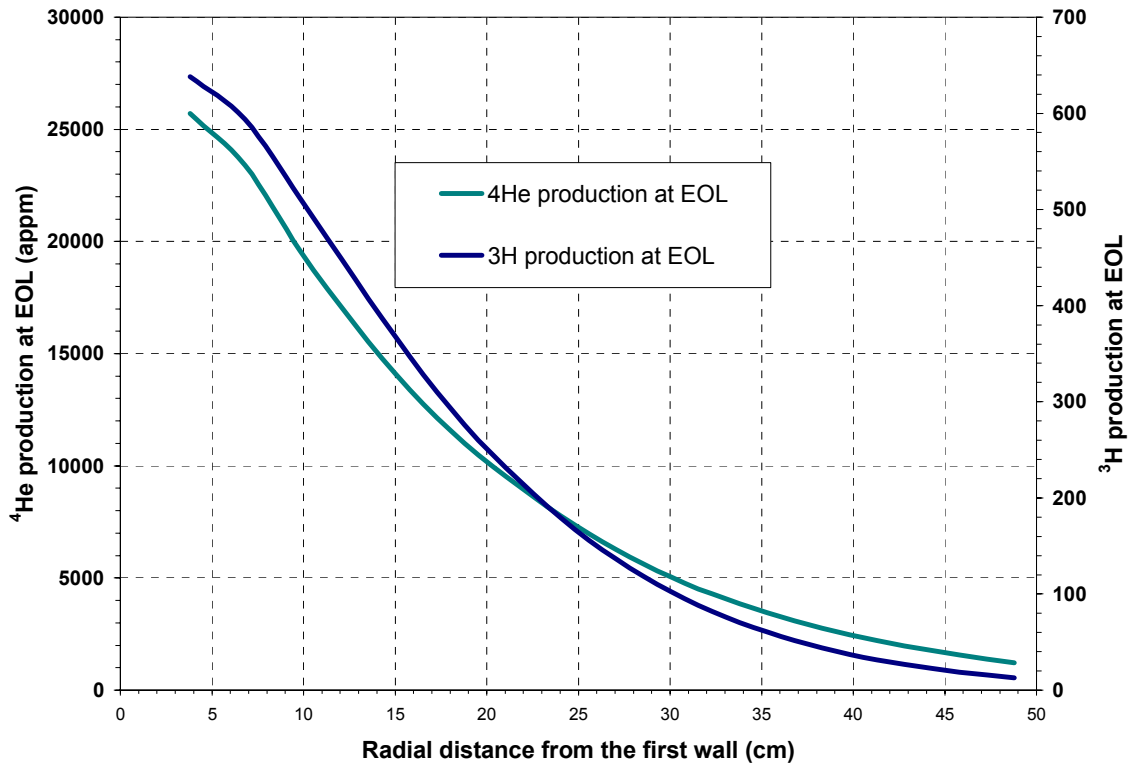
Fig. 4-5   Radial profile of [4]He and ^{3}H production in beryllium at End-Of-Life in the central outboard module of the Helium Cooled Pebble Bed blanket, in the reference fusion power plant of the Power Plant Conceptual Study [Che02]. 3D MCNP transport and FISPACT inventory calculations using 20° torus sector. Globally, in 3.1 t of beryllium pebbles, 12.1 kg of [4]He and 218 g of ^{3}H are generated.

In a range of operating temperatures from 715 to 974 K (442 – 701 ºC), ANFIBE 0 predicts that a very large fraction of generated tritium, about 80%, is retained in beryllium, mostly in bubbles inside the grain. Such result turns out to be in substantial agreement with a previous assessment performed by ANFIBE 0 [Sca95] [Dal94], where a value around 50% was found, as in that case a material with much finer grains than the pebbles in the present assessment (10 microns radius instead of 100) was considered. On the basis of the results of the integrated macroscopic/microscopic validation procedure applied for ANFIBE 0 and ANFIBE 1 in Chapter 3, ANFIBE 0 prediction has to be considered extremely conservative and unrealistic, because of a remarkable overestimation of the precipitation rate of tritium atoms into bubbles inside the grain.

On the contrary, ANFIBE 1 predicts that practically the whole tritium generated under irradiation reaches the grain boundaries in the range of temperature considered; therefore it is in a very favourable position to be released. ANFIBE 1 predictions, due to the still open issues in some parts of the analytical model and needs for re-calibration and further validation (as discussed in Chapter 3, paragraph 3.13), are not exhaustive and should be rather intended as a provisional projection. Due to the high operation temperature of the beds, ANFIBE 1 as-
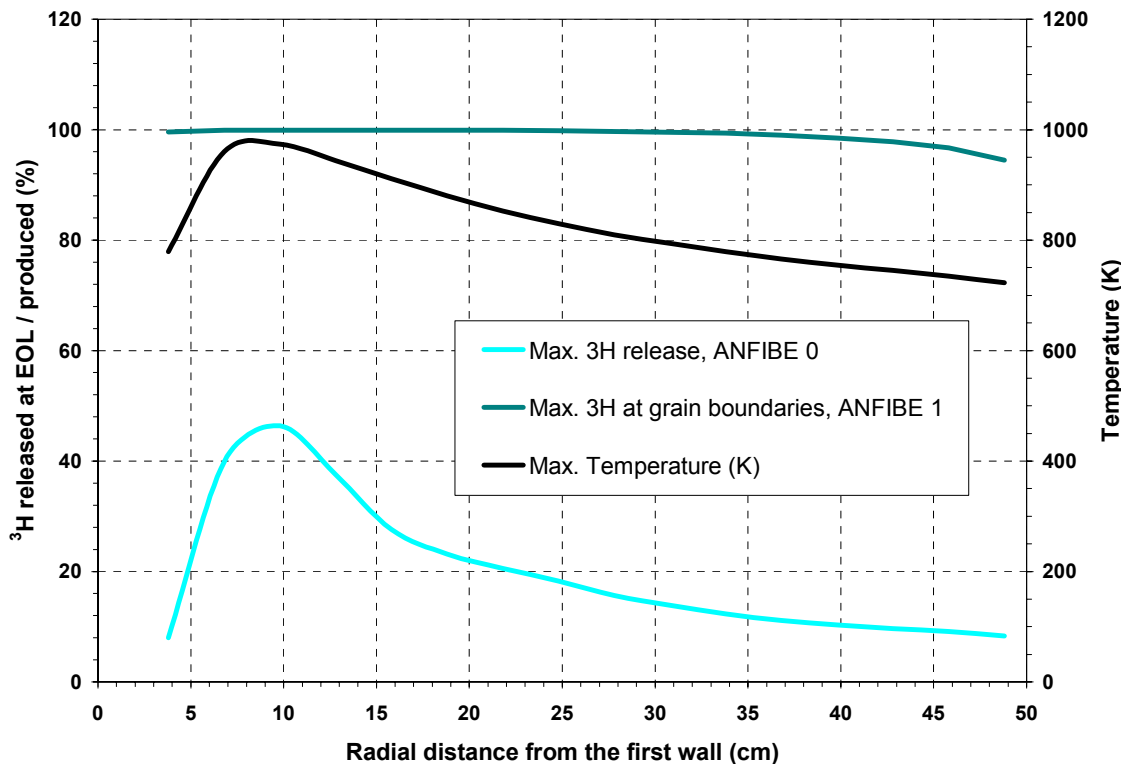
Fig. 4-6   Radial profiles of tritium release according to ANFIBE 0 and of tritium at grain boundaries according to ANFIBE 1 in beryllium pebbles at the End-Of-Life of the Helium Cooled Pebble Bed blanket central outboard module, in the reference fusion power plant of the Power Plant Conceptual Study. The maximum of the parabolic temperature profile between the helium cooled plates is considered. In the assumption that the whole tritium at grain boundaries is released, because of the presence of external grain boundaries or of interconnected porosity networks, ANFIBE 1 predicts a negligible residual tritium inventory in the module, to be compared with the 171 g predicted by ANFIBE 0.

sessment, independently from the analytical prediction, appears to be more realistic than that by ANFIBE 0, since, on one hand, it is known that tritium is mobile and, on the other hand, it has been shown in Chapter 2 that it practically does not precipitate into bubbles inside the grain. It has to be pointed out that a high tritium mobility, with a linear precipitation model like in ANFIBE 0, does not prevent in itself a fast precipitation: the higher tritium release predicted by ANFIBE 1 is essentially related to the introduction of a precipitation hindering factor for tritium, which, for the same diffusivity, limits precipitation and enhances migration to grain boundaries.

Tritium at grain boundaries is actually released if at EOL a completely interconnected and open grain boundary porosity network is present or if grain boundary separation due to mi-

crocracking has occurred, since in these conditions the assumption of a percolation probability of 100% in ANFIBE 1 is confirmed (see paragraph 3.13.3). If this were not the case, only a fraction of tritium at grain boundaries would be released to the outside, starting from a minimum of about 20% (roughly equal to the fraction of external grain surface for 1 mm diameter pebbles with 100 micron grain radius according to Eq. 3-16, paragraph 3.8) at the beginning of irradiation and approaching 100% as grain boundary bubbles form interconnected porosities. In this case, the assumption of complete percolation in ANFIBE 1 would lead to an overestimation of tritium release. On the other hand, with the assumption of complete percolation, ANFIBE 1 was indeed found to underestimate in-pile tritium release for the pebbles from COBRA-1A irradiation (Fig. 3-7f and Fig. 3-9f, paragraph 3.9.2) and the assumption is in any case coherent with the measured values of the precipitation hindering factor (paragraph 2.5).

In order to evaluate to which extent the assumption of completely open porosities at grain boundaries in beryllium pebbles at EOL of the blanket module is realistic, a qualitative assessment of the expected microstructure is possible, by extrapolating available data on bubble kinetics.

For the weakly irradiated pebbles from the BERYLLIUM experiment analysed in Chapter 2 (480 appm ^{4}He produced in 97 days irradiation at 780 K), during out-of-pile thermal ramp annealing at 10 K min^{-1} in vacuum (Fig. 2-3, paragraph 2.3.2), it has been seen that at 1340 K, after 6500 s from the beginning of the thermal ramp, a large fraction of porosities at grain boundaries are connected and cracks appear at the surface (Fig. 2-22, paragraph 2.4). Recent results obtained by microtomography [Rab04] have also proved that at 1500 K, after 7500 s, all porosities, both at grain boundaries and inside the grain, are completely interconnected. The material for the reactor has a similar microstructure than the pebbles from the BERYLLIUM irradiation, therefore it is reasonable to assume that the same percolation structures, which are formed in a shorter time during the fast thermal ramp annealing of the pebbles from BERYLLIUM, are also formed during much longer irradiation time in the reactor (40000 hours, $1.44 \cdot 10^8$ seconds), at lower temperatures. A guess of the equivalent conditions in the reactor at EOL can be made on the basis of the following simple model:

$$\frac{\exp\left(-\dfrac{Q_{DHe}}{kT_{BERYLLIUM}}\right)}{\exp\left(-\dfrac{Q_{DHe}}{kT_{reactor}}\right)} = \frac{t_{EOL}}{t_{BERYLLIUM}} \tag{4.2}$$

where t is the time and Q_{DHe}/k is the diffusion enthalpy of helium, divided by Boltzmann's constant (a value of 29380 K has been measured in Chapter 2, Eq. 2-15). According to Eq. 4-2, the percolation structures observed above 1300 K during fast thermal ramp annealing of the pebbles from the BERYLLIUM irradiation would be observed in the reactor at EOL above 900 K. In general, whilst in the thermal ramp annealing the key factor in determining gas re-

lease is temperature (if a certain release is not observed at a certain temperature, it will be certainly observed at a higher temperature), in the reactor it is time. Therefore, even in the assumption that a fully interconnected grain boundary porosity network was not present in the reactor at EOL and tritium were still trapped in closed grain boundary bubbles, it would be sufficient to bake the pebble beds above 900 K for a certain time or to extend the lifetime of the blanket modules to release practically the whole tritium inventory.

A further assumption in ANFIBE 1 is related to the precipitation model. The values of the precipitation hindering factor implemented in ANFIBE 1 have been measured during fast out-of-pile thermal annealing, where the conditions are very far from thermodynamic equilibrium. In conditions nearer to equilibrium, the deviation of the precipitation model from linearity is expected to be smaller [Ron87], therefore precipitation faster. Nevertheless, the very small values found out-of-pile for the precipitation hindering factor have been confirmed also in-pile from the observation that much less bubbles are formed than predicted by an unbiased pre-cipitation model (paragraph 3.10.2). Furthermore, it has been found that, independently from the linearity of the precipitation term, in-pile re-solution effect always plays a very important additional role in reducing the precipitation rate and such effect is enhanced by a fusion spectrum. Therefore it cannot be concluded that the assumption of a constant precipitation hindering factor leads in ANFIBE 1 to an overestimation of tritium at grain boundaries and consequently of tritium release.

In conclusion, ANFIBE 1 extrapolated predictions to the EOL of a fusion power reactor, though approximate, appear to be significant. From the assessment presented above, the issue of tritium retention in beryllium in the HCPB blanket appears to be, if not completely solved, much less serious than it was believed in the past.

The improvement and final confirmation of the prediction and extrapolation capability of the ANFIBE code will be possible as soon as beryllium pebbles, irradiated at higher neutron flu-ence and temperature than in COBRA-1A irradiation and approaching the EOL dose in a fusion power reactor, become available, e.g. in the next years from the irradiation pro-gramme HIDOBE and, in the longer term, from irradiation experiments in the International Fusion Material Irradiation Facility (IFMIF).

4.4 Discussion

After the development and validation of an improved version of the ANFIBE code performed in the previous parts of this study, the code has been extrapolated to predict tritium release and retention in beryllium in the central outboard module of the Helium Cooled Pebble Bed blanket, in the reference commercial fusion power plant Model B defined in the European Power Plant Conceptual Study.

In a range of operating temperatures between 450 and 700 ºC, whilst the previous version of the code predicts that a large fraction of tritium produced under irradiation (80% for the mate-rial considered) is retained in beryllium, essentially in bubbles inside the grain, according to

ANFIBE 1 practically the whole of tritium is at grain boundaries and it is released if a completely interconnected network of grain boundary porosities is present. By extrapolation of the microstructure of weakly irradiated beryllium pebbles from the BERYLLIUM experiment during fast thermal ramp annealing, it is expected that such condition is likely to occur in the reactor above 900 K; for lower temperatures the formation of porosity networks is only partial and to release all tritium at grain boundaries it is necessary to enhance porosity development and microcracking by, for example, baking above 900 K for a limited time.

On the basis of the present study, the issue of tritium retention in beryllium in the Helium Cooled Pebble Bed blanket appears to be much less serious than in the past.

5 Conclusions

An experimental and theoretical study of the behaviour of helium and tritium in neutron-irradiated beryllium has been presented. The study was aimed at improving and better validating the ANFIBE code, in view to enable reliable extrapolated predictions of tritium retention and release in beryllium pebbles, which are foreseen as a neutron multiplier in the Helium Cooled Pebble Bed (HCPB) blanket, at the End-Of-Life of the blanket modules in a fusion power reactor. Since tritium retention in beryllium is considered to be a key safety issue of the HCPB blanket, such assessment is required in the frame of the on-going European Power Plant Conceptual Study on the safety, viability and attractiveness of fusion power.

The first part of the study was meant to provide significant experimental data for the improvement and validation of the helium and tritium kinetics model in the ANFIBE code, in the limit of the presently available neutron-irradiated beryllium samples. An experimental study of out-of-pile helium and tritium release from different samples, irradiated in a large range of neutron fluence and temperature conditions, has been performed by a Knudsen-cell technique. In particular, pebbles irradiated at low fluence in the BERYLLIUM and EXOTIC 8 experiments have been investigated, as well as highly irradiated samples from the disposed moderator of Belgian Reactor 2. In order to understand the relationship between macroscopic release and microscopic gas diffusion phenomena and to measure key parameters in the analytical model of the ANFIBE code, at different release stages the sample microstructure has been characterised by optical, scanning and transmission electron microscopy, as well as by microtomography based on monochromatic synchrotron radiation. As a third step, an inverse analysis of the gas release experiments has been performed, by a model where gas precipitation into bubbles inside the grain and intragranular bubble venting was taken into account, beside atomic diffusion. Since the diffusion and precipitation model is substantially the same as in the ANFIBE code, such analysis has made it possible to measure key parameters, needed to calibrate the gas kinetics model in ANFIBE especially for pebbles. In particular, the characteristic migration length of gas atoms to grain boundaries, and the helium and tritium thermal diffusivities in irradiated beryllium pebbles have been measured. A further fundamental result of the analysis was the measurement of the actual precipitation rate of gas atoms into bubbles inside the grain, which turned out to be much lower than the theoretical value related to the bubble population, especially for tritium: the confirmation for beryllium of the non–linearity of the gas precipitation model, already observed for UO_2, was provided. As a consequence, it was shown that the gas precipitation model had to be corrected by introducing *a precipitation hindering factor,* which enhances gas release and limits intragranular swelling. The factor has been assumed constant and equal to the measured values: this is an approximate but effective representation of the non-linearity of gas precipitation.

The second part of the study was dedicated to the improvement and validation of the ANFIBE code. A new version of the code, ANFIBE 1, was developed from the previous version 0 and validated on the basis of the experimental results presented in the first part, as well as of other data available in the literature from the Post Irradiation Examinations of COBRA-1A

irradiation. An integrated macroscopic/microscopic validation procedure was defined and applied, where for the first time not only macroscopic gas release, but also the related evolution of microscopic quantities (gas in solution, gas in bubbles), were compared with the available experimental data. In all benchmarks considered, ANFIBE 1 describes gas release in a satisfactory way, with a trend to underestimate helium and tritium release also in-pile for pebbles. ANFIBE 1 represents a remarkable improvement with respect to the previous version 0, where gas precipitation was largely overestimated.

In the third part of the study, ANFIBE 1 was applied far outside its validation range, to give an approximate assessment of tritium release and retention at End-Of-Life conditions of beryllium pebbles in the reference fusion power reactor, considered in the Power Plant Conceptual Study. The code predicts that practically the whole of tritium inventory is at grain boundaries and it is released if a completely interconnected and open network of grain boundary porosities is present. Such condition is actually expected to occur above 900 K, for lower temperatures the development of interconnected porosity networks can be enhanced by a baking above 900 K for a limited time. Such assessment is believed to be much more realistic than the previous predictions of 80% tritium retention by ANFIBE 0.

On the basis of the present study, the issue of tritium retention in beryllium in the Helium Cooled Pebble Bed blanket appears to be much less serious than in the past.

Literature

[Aal02]   J. K. Aaldijk, D.J. Ketema, Irradiation of ceramic breeder material EXOTIC (R212 8/8), Report K5079/01.4662/I, NRG, Petten, The Netherlands, 2002

[Abr90]   E. Abramov, M.P. Riehm and D.A. Thompson, Deuterium permeation and diffusion in high-purity beryllium, J. Nucl. Mater. 175 (1990) 90-95

[Ame64]   S. Amelincxx, The direct observation of dislocations, Academic Press, New York and London, 1964, p. 193

[Ber02]   L. C. Bernard, J. L. Jacoud and P. Vesco, An efficient model for the analysis of fission gas release, J. Nucl. Mater. 302 (2002) 125-134

[Bes74]   A. G. Bespalov et al., Diffusivity of He in irradiated beryllium, Trans. Physical-Energetic Inst. Moscow 443 (1974)

[Boo57]   A.H. Booth, A method for calculating fission gas diffusion from UO_2 and its application to the X-2-f loop tests, Report AECL-496, 1957

[Bue02]   L. Bühler, Continuum models for pebble beds in fusion blankets, Report FZKA 6561, Forschungszentrum Karlsruhe, March 2002

[Cau02]   R. A. Causey, Hydrogen isotope retention and recycling in fusion reactor plasma-facing components, J. Nucl. Mater. 300 (2002) 91-117

[Cha02]   V. P. Chakin, Z. Ye Ostrovsky, Evolution of beryllium microstructure under high-dose neutron irradiation, J. Nucl. Mater. 307-311 (2002) 657-663

[Che02]   Y. Chen, U. Fischer, P. Pereslavtsev and F. Wasastjerna, The EU Power Plant Conceptual Study - Neutronic Design Analyses for Near Term and Advanced Reactor Models, Report FZKA 6763, Forschungszentrum Karlsruhe, 2002

[Con96]   R. Conrad, R. May, BERYLLIUM final irradiation report, Report P/F1/96/15, EC-JRC-IAM, Petten, November 1996

[Coo03]   I. Cook, N.P. Taylor, D.J. Ward, Four near-term and advanced fusion power plants: systems analysis; economics; prime safety and environmental characteristics, 20th IEEE/NPSS Symp. on Fusion Engineering (SOFE), San Diego, California, October 14-17, 2003

[Dal94]   M. Dalle Donne (ed.), European DEMO BOT solid breeder blanket, Report KfK 5429, Kernforschungszentrum Karlsruhe, 1994

[Dru02]   F. Druyts, J. Fays, X. Sillen, P. Van Iseghem, Beryllium waste conditioning strategies, 2. Conditioning methods for irradiated beryllium waste, Report R-3625, SCK-CEN, Mol, Belgium, 2002

[Fas76]   J. D. Fast, Gases in metals, The MacMillan Press, London, 1976

[Fis02]   S. B. Fisher, R. J. White, P. M. A. Cook, S. Bremier, R. C. Corcoran, R. Stratton, C. T. Walker, P. K. Ivison and I. D. Palmer, Microstructure of irradiated SBR MOX fuel and its relationship to fission gas release, J. Nucl. Mater. 306 (2002) 153-172

[Fis04]   U. Fischer, Y. Chen, D. Leichtle, A. Moeslang, S. Simakov, P. Vladimirov, Nuclear irradiation parameters of beryllium under fusion, fission and IFMIF irradiation conditions, Proc. 6th IEA International Workshop on Beryllium Technology for Fusion, Myazaki, Japan, December 2-5, 2003, Report JAERI-Conf 2004-2006, JAERI, March 2004, pp. 146-152

[Fis88]   U. Fischer, Optimal use of beryllium for fusion reactor blankets, Fusion Technology 1986, Proc. 14th Symp. on Fusion Technology, Avignon, France, September 8-12, 1986, Pergamon Press (1986), pp. 1179-1184

[Gag92]   P. Gagnol, J.-P. Hiernaut, Développement de la technique combinée spectrométrie de masse-effusion de Knudsen, Technical Note K 0292164, Joint Research Centre, Institute of Transuranium Elements, November 1992

[Gel97]   D. S. Gelles, L. R. Grenwood, B. M. Oliver, D. L. Baldwin, R. M. Ermi, H. Tsai, Post-irradiation examination of beryllium, Report Battelle, December 1997

[Heg04]   J. B. J. Hegeman, J. Van der Laan, A. J. Magielsen, A. Moeslang, E. Rabaglino, G. Piazza, J. Reimann, M. A. G. Oojevaar; M. P. Stijkel; S. Kamer, The HFR Petten high dose irradiation programme of beryllium for blanket application HIDOBE, Proc. 6th IEA Internat. Workshop on Beryllium Technology for Fusion, Miyazaki, Japan, December 3-6, 2003, Report JAERI-Conf 2004-006, JAERI, March 2004, pp. 141-145

[Her01]   S. Hermsmeyer, U. Fischer, M. Fütterer, K. Schleisiek, I. Schmuck, H. Schnauder, An improved European helium cooled pebble bed blanket, Fus. Eng. Des. 58-59 (2001) 689-693

[Her03]   S. Hermsmeyer, B. Dolenski, J. Fiek, U. Fischer, C. Koehly, S. Malang, P. Pereslatsev, J. Rey, Z. Xu, 20th IEEE/NPSS Symp. on Fusion Engineering (SOFE), San Diego, Calif., October 14-17, 2003

[Her99]   S. Hermsmeyer, S. Gordeev, K. Kleefeldt, K. Schleisiek, I. Schmuck, H. Schnauder, U. Fischer, S. Malang, M. Fütterer, O. Ogorodnikowa, Improved Helium Cooled Pebble Bed blanket, Report FZKA 6399, Forschungszentrum Karlsruhe, 1999

[Hie00]   J.-P. Hiernaut, Description et utilization de la méthode de Knudsen, Unpublished report, Joint Research Centre, Institute of Transuranium Elements, June 2000

[Hie01]   J. P. Hiernaut, C. Ronchi, Fission gas release and volume diffusion enthalpy in UO_2 irradiated at low and high burn-up, J. Nucl. Mater. 294 (2001) 39-44

[Hir65]   P. B. Hirsch, A. Howie, R. B. Nicholson, D. W. Pashley, M. J. Whelan, Electron microscopy of thin crystals, Butterworths, London, 1965

[Iwa99]   T. Iwadachi, Trial production of beryllium pebbles made by Inert Gas Atomisation and the results of basic characterisation, Proc. 4th IEA international workshop on beryllium technology for fusion, Report FZKA 6462, Forschungszentrum Karlsruhe, 1999, p. 1

[Jon67a]   P.M. S. Jones, R. Gibson, Hydrogen in beryllium, AWRE report 0-2/67, Atomic Weapons Research Establishment, 1967

[Jon67b]   P.M.S. Jones, R. Gibson, Hydrogen in beryllium, J. Nucl. Mater. 21 (1967) 353-354

[Kle01]   H. Kleykamp, Selected thermal properties of beryllium and phase equilibria in beryllium systems relevant for nuclear fusion reactor blankets, J. Nucl. Mater. 294 (2001) 88-93

[Kley99]   H. Kleykamp, Chemical interactions in the EXOTIC-7 experiment, J. Nucl. Mater. 273 (1999) 171-176

[Lae89]   R. Laesser, Tritium and helium-3 in metals, Springer-Verlag, 1989

[Las00]   K. Lassmann, H. Benk, Numerical algorithms for intragranular fission gas release, J. Nucl. Mater. 280 (2000) 127-135

[Las95]   K. Lassmann, J. Van de Laar, C.T. Walker, F. Lindstrom, Modelling the high burn-up UO_2 structure in LWR fuel, J. Nucl. Mater. 226 (1995) 1-8

[Lee00]   Chan Bock Lee, Youn Ho Jung, An attempt to explain the high burn-up structure formation mechanism in UO_2 fuel, J. Nucl. Mater. 279 (2000) 207-215

[Luc84] P. Luchini, A. Pozzi, C. Ronchi, Evaluation of the statistical distribution of spheroidal objects from measurements on metallographic cross sections, Meccanica 19 (1984) 127-132

[Mal99] S. Malang, Limitations on blanket performance, Fus. Eng. Des. 46 (1999) 193-206

[Mar02] G. Marbach, I. Cook, D. Maisonnier, The EU Power Plant Conceptual Study, Fus. Eng. Des. 63-64 (2002) 1-9

[Moe02] A. Moeslang, P. Vladimirov, Neutronics calculations and design for the medium flux test module of IFMIF, Fus. Eng. Des. 63-64 (2002) 121-126

[Moe03] A. Moeslang, personal communication, Forschungszentrum Karlsruhe, 2003

[Pia02] G. Piazza, in W. Bahm (ed.), Nuclear Fusion Programme Annual Report of the Association Forschungszentrum Karlsruhe / EURATOM, October 2000 - September 2001, Report FZKA 6650/EUR 20162 EN, Forschungszentrum Karlsruhe, 2002, p. 96

[Pia03] G. Piazza, J. Reimann, G. Hofmann, S. Malang, A. A. Goraieb and H. Harsch, Heat transfer in compressed beryllium pebble beds, Fusion Engineering and Design 69 (2003) 227-231

[Pok96] A.S. Pokrovsky, S.A. Fabritsiev, R.M. Bagautdinov, Yu. Goncharenko, High temperature beryllium embrittlement, J. Nucl. Mater. 233-237 (1996) 841-846

[Rab02a] E. Rabaglino, J.P. Hiernaut, C. Ronchi, F. Scaffidi-Argentina, Helium and tritium kinetics in irradiated beryllium pebbles, J. Nucl. Mater. 307-311(2002) 1424-1429

[Rab02b] E. Rabaglino, C. Ferrero, J. Reimann, C. Ronchi, T. Schulenberg, Study of the microstructure of neutron irradiated beryllium for the validation of the ANFIBE code, Fus. Eng. Des. 61-62c (2002) 769-773

[Rab03] E. Rabaglino, J. Baruchel, E. Boller, A. Elmoutaouakkil, C. Ferrero, C. Ronchi, T. Wiss, Study by microtomography of 3D porosity networks in irradiated beryllium, Nucl. Instr. Meth. B 200 (2003) 352-357

[Rab03b] E. Rabaglino, C. Ronchi, J.-P. Hiernaut, F. Capone, J.-Y. Colle, M. Murray-Farthing, R. Rolli, M. Holzer, H. Thiele, T. Wiss, Helium and tritium release and sub-microscopic restructuring in beryllium irradiated at high dose and low temperature, 6th IEA Internat. Workshop on Beryllium Technology for Fusion, Miyazaki, Japan, December 3-6, 2003

[Rab03c]   E. Rabaglino, C. Ronchi, A. Cardella, Recent progress in the modelling of helium and tritium behaviour in irradiated beryllium pebbles, Fus. Eng. Des. 69 (2003) 455-461

[Rab04]   E. Rabaglino, C. Ronchi, C. Ferrero, G. Janeschitz, R. A. Pieritz, Quantitative characterisation by microtomography of 3D percolation patterns in weakly irradiated beryllium, Technical Meeting on X-Ray Tomography of Nuclear Materials, Karlsruhe, January 22-23, 2004

[Rei02]   J. Reimann, L. V. Boccaccini, M. Enoeda, A. Y. Ying, Thermomechanics of solid breeder and beryllium pebble bed materials, Fus. Eng. Des. 61-62 (2002) 319-331

[Ron02]   C. Ronchi, E. Rabaglino, EFFUSX code Version for irradiated beryllium, unpublished, Joint Research Centre, Institute for Transuranium Elements, 2002

[Ron04]   C. Ronchi, M. Sheindlin, D. Staicu, M. Kinoshita, Effect of burn-up on the thermal conductivity of uranium dioxide up to 100.000 MWd t^{-1}, J. Nucl. Mater. 327 (2004) 58-76

[Ron04b]   C. Ronchi, J.-P. Hiernaut, Helium diffusion in uranium and plutonium oxides, J. Nucl. Mater. 325 (2004) 1-12

[Ron79]   C. Ronchi, Physical processes and mechanisms related to fission gas swelling in MX-type nuclear fuels, J. Nucl. Mater. 84 (1979) 55-84

[Ron81]   C. Ronchi, Extrapolated equation of state for rare gases at high temperatures and densities, J. Nucl. Mater. 96 (1981) 314-328

[Ron87a]   C. Ronchi, On diffusion and precipitation of gas-in-solid, J. Nucl. Mater. 148 (1997) 316 - 323

[Ron87b]   C. Ronchi, J. Sakellaridis, C. Syros, Boundary loss term in the diffusion of radioactive volatile fission products, Nucl. Sc. Eng. 95 (1987) 282-295

[Ron88]   C. Ronchi, J. Van de Laar, The fuel performance code FUTURE, Report EUR 11387 EN, EC-JRC-ITU, Karlsruhe, Germany, 1988

[Ron96]   F. Capone, J. P. Hiernaut, M. Martellenghi, C. Ronchi, Mass spectrometric measurements of fission product effusion from irradiated light water reactor fuel, Nucl. Sc. Eng. 124 (1996) 436-454

[Ron99]   F. Capone, J. Y. Colle, J. P. Hiernaut, C. Ronchi, Mass spectrometric measurement of the ionisation energies and cross sections of uranium and plutonium oxide vapors, J. Phys. Chem. A 103 (1999) 10899-10906

[Sca01a]   F. Scaffidi-Argentina, Tritium and helium release from neutron irradiated beryllium pebbles from the EXOTIC 8 irradiation experiment, Fus. Eng. Des. 58-59 (2001) 641-645

[Sca01b]   F. Scaffidi-Argentina, G. Piazza, A. Goraieb, E. Boller, A. Elmoutaouakkil, C. Ferrero, J. Baruchel, Non destructive three dimensional analysis of the packing of a binary beryllium pebble bed, Fus. Eng. Des. 58-59 (2001) 707-712

[Sca95]   F. Scaffidi-Argentina, Modellierung des Schwellens und der Tritium-Freisetzung von bestrahltem Beryllium, Report FZKA 5632, Forschungszentrum Karlsruhe, 1995

[Sca95b]   F. Scaffidi-Argentina, H. Werle, Tritium release from neutron irradiated beryllium: kinetics, long-time annealing and effect of crack formation, Proc. 2nd IEA Int. Workshop on Beryllium Technology for Fusion, Jackson Lake Lodge, Wyoming, USA, September 6-8, 1995, CONF-9509218 (1995), pp. 235-248

[Sca95c]   F. Scaffidi-Argentina, C. Ronchi, ANFIBE Code Version 0, unpublished, 1995

[Sca97a]   F. Scaffidi-Argentina, M. Dalle Donne, C. Ronchi, C. Ferrero, ANFIBE: a comprehensive model for swelling and tritium release from neutron irradiated beryllium - I: theory and model capabilities, Fus. Tech. 32 (1997) 179-195

[Sca97b]   F. Scaffidi-Argentina, Effect of neutron irradiation swelling on the heat transfer behavior of a beryllium pebble bed, Fusion Technology 1996, Proc. 19th Symp. On Fusion Technology, Lisbon, Portugal, September 16-20, 1996, North Holland (1997), pp. 1491-1494

[Sca97c]   F. Scaffidi-Argentina, H. Werle, Tritium release from neutron irradiated beryllium pebbles, Fusion Technology 1996, Proc. 19th Symp. On Fusion Technology, Lisbon, Portugal, September 16-20, 1996, North Holland (1997), pp. 1431-1434

[Sca98]   F. Scaffidi-Argentina, M. Dalle Donne, C. Ronchi, C. Ferrero, ANFIBE: a comprehensive model for swelling and tritium release from neutron irradiated beryllium - II: comparison of model predictions with experimental results, Fus. Tech. 33 (1998) 146-163

[Ses01]   A. L. Sessions, T. W. Burgoyne, J. M. Hayes, Correction of H3+ contributions in hydrogen isotope ratio monitoring mass spectrometry, Anal. Chem. 73 (2001) 192-199

[Sha88]   V. I. Shapovalov, Yu. M. Dukel'ski, The beryllium-hydrogen phase diagram, Russian Metallurgy 5 (1988) 201-203

[Swa86]   W. A. Swansiger, Tritium solubility in high purity beryllium, J. Vac. Sci. Technol., A4 (3) (1986) 1216-1217

[Sys02]   D.N. Syslov, V.P. Chakin, R.N. Latypov, Influence of high dose neutron irradiation on thermal conductivity of beryllium, J. Nucl. Mater. 307-311(2002) 364-367

[Taz94]   I.L. Tazhibaeva, V.P. Shestakov, E.V. Chikhray, et al. , Deuterium permeation through beryllium with surface element composition control, Fusion Technology 1994, Proc. 18th Symposium on Fusion Technology, Karlsruhe, Germany, August 22-26, 2004, North Holland, 1995, p. 427-431

[Tur71]   J. A. Turnbull, The distribution of intragranular fission gas bubbles in UO_2 during irradiation, J. Nucl. Mater. 38 (1971) 203-212

[Une00]   K. Une, M. Hiraia, K. Nogitaa, T. Hosokawaa, Y. Suzawab,S. Shimizuc and Y. Etoh, Rim structure formation and high burn-up fuel behavior of large-grained UO2 fuels, J. Nuc. Mater. 278 (2000) 54-63

[Van02]   V. Van Alsenoy, F. Druyts, M. Gysemans, L. Sannen, C. De Raedt, J. Fays, Beryllium waste conditioning strategies 1. Physical, chemical and radiological properties of the beryllium waste from the BR2 reactor of SCK-CEN, Report R-3598, SCK-CEN, Mol, Belgium, 2002

[Ver72a]   L. Verlet, J. J. Weis, Perturbation theory for the thermodynamic properties of simple liquids, Mol. Phys. 24-5 (1972) 1013-1024

[Ver72b]   L. Verlet, J. J. Weis, Equilibrium theory of simple liquids, Phys. Rev. A 5 (1972) 939-952

[Wil96]   D. B. Williams, C. Barry Carter, Transmission Electron Microscopy, Plenum Press, New York, 1996

[Wol81]   W. G. Wolfer, High density equation of state for helium and its application to bubbles in solids, Proc. 10th Conf. on Effects of Radiation on Materials, ASTM STP 725, D. Kramer, H.R. Brager, J. S. Perrin Eds., ASTM, 1981, pp. 201-212

[Wol84]   W. G. Wolfer, B. B. Glasgow, M. F. Wehner, H. Trinkaus, Helium equation of state for small cavities: recent developments, J. Nucl. Mater. 122-123 (1984) 565-570

[Wol85]   W. G. Wolfer, An assessment of radiation effects in beryllium, Fus. Tech. 8 (1985)1157-1164

Annex A   The gas kinetics model in ANFIBE

The analytical model for helium and tritium kinetics in the ANFIBE code consists of two separate sets of reaction-rate equations which have an identical structure but contain different unknowns and parameters, in one case referred to helium, in the other to tritium. The gas-dependent parameters are the atomic diffusion coefficient D and the precipitation hindering factor χ, the gas-in solid equilibrium solubility, contained in χ, as well as the radioactive decay constant λ for tritium. The analytical model for bubble kinetics considers bubbles containing both helium and tritium.

The description of the terms of the equations which have been the object of study, experimental validation and improvement in this work is in bold characters. A detailed explanation of the other terms is given in [Sca95] and [Sca97a].

The three set of equations (for helium kinetics, tritium kinetics and bubble kinetics) are solved in ANFIBE separately by different numerical techniques and, for some equations, analytically.

A.1   Helium and tritium kinetics

Eq. A-1   Concentration of helium or of tritium in dynamic solution c

$\dfrac{\partial c}{\partial t} =$	**Time derivative of the concentration of gas in solution**
$+\,\beta$	Gas atom production rate from nuclear reactions (only in-pile)
$-\,\chi\ k_{sc}^2 D c$	**Precipitation rate of gas atoms into intragranular bubbles**
$-\,k_{sg}^2 D c$	**Migration rate of gas atoms to grain boundaries (or precipitation rate of gas atoms into grain boundary bubbles)**
$+\,\eta b$	**Rate of re-solution into the lattice of gas trapped in intragranular bubbles due to atom recoils under neutron irradiation**
$-\,\dfrac{6\pi\ r_i^2 c N_i D_i}{a}$	Random walk rate of gas atom sweeping due to intragranular bubble migration
$-\,\pi\ r_i^2 c N_i v_i$	Thermal-gradient-driven rate of gas atom sweeping due to intragranular bubble migration
$-\,\psi\ c$	Rate of gas atom sweeping by grain boundaries due to grain growth
$-\,\lambda\ c$	**Rate of radioactive decay of gas atoms** (for tritium out-of-pile only, since in-pile decay is taken into account in β)
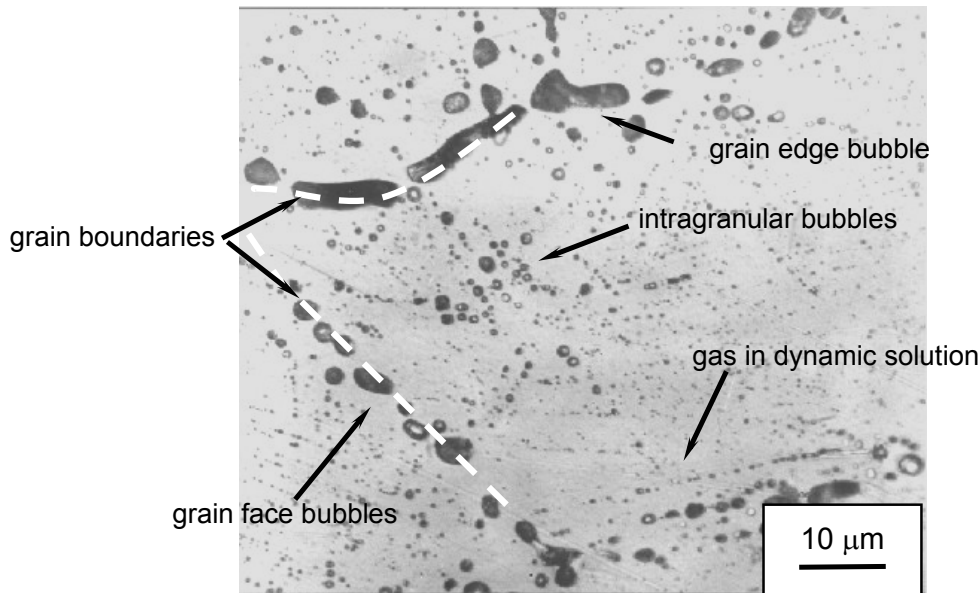
Fig. A-1   Bubbles inside the grain and at grain boundaries in an irradiated beryllium peb-
            ble. Some of the average quantities described by the gas kinetics model of the
            ANFIBE code are shown.

Eq. A-2   Concentration of helium or of tritium in intragranular bubbles b

$\dfrac{\partial b}{\partial t} =$	**Time derivative of the concentration of gas in intragranular bubbles**
$+ k_{sc}^2 \chi \; Dc$	**Precipitation rate of gas atoms into intragranular bubbles**
$- \eta b$	**Rate of re-solution into the lattice of gas trapped in intragranular bubbles due to atom recoils under neutron irradiation**
$+ \dfrac{6\pi \; r_i^2 c N_i D_i}{a}$	Random walk rate of gas atom sweeping due to intragranular bubble migration
$- \dfrac{3 v_i b}{\alpha}$	Thermal-gradient-driven bubble migration rate to grain boundaries
$- k_{gb}^2 D_i b$	Random walk migration rate of intragranular bubbles to grain boundaries
$- \pi \; r_i^2 c N_i v_i$	Thermal-gradient-driven rate of gas atom sweeping due to intragranular bubble migration
$- \psi \; b$	Rate of intragranular bubble sweeping by grain boundaries due to grain growth
$- U b$	Rate of intragranular bubble venting at high temperatures
$- \lambda \; b$	**Rate of radioactive decay of gas atoms** (for tritium out-of-pile only, since in-pile decay is taken into account in β)

Eq. A-3   Concentration of helium or of tritium in grain-face bubbles g

$\dfrac{\partial g}{\partial t} =$	**Time derivative of the concentration of gas in grain-face bubbles**
$+ Fk_{sg}^2 Dc$	**Migration rate of gas atoms to grain faces (or precipitation rate of gas atoms into grain face bubbles)**
$+ Fk_{gb}^2 D_i b$	Random walk migration rate of intragranular bubbles to grain faces
$+ F\dfrac{3v_i b}{\alpha}$	Thermal-gradient-driven migration of intragranular bubbles to grain faces
$+ F\psi(c + b)$	Rate of sweeping of intragranular bubbles and soluted gas atoms by grain faces due to grain growth
$- \dfrac{v_f g}{\alpha_f}$	Thermal-gradient-driven migration of grain face bubbles to grain edges
$- \lambda g$	**Rate of radioactive decay of gas atoms** (for tritium out-of-pile only, since in-pile decay is taken into account in β)

Eq. A-4   Concentration of helium or of tritium in grain-edge bubbles w

$\dfrac{\partial w}{\partial t} =$	Time derivative of the concentration of gas in grain-edge bubbles
$+ (1-F)k_{sg}^2 Dc$	**Migration rate of gas atoms to grain edges (or precipitation rate of gas atoms into grain-edge bubbles)**
$+ (1-F)k_{gb}^2 D_i b$	Random walk migration rate of intragranular bubbles to grain edges
$+ (1-F)\dfrac{3v_i b}{\alpha}$	Thermal-gradient-driven migration of intragranular bubbles to grain edges
$+ (1-F)\psi(c + b)$	Rate of sweeping of intragranular bubbles and soluted gas atoms by grain edges due to grain growth
$- \lambda w$	**Rate of radioactive decay of gas atoms** (for tritium out-of-pile only, since in-pile decay is taken into account in β)

A.2 Bubble kinetics

Eq. A-5   Concentration of intragranular bubbles N_i

$\dfrac{\partial N_i}{\partial t} =$	Time derivative of the concentration of intragranular bubbles
$+ \chi 16\pi\ \lambda\ DN_n c^2 A^2$	Intragranular bubble nucleation rate
$- \eta * N_i$	**Intragranular bubble destruction rate due to atom recoils under neutron irradiation (only in-pile)**

$-16\pi r_i D_i N_i^2$	Random walk loss rate of intragranular bubbles due to collision and coalescence
$-\theta' r_i^2 v_i N_i^2$	Thermal-gradient-driven loss rate of intragranular bubbles due to collision and coalescence. The term θ' in the thermal-gradient-driven motion is a heterogeneity factor that takes into account the dimensions of bubbles and consequently their related biased velocities. If θ' is equal to zero, then all bubbles have the same velocity and there is no capture of the small, faster bubbles.
$-\theta \dfrac{3 v_i N_i}{\alpha}$	Thermal-gradient-driven migration rate of intragranular bubbles to grain boundaries
$-k_{gb}^2 D_i N_i$	Thermal-gradient-driven migration rate of intragranular bubbles to grain boundaries

<div align="center">

Eq. A-6   Concentration of grain-face bubbles N_f

</div>

$\dfrac{\partial N_f}{\partial t} =$	Time derivative of the concentration of grain-face bubbles
$+ F k_{gb}^2 D_i N_i$	Thermal-gradient-driven migration rate of intragranular bubbles to grain faces
$+ F \dfrac{3 v_i N_i}{\alpha}$	Thermal-gradient-driven migration rate of intragranular bubbles to grain faces
$-16\pi r_f D_f N_f^2$	Random walk loss rate of grain-face bubbles due to collision and coalescence
$-\theta' r_f^2 v_f N_f^2$	Thermal-gradient-driven loss rate of grain-face bubbles due to collision and coalescence
$-\theta \dfrac{v_f N_f}{\alpha_f}$	Thermal-gradient-driven migration rate of grain-face bubbles to grain edges

<div align="center">

Eq. A-7   Concentration of grain-edge bubbles N_e

</div>

$\dfrac{\partial N_e}{\partial t} =$	Time derivative of the concentration of grain-edgebubbles
$+ (1-F) k_{gb}^2 D_i N_i$	Thermal-gradient-driven migration rate of intragranular bubbles to grain edges
$+ (1-F) \dfrac{3 v_i N_i}{\alpha}$	Thermal-gradient-driven migration rate of intragranular bubbles to grain edges
$-16\pi r_f D_f N_f^2$	Random walk loss rate of grain-edge bubbles due to coalescence
$-\theta' r_e^2 v_e N_e^2$	Thermal-gradient-driven loss rate of grain-face bubbles due to collision and coalescence
$+\theta \dfrac{v_f N_f}{\alpha_f}$	Thermal-gradient-driven migration rate of grain-face bubbles to grain edges

A.3   Symbols in the gas kinetics equations

A Avogadro's number

a Beryllium lattice spacing (m^{-1})

b Helium or tritium atoms in intragranular bubbles per unit volume of beryllium (mol m^{-3})

c Helium or tritium atoms in dynamic solution per unit volume of beryllium (mol m^{-3})

D Atomic diffusion coefficient of helium or of tritium in beryllium (m^2 s^{-1})

D_e Edge bubble diffusion coefficient in beryllium (m^2 s^{-1})

D_f Face bubble diffusion coefficient in beryllium (m^2 s^{-1})

D_i Intragranular bubble diffusion coefficient (m^2 s^{-1})

D_v Atomic vacancy diffusion coefficient (m^2 s^{-1})

F Ratio of face bubble surface to specific surface

g Helium or tritium atoms in gain-face bubbles per unit volume of beryllium (mol m^{-3})

k_{sc} Sink strength of intragranular bubbles (m^{-1})

k_{sg} Sink strength of grain boundary bubbles (m^{-1})

k_{gb} Sink strength of grain boundaries for intragranular bubbles (m^{-1})

N_e Concentration of grain-edge bubbles (m^{-3})

N_f Concentration of grain-face bubbles (m^{-3})

N_i Concentration of intragranular bubbles (m^{-3})

N_n Concentration of vacancy clusters produced by recoil atoms (mol m^{-3})

r_e Average edge bubble radius (m)

r_f Average face bubble radius (m)

r_i Average intragranular bubble radius (m)

v_e Edge bubble migration velocity (m s^{-1})

v_f Face bubble migration velocity (m s^{-1})

v_i Intragranular bubble migration velocity (m s^{-1})

w Helium or tritium atoms in edge bubbles per unit volume of beryllium (mol m^{-3})

Greek symbols:

α Average grain size (m)

β Helium or tritium production rate from nuclear reactions (mol m^{-3} s^{-1})

η Atomic resolution rate from intragranular bubbles (s^{-1})

η^* Intragranular bubble destruction rate (s^{-1})

θ, θ' Heterogeneity factors which represent a bias in the velocity of bubbles

λ Radioactive decay constant (s^{-1})

χ Helium or tritium precipitation hindering factor

ψ Sweeping rate of grain boundaries due to grain growth

Annex B   Nomenclature

ANFIBE   ANalysis of Fusion Irradiated BEryllium (computer code)

BR2   Belgian Reactor 2 (located in SCK-CEN, Mol, Belgium)

CMT   Computer-aided MicroTomography

DEMO   DEMOnstration fusion power reactor

EFDA   European Fusion Development Agreement

EOI   End-Of-Irradiation

EOL   End-Of-Life

EOS   Equation Of State

FRP   Fluoride Reduction Process

HCPB   Helium Cooled Pebble Bed

HBS   High Burn-up Structure

HFR   High Flux Reactor (located in Petten, the Netherlands)

IFMIF   International Fusion Material Irradiation Facility

IGA   Inert Gas Atomisation

ITER   International Thermonuclear Experimental Reactor

JRC-ITU   Joint Research Centre, Institute for Transuranium Elements

NGK   Nippon Gaishi Co.

OM   Optical microscopy

PPCS   Power Plant Conceptual Study

PIE   Post Irradiation Examinations

REP   Rotating Electrode Process

SEM   Scanning Electron Microscopy

STEM   Scanning Transmission Electron Microscopy

TEM   Transmission Electron Microscopy

VHP   Vacuum Hot Pressing

Acknowledgments

Table captions

Figure captions